

AD-A241 374



2

NAVAL POSTGRADUATE SCHOOL

Monterey, California



THESIS



SEASONAL VARIABILITY OF THE GEOSTROPHIC
VELOCITY AND WATER MASS STRUCTURE
OFF POINT SUR, CALIFORNIA

by

Timothy Daniel Tisch

September 1990

Thesis Advisor:
Co-advisor:

Steven R. Ramp
Curtis A. Collins

Approved for public release; distribution unlimited.

91-12677

91 10 1991

Unclassified

Security Classification of this page

REPORT DOCUMENTATION PAGE

1a Report Security Classification Unclassified			1b Restrictive Markings		
2a Security Classification Authority			3 Distribution Availability of Report		
2b Declassification/Downgrading Schedule			Approved for public release; distribution is unlimited.		
4 Performing Organization Report Number(s)			5 Monitoring Organization Report Number(s)		
6a Name of Performing Organization Naval Postgraduate School		6b Office Symbol (If Applicable) OC	7a Name of Monitoring Organization Naval Postgraduate School		
6c Address (city, state, and ZIP code) Monterey, CA 93943-5000			7b Address (city, state, and ZIP code) Monterey, CA 93943-5000		
8a Name of Funding/Sponsoring Organization		8b Office Symbol (If Applicable)	9 Procurement Instrument Identification Number		
8c Address (city, state, and ZIP code)			10 Source of Funding Numbers		
			Program Element Number	Project No	Task No
			Work Unit Accession No		
11 Title (Include Security Classification) SEASONAL VARIABILITY OF THE GEOSTROPHIC VELOCITY AND WATER MASS STRUCTURE OFF POINT SUR, CALIFORNIA					
12 Personal Author(s) Tisch, Timothy Daniel					
13a Type of Report Master's Thesis		13b Time Covered From To		14 Date of Report (year, month, day) September 1990	
15 Page Count 163					
16 Supplementary Notation The views expressed in this thesis are those of the author and do not reflect the official policy or position of the Department of Defense or the U.S. Government.					
17 Cosati Codes			18 Subject Terms (continue on reverse if necessary and identify by block number)		
Field	Group	Subgroup	California Current, California Undercurrent, spiciness anomaly, geostrophic velocity, water mass characteristics		
19 Abstract (continue on reverse if necessary and identify by block number)					
<p>The Point Sur Transect was established in 1987 by the Department of Oceanography at the Naval Postgraduate to further the present understanding of long term variability of current and temperature in eastern boundary regions. Of particular interest is the temporal variability of poleward flows, their role in gyre-scale processes, and a more complete understanding of their dynamics. The POST extends offshore, normal to bottom topography, along 36° 20'N, to 123° 01.7'W where it doglegs southwest along the California Cooperative Oceanic Fisheries Investigation (CalCOFI) line 67. Station spacing along the POST is 5-10 km inshore, increasing to 20-40 km offshore. The transect has been occupied 6-8 times per year since 1988, to resolve the flow at seasonal and interannual time scales.</p> <p>Seven of these cruises were selected for seasonal comparisons of alongshore geostrophic velocities and water mass characteristics. Geostrophic velocities were referenced to the 1000 decibar surface based on available PEGASUS observations. Anomalies of spiciness calculated as deviations from an average offshore T-S profile have been used to identify the location and spatial extent of the eastern Pacific water masses. The California Undercurrent (positive spiciness anomaly) was a prominent feature in 6 of the 7 sections analyzed, and was very weak during a period of uncommonly strong equatorward wind stress. The position of the core varied from 12 to 42 km from shore while its strength varied from 10 to 35 cm s⁻¹, with the maximum flow occurring in winter. The vertical extent of the Undercurrent core covered a region of the continental slope from 70 to 460 m throughout these seven cruises. The nature of the alongshore geostrophic velocities and the location and spatial extent of the undercurrent appear strongly related to specific wind events, both local and remote. Remote wind forcing from</p>					
20 Distribution/Availability of Abstract			21 Abstract Security Classification		
<input checked="" type="checkbox"/> unclassified/unlimited <input type="checkbox"/> same as report <input type="checkbox"/> DTIC users			Unclassified		
22a Name of Responsible Individual Steven R. Ramp			22b Telephone (Include Area code) (408) 646-3162		22c Office Symbol OC/Ra

DD FORM 1473, 84 MAR

83 APR edition may be used until exhausted

security classification of this page

All other editions are obsolete

Unclassified

Unclassified

Security Classification of this page

Line # 19 (CONT)

the south was believed to cause anomalous, strong poleward flow throughout the entire water column during a period of local equatorward wind stress, while an intrusion of warm, salty water was believed to cause a deep penetration (to 700 m) of the California Current in winter.

These observations revealed primarily interannual rather than seasonal variability. This is not surprising since only seven cruises were selected for study whereas earlier studies utilized many years of data collected along the CalCOFI sampling grid to determine the seasonal means. This study excelled over the continental shelf and slope where the station spacing of the POST is considerably closer than the CalCOFI scheme, which allowed for the study of narrow coastal jets not well resolved by the CalCOFI grid.

S/N 0102-LF-014-6601

security classification of this page

Unclassified

Approved for public release; distribution is unlimited.

Seasonal Variability of the Geostrophic Velocity and Water Mass Structure
off Point Sur, California

by

Timothy Daniel Tisch
Lieutenant, NOAA Corps
B.S., State University of New York, Maritime College, 1982

Submitted in partial fulfillment of the requirements
for the degree of

MASTER OF SCIENCE IN PHYSICAL
OCEANOGRAPHY

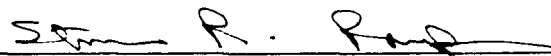
from the

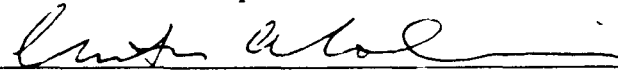
NAVAL POSTGRADUATE SCHOOL
September 1990

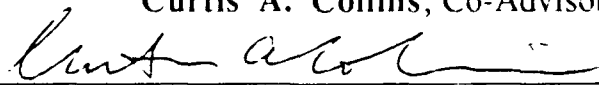
Author:


Timothy Daniel Tisch

Approved by:


Steven R. Ramp, Thesis Advisor


Curtis A. Collins, Co-Advisor


Curtis A. Collins, Chairman, Department of Oceanography

ABSTRACT

The Point Sur Transect (POST) was established in 1987 by the Department of Oceanography at the Naval Postgraduate School to further the present understanding of long term variability of current and temperature in eastern boundary regions. Of particular interest is the temporal variability of poleward flows, their role in gyre-scale processes, and a more complete understanding of their dynamics. The POST extends offshore, normal to bottom topography, along $36^{\circ} 20'N$, to $123^{\circ} 01.7'W$ where it doglegs southwest along the California Cooperative Oceanic Fisheries Investigation (CalCOFI) line 67. Station spacing along the POST is 5-10 km inshore, increasing to 20-40 km offshore. The transect has been occupied 6-8 times per year since 1988, to resolve the flow at seasonal and interannual time scales.

Seven of these cruises were selected for seasonal comparisons of alongshore geostrophic velocities and water mass characteristics. Geostrophic velocities were referenced to the 1000 decibar surface based on available PEGASUS observations. Anomalies of spiciness calculated as deviations from an average offshore T-S profile have been used to identify the location and spatial extent of the eastern Pacific water masses. The California Undercurrent (positive spiciness anomaly) was a prominent feature in 6 of the 7 sections analyzed, and was very weak during a period of uncommonly strong equatorward wind stress. The position of the core varied from 12 to 42 km from shore while its strength varied from 10 to 35 cm s^{-1} , with the maximum flow occurring in winter. The vertical extent of the Undercurrent core covered a region of the continental slope from 70 to 460 m throughout these seven cruises. The nature of the alongshore geostrophic velocities and the location and spatial extent of the undercurrent

appear strongly related to specific wind events, both local and remote. Remote wind forcing from the south was believed to cause anomalous, strong poleward flow throughout the entire water column during a period of local equatorward wind stress, while an intrusion of warm, salty water was believed to cause a deep penetration (to 700 m) of the California Current in winter.

These observations revealed primarily interannual rather than seasonal variability. This is not surprising since only seven cruises were selected for study whereas earlier studies utilized many years of data collected along the CalCOFI sampling grid to determine the seasonal means. This study excelled over the continental shelf and slope where the station spacing of the POST is considerably closer than the CalCOFI scheme, which allowed for the study of narrow coastal jets not well resolved by the CalCOFI grid.

v



Accession For	
NTIS GRA&I	<input checked="" type="checkbox"/>
DTIC TAB	<input type="checkbox"/>
Unannounced	<input type="checkbox"/>
Justification	
By	
Distribution/	
Availability Codes	
Dist	Avail and/or Special
A-1	

TABLE OF CONTENTS

I. INTRODUCTION.....	1
II. DATA COLLECTION AND PROCESSING.....	7
A. DATA COLLECTION	7
B. DATA PROCESSING	12
III. CALIBRATION PROCEDURE FOR HYDROGRAPHIC DATA .	15
A. STANDARD PRE- AND POST- CRUISE CALIBRATION PROCEDURE	15
B. POST-CRUISE SALINITY CALIBRATION PROCEDURE	17
1. Calibration of Large Neil Brown CTD.....	19
2. Calibration of Small Neil Brown CTD before repair	22
a. Pressure effect and its removal	25
b. Final adjustment of Small Neil Brown CTD salinities	26
3. Calibration of Small Neil Brown CTD after repair.....	29
IV. ANALYSIS	33
A. DESCRIPTION OF WATER MASS CHARACTERISTICS	33
1. Analysis of spiciness and spiciness anomaly	34
a. August 1988 Water Mass Analysis (seasonal normal).....	37
b. May 1988 Water Mass Analysis (weak poleward flow)	41
c. November 1988 Water Mass Analysis (strong mesoscale feature)	43
d. February 1989 Water Mass Analysis (strong equatorward flow near coast).....	48
e. May 1989 Water Mass Analysis (poleward flow near coast)	50
f. July 1989 Water Mass Analysis (anomalous poleward flow)	52
g. November 1989 Water Mass Analysis (deep equatorward flow)	56

B. DESCRIPTION OF ALONGSHORE GEOSTROPHIC FLOW	60
1. Geostrophy and its limitations	60
2. Calculation of alongshore geostrophic velocity.....	63
3. Estimation of error in dynamic height and geostrophic velocity	63
a. Determination of error in specific volume anomaly.....	66
b. Determination of error in dynamic height.....	68
c. Determination of error in geostrophic velocity	70
d. Effect of internal tides on errors in dynamic height.....	73
4. Analysis of alongshore geostrophic velocity.....	75
a. August 1988 alongshore geostrophic velocities (seasonal normal)	75
b. May 1988 alongshore geostrophic velocities (weak poleward flow).....	78
c. November 1988 alongshore geostrophic velocities (strong mesoscale feature)	81
d. February 1989 alongshore geostrophic velocities (strong equatorward flow near coast).....	83
e. May 1989 alongshore geostrophic velocities (poleward flow near coast).....	85
f. July 1989 alongshore geostrophic velocities (anomalous poleward flow).....	90
g. November 1989 alongshore geostrophic velocities (deep equatorward flow).....	94
V. DISCUSSION	100
A. WATER MASS CHARACTERISTICS	100
B. ALONGSHORE GEOSTROPHIC VELOCITIES.....	103
VI. CONCLUSIONS AND RECOMMENDATIONS	111
A. CONCLUSIONS	111
B. RECOMMENDATIONS.....	112

APPENDIX A: CALIBRATION INFORMATION AND DEEP T-S CURVES	115
APPENDIX B: PROPAGATION OF VARIANCES AND COVARIANCES AND FUNDAMENTAL PROPERTIES OF A UNIFORM DISTRIBUTION	130
REFERENCES.....	142
INITIAL DISTRIBUTION LIST	147

LIST OF TABLES

Table 1.	POINT SUR TRANSECT CRUISE PERIODS AND DATA TYPES	10
Table 2.	TEMPERATURE AND PRESSURE CALIBRATION COEFFICIENTS	17
Table 3.	SALINITY CALIBRATION COEFFICIENTS FOR THE LARGE NEIL BROWN CTD	25
Table 4.	CALIBRATION COEFFICIENTS FOR REMOVAL OF THE SMALL NEIL BROWN CTD PRESSURE DEPENDENCE	31
Table 5.	SALINITY CALIBRATION COEFFICIENTS FOR THE SMALL NEIL BROWN CTD	31
Table 6.	WATER MASSES OF THE CALIFORNIA CURRENT SYSTEM...	33
Table 7.	NORMALIZED ALONGTRACK DIFFERENTIAL DRIFT OF THE VESSEL	72
Table 8.	SPATIAL EXTENT AND CORE VELOCITIES OF THE CALIFORNIA UNDERCURRENT	107

LIST OF FIGURES

Figure 1.	Sampling schemes along the Point Sur Transect.....	8
Figure 2.	CalCOFI sampling scheme along the central California coast	9
Figure 3.	NOAA weather buoys used to calculate alongshore component of wind stress	14
Figure 4.	Scattergram of initial salinity difference for STMAY 1988	20
Figure 5.	Scattergram of intermediate salinity difference for STMAY 1988	21
Figure 6.	Scattergram of final salinity difference for STMAY 1988	23
Figure 7.	Linear Regression used to fit STMAY 1988 CTD salinities to bottle salinities	24
Figure 8.	Pressure effect on small Neil Brown CTD (February 1989)	27
Figure 9.	Comparison of salinity differences before and after removing pressure effect from CTD data (February 1989)	28
Figure 10.	Linear Regression to fit February 1989 CTD salinities to bottle salinities	30
Figure 11.	The eight T-S profiles used to obtain the average offshore profile.....	35
Figure 12.	Average offshore T-S profile used in calculation of spiciness anomaly	36
Figure 13.	Vertical section of temperature for cruise CUC-August 1988	37
Figure 14.	Vertical section of salinity for cruise CUC-August 1988	38
Figure 15.	Vertical section of spiciness for cruise CUC-August 1988.....	39
Figure 16.	Vertical section of spiciness anomaly for cruise CUC-August 1988	40
Figure 17.	Vertical section of density anomaly for the May 1988 Student Cruise	42
Figure 18.	Vertical section of spiciness anomaly for the May 1988 Student Cruise	44

Figure 19.	Vertical section of density anomaly for cruise CUC-November 1988	45
Figure 20.	NOAA AVHRR satellite image from 0004 GMT, 21 November 1988	46
Figure 21.	Vertical section of spiciness anomaly for cruise CUC-November 1988	47
Figure 22.	NOAA AVHRR satellite image from 2058 GMT, 5 February 1989	48
Figure 23.	Vertical section of spiciness anomaly for cruise CUC-February 1989	49
Figure 24.	Vertical section of salinity for the May 1989 Student Cruise	51
Figure 25.	Vertical section of spiciness anomaly for the May 1989 Student Cruise	52
Figure 26.	Vertical section of density anomaly for the May 1989 Student Cruise	53
Figure 27.	Vertical section of spiciness anomaly for cruise CUC-July 1989...	54
Figure 28.	Vertical section of salinity for cruise CUC-July 1989.....	55
Figure 29.	Vertical section of density anomaly for cruise CUC-November 1989	57
Figure 30.	Vertical section of spiciness anomaly for cruise CUC-November 1989	58
Figure 31.	Vertical section of salinity for cruise CUC-November 1989.....	59
Figure 32.	Extrapolation of dynamic height relative to 1000 decibars.	64
Figure 33.	Alongshore component of wind stress during cruise CUC-August 1988	76
Figure 34.	Vertical section (0-1000dbar) of alongshore geostrophic velocity for cruise CUC-August 1988	77
Figure 35.	Alongshore component of wind stress during the May 1988 Student Cruise.....	79

Figure 36.	Vertical section (0-1000 dbar) of alongshore geostrophic velocity for the May 1988 Student Cruise.....	80
Figure 37.	Vertical section (0-1000 dbar) of alongshore geostrophic velocity for cruise CUC-November 1988	82
Figure 38.	Alongshore component of wind stress during cruise CUC-November 1988	84
Figure 39.	Alongshore component of wind stress during cruise CUC-February 1989	85
Figure 40.	Vertical section (0-1000 dbar) of alongshore geostrophic velocity for CUC-February 1989	86
Figure 41.	Vertical section of density anomaly for cruise CUC-February 1989	87
Figure 42.	Alongshore component of wind stress during the May 1989 Student Cruise.....	88
Figure 43.	Vertical section (0-1000 dbar) of alongshore geostrophic velocity for the May 1989 Student Cruise.....	89
Figure 44.	NOAA AVHRR satellite image from 2044 GMT, 3 May 1989	92
Figure 45.	Alongshore component of wind stress during cruise CUC-July 1989	93
Figure 46.	Vertical section (0-1000 dbar) of alongshore geostrophic velocity for cruise CUC-July 1989	94
Figure 47.	Alongshore component of wind stress during cruise CUC-November 1989	96
Figure 48.	Vertical section (0-1000 dbar) of alongshore geostrophic velocity for cruise CUC-November 1989	97
Figure 49.	Vertical section (0-4500 dbar) of alongshore geostrophic velocity for cruise CUC-November 1989	99
Figure 50.	Mean salinity on the surface where $\sigma_t = 25.0$ for July	101
Figure 51.	Horizontal sections of salinity at 10 m depth from CalCOFI data.....	103

Figure 52. Vertical section (0-400 m) of seasonal alongshore geostrophic velocity relative to 500 dbar along CalCOFI line 70 off

Point Sur..... 105

ACKNOWLEDGMENTS

A scientific paper such as this is rarely the result of one individual's efforts. The support and guidance from faculty advisors, technical staff, and family play an important role in the final product. I would first like to thank my advisors Prof. Steve Ramp and Prof. Curt Collins for their collective wisdom on this subject and for providing much insight into the processing and interpretation of the acquired oceanographic data. Next, I would like to thank Mr. Paul Jessen for his extreme patience and dedication and the numerous hours he spent writing the programs necessary for this study. I would also like to express my sincere appreciation to CDR. Kurt Schnebele for his guidance on the analysis of errors, both in calibrating the data and in geostrophic velocities, and CDR. Dan Tracy who was a source of encouragement during our stay at the Naval Postgraduate School. Finally, and most importantly, I would like to thank my family, especially my wife Kathleen, for their continued support and toleration of the many lonely hours endured while this work was in progress. Without this support none of this work could have been accomplished.

I. INTRODUCTION

Large scale atmospheric forcing in the eastern Pacific Ocean consists of the North Pacific (sub-tropical) high, the Aleutian low, and in the summer the thermal low over the western United States. The North Pacific high is most intense during the summer months while the Aleutian low is most intense during the winter months. The high migrates annually from a maximum southern position at 28°N , 130°W in February to a maximum northern position at 38°N , 150°W in August (Huyer 1983). The U.S. thermal low is centered near 35°N and enhances the equatorward wind stress over the coastal waters off northern California (Reinecker and Ehret 1988). A region of positive wind stress curl exists near the coast throughout the year, being well developed from May to September and having greater spatial variability during winter (Nelson 1977).

This large-scale atmospheric forcing creates the anticyclonic North Pacific gyre. Its northern side is comprised of the West Wind Drift and the North Pacific Current which flow easterly. The eastern limb of this gyre is the California Current (CC). Offshore the CC is a surface current (0-300 m deep) carrying water equatorward throughout the year along the west coast of North America (Lynn and Simpson 1987). Near 20°N it turns westward as part of the North Equatorial Current. The average speed of the CC off the coast of California is generally less than 25 cm s^{-1} (Reid and Schwartzlose 1962).

Within 150 km of the coast there is a fall-winter reversal of the surface flow known as the California Countercurrent (CCC, Simpson et al. 1986) or Inshore Countercurrent (IC, Lynn and Simpson 1987). This poleward flow from

October to March is generally referred to as the Davidson Current (DC) north of Point Conception. Hereinafter it will be referred to as the DC.

The California Undercurrent (CUC) flows poleward throughout the year. It has been observed from off Baja California (Wooster and Jones 1970) to as far north as Oregon (Halpern et al. 1978). The continuity of the CUC has not been observed. It has its origin in the eastern equatorial Pacific and is centered primarily over the continental slope. The location, strength and core depth as determined from moored current meters and inferred from hydrographic measurements show considerable seasonal variability and can be related to the seasonal variability in wind stress and wind stress curl (Hickey 1979).

Collectively these currents comprise what is known as the California Current System (CCS). The water properties which make up this system are determined by four water masses, each of which can be defined by its temperature (T), salinity (S), dissolved oxygen (DO) and nutrient content as it enters into the CCS. Pacific Subarctic water is formed at the Subarctic Convergence through mixing of the warmer, saline waters of the Kuroshio Extension and the cooler, fresher waters of the Oyashio Current and enters the CC near 48°N (Pickard and Emery 1982). It is characterized by relatively low temperature, low salinity, high dissolved oxygen and high nutrients (Reid et al. 1958). Equatorial Pacific water forms in the eastern tropical Pacific and is characterized by relatively high temperature, high salinity, low dissolved oxygen and high nutrients. It enters the CCS from the south and is carried northward by the CUC. Eastern North Pacific Central enters the CCS from the west and is characterized by relatively high temperature, high salinity, low dissolved oxygen and low nutrients (Reid et al. 1958). Upwelled water within 50 km of the coast is identified by relatively

cold temperature, high salinity, high nutrients and low dissolved oxygen (Sverdrup 1938; Reid et al. 1958). These water properties appear in varying proportions throughout the CCS due to mixing which occurs as the CC flows southward and the CUC northward.

Wickham (1975) used 5 km station spacing off Point Sur and Monterey Bay to define very narrow streams of anomalously high temperature and salinity, which he termed southern water. Vertical distributions of this southern water were extremely complex. He noted two regions of warmer southern water in bands 10-20 km in width, which appeared as intrusions from the south. Vertical cross-sections indicated that these intrusions are generally found between 200-500 m depths. Alongshore geostrophic velocities along 36° 20'N exhibited a banded structure. A narrow band of poleward flow was found between 50 m and 200 m near the shelf edge. Offshore he observed alternating bands (5 km width) of poleward and equatorward flow, with maximum speeds of +40 cm s⁻¹ and -80 cm s⁻¹, respectively. Current patterns exhibited by both drogue measurements and geostrophy were in agreement with the banded nature of southern water flowing poleward.

Chelton (1984) and Lynn and Simpson (1987) have utilized the California Cooperative Oceanic Fisheries Investigations (CalCOFI) data sets to examine the seasonal variability of alongshore geostrophic currents and physical characteristics, respectively. This large scale hydrographic sampling grid was initiated in 1949 and since 1950 stations have been occupied between 4 and 12 times per year (Chelton 1984). The sampling grid consists of a series of parallel lines which are oriented normal to the coast. Standard station and line spacing are both 74 km, with station spacing decreasing to 40 km near the coast (Lynn and Simpson

1987). While this data set provides excellent temporal coverage, the coarse station spacing and limited vertical extent (upper 500 m) do not allow for detailed analysis of the smaller scale phenomenon which occur in coastal regions. The seasonal average geostrophic flow in the upper 100 m relative to 500 m off Point Sur and Point Conception is equatorward flow from February to September and poleward from October to January. The deeper flow (below 100 m) is different along these sections with poleward flow throughout the year at Point Conception, while off Point Sur it has a poleward maximum in December and weak equatorward flow from March to May. The surface flow throughout this region was found to lead the annual wind forcing, computed from the spatial averages of Nelson (1977), by about one month while the deep poleward flow was found to lag the local poleward barotropic pressure gradient by about two months (Chelton 1984). Chelton (1984) estimates the total alongshore pressure gradient ($p_y = \text{barotropic component} + \text{baroclinic component}$) as

$$\frac{\partial p}{\partial y} = \rho_0 g \frac{\partial h}{\partial y} + g \int_D^0 \frac{\partial \rho}{\partial y} dz$$

where the p is pressure, g the gravitational acceleration, h the sea surface elevation, D is depth, ρ the water density, and ρ_0 the water density at the surface.

Analysis of dynamic height fields have led to the definition of three domains within the CCS: oceanic, coastal, and an intervening transition zone. The transition zone is coincident with the core of the CC and is hypothesized to result from recurrent eddies and energetic meanders. Seasonal variability in the fields of temperature, salinity, σ_t (defined as $\sigma_t = \rho_{s,t,0} - 1000$, where ρ has units of kg m^{-3}), and oxygen is related to variations in the CC, DC, and CUC through vertical adjustments in the density field and through changes in transport (Lynn

and Simpson 1987). This transition zone differs from that described in the Coastal Transition Zone (CTZ) program where it is defined as the area encompassing the offshore (greater than 50 km) region of cold "filaments" often seen in satellite imagery (Brink and Hartwig 1985).

The Central California Coastal Circulation Study (CCCCS) (February 1984 and July 1984) provided higher resolution (than CalCOFI) CTD and current meter coverage from San Francisco to Point Conception and was aimed at a detailed description of the coastal circulation on the continental shelf and upper slope (Chelton et al. 1988). During the first half of 1984 the mean flow between Point Conception and Point Sur was poleward and in opposition to the equatorward wind stress. A three week period of calm winds during July 1984 resulted in a 100 km wide surface poleward flow (observed in current meter measurements, satellite sea surface temperature imagery, buoy drift trajectories, and inferred from the hydrographic data) which extended 300 km off the central California coast. In July 1981 a similar but weaker occurrence produced a poleward surface flow which extended to 150 km off the coast. Poleward flow at the surface over the continental shelf is normally observed during spring and summer, however, poleward flow at the surface over the continental slope was previously not observed after February (Chelton et al. 1988).

In 1987, the Point Sur Transect (hereinafter referred to as the POST) was established by the Department of Oceanography at the Naval Postgraduate School (NPS) to further the present understanding of long term variability in eastern boundary regions. Of particular interest is the time variability of poleward flows, their role in gyre-scale processes, and a more complete understanding of the dynamics involved.

The purpose of this study is to describe the seasonal variability of the alongshore geostrophic currents and water mass structure off Point Sur using hydrographic data four times per year collected from spring 1988 through winter 1989 along the POST. Data collection and processing will be discussed in Chapters II and III. Analysis of water mass characteristics and alongshore geostrophic velocities are discussed in Chapter IV and comparisons with earlier studies conducted off Point Sur are made in Chapter V. A discussion and conclusion follows.

II. DATA COLLECTION AND PROCESSING

The POST, as established in 1987, extends offshore, normal to bottom topography, along $36^{\circ} 20'N$, to $123^{\circ} 01.7'W$ where it meets and thereafter coincides with the California Cooperative Oceanic Fisheries Investigation (CalCOFI) line 67 (the Monterey Bay line). It follows line 67 to allow for comparison with previous studies which have utilized the CalCOFI data set. As of January 1990 there have been 16 cruises (Table 1) along the POST using either one of two sampling schemes. The first, used for the NPS student cruises, consists of 19 stations and extends to approximately 370 km offshore (Figure 1a). The second, used for CUC cruises, consists of 22 stations and is approximately 215 km in length, terminating in the vicinity of station 15 of the NPS student cruise sampling scheme (Figure 1b). The former provides greater offshore coverage while the latter provides a more extensive coverage of the inshore end of the transect for a more detailed study of the CUC. Both of these schemes provide higher resolution coverage than the CalCOFI sampling scheme in this region (Figure 2). Of the 16 cruises along the POST, a total of 7, indicated by asterisks in Table 1, were selected for detailed analysis. These cruises provide a suitable seasonal description of the POST. When cruises were within a month of one another only one was selected.

A. DATA COLLECTION

Data collected along the POST consists primarily of three types: hydrographic (CTD), acoustic Doppler current profiler (ADCP), and more

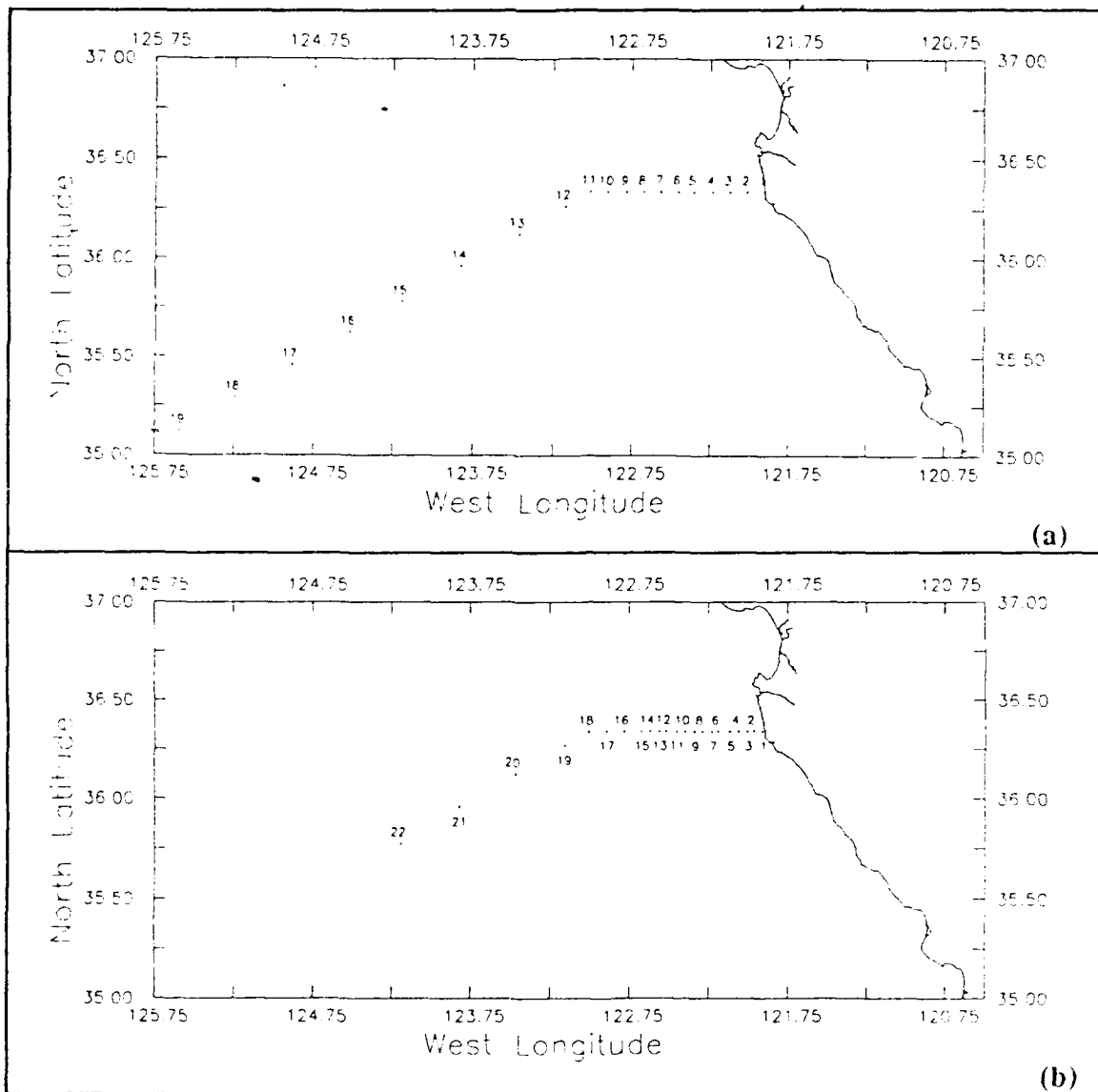


Figure 1. Sampling schemes along the Point Sur Transect:
 (a) NPS student cruise sampling scheme; (b) California
 undercurrent cruise sampling scheme.

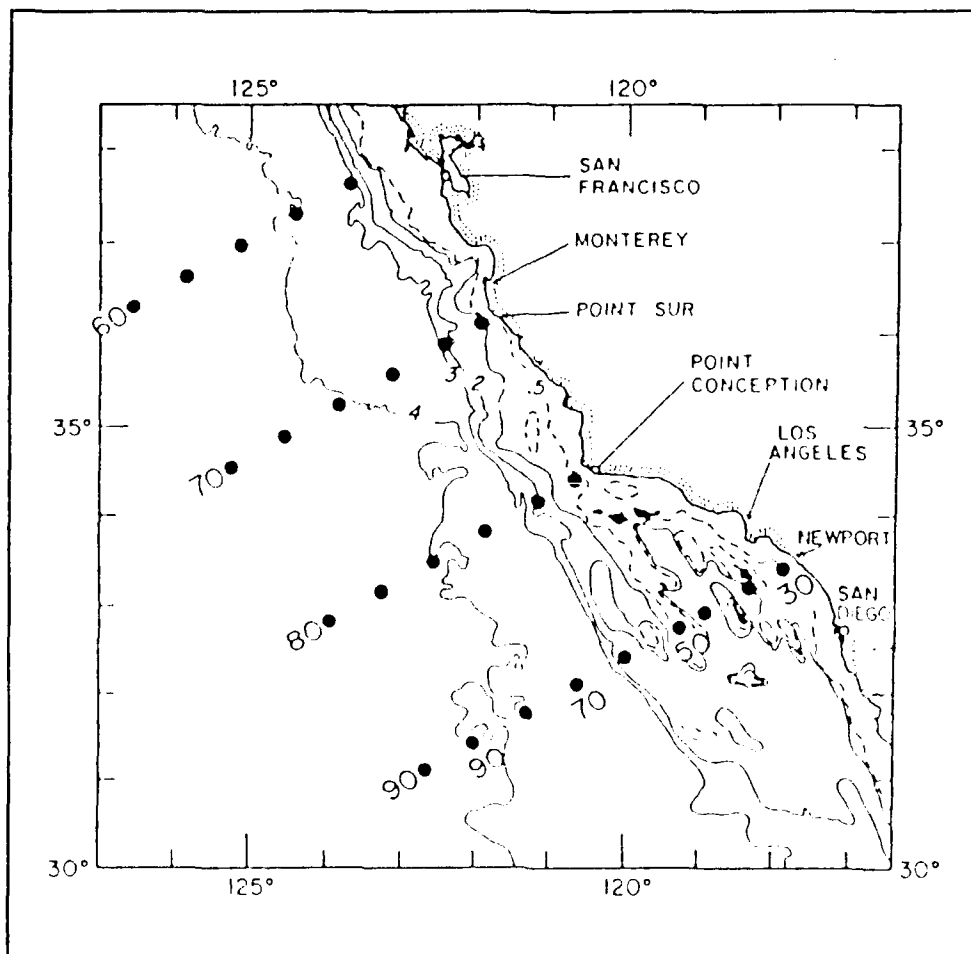


Figure 2. CalCOFI sampling scheme along the central California coast: Dots represent hydrographic stations along cardinal lines which lie in water deeper than 500m and were occupied more than 40 times between 1950 and 1979. (Source: Chelton 1984)

Table 1. POINT SUR TRANSECT CRUISE PERIODS AND DATA TYPES: Includes all cruises through January 1990. Cruises used in this study are indicated by asterisks.

Cruise	Dates	Vessel	Data Type
STNOV 1987	11/4 - 11/11	R/V Point Sur	CTD, ADCP
CUC-April 1988	4/15- 5/1	USNS DeSteiguer	CTD, ADCP, PEGASUS
STMAY 1988 *	5/4 - 5/11	R/V Point Sur	CTD, ADCP
CUC-August 1988 *	8/3 - 8/7	R/V Point Sur	CTD, ADCP, PEGASUS
CUC-September 1988	9/22 - 9/27	R/V Point Sur	CTD, ADCP, PEGASUS
STNOV 1988	11/1 - 11/8	R/V Point Sur	CTD, ADCP
CUC-November 1988 *	11/14 - 11/19	R/V Point Sur	CTD, ADCP, PEGASUS
CUC-February 1989 *	2/3 - 2/7	R/V Point Sur	CTD, ADCP, PEGASUS
CUC-March 1989	3/24 - 3/30	R/V Point Sur	CTD, ADCP, PEGASUS
CUC-May 1989	5/10 - 5/26	USNS DeSteiguer	CTD, ADCP, PEGASUS
STMAY 1989 *	5/4 - 5/8	R/V Point Sur	CTD, ADCP
CUC-July 1989 *	7/28 - 8/3	R/V Point Sur	CTD, ADCP, PEGASUS
CUC-September 1989	9/25 - 9/30	R/V Point Sur	CTD, ADCP, PEGASUS
STNOV 1989	11/1 - 11/8	R/V Point Sur	CTD, ADCP
CUC-November 1989 *	11/15 - 11/22	R/V Point Sur	CTD, ADCP, PEGASUS
CUC-January 1990	1/17 - 1/24	R/V Point Sur	CTD, ADCP, PEGASUS

recently data collected using the PEGASUS, a free-falling acoustically tracked dropsonde that measures temperature, salinity, velocity, and pressure. To provide additional temperature information, expendable bathythermographs (XBT's) were also utilized on some student cruises. A listing of the data collected on each individual cruise, including the vessel used, can be found in Table 1. Data analysis in this thesis has been limited to hydrographic information from CTD casts.

Hydrographic data was collected using Neil Brown Mark III-B CTDs. The only distinction between these two instruments is the physical size of their pressure casings. Because of this, they have been commonly referred to as either the "large" or "small " Neil Brown CTD, a convention which will be used throughout this thesis. The Neil Brown Mark III-B CTD has a resolution of ± 0.001 PSU, $\pm 0.005^{\circ}\text{C}$, and 0.0015% of the depth range, and is considered accurate to within ± 0.005 PSU, $\pm 0.005^{\circ}\text{C}$, and 0.1% of the depth range for salinity, temperature, and pressure, respectively. On each cruise, a General Oceanics Rosette sampler, equipped with twelve 5-liter bottles, was attached to the CTD for *in situ* water sampling. These samples were used for post-cruise calibration of the hydrographic data. Conductivity, temperature, and pressure data were acquired on the downcast at each station, while bottle samples were collected on the upcast. Winch speeds were approximately 0.5 m s^{-1} for the upper and lower 150 m of the cast and 1.0 m s^{-1} in between.

Raw wind data from the NOAA weather buoys (Figure 3) located off Monterey Bay (B46042) and Cape San Martin (B46028) was obtained from Mr. Dave Husby, Pacific Fisheries Environmental Group (PFEG). Data gaps ranging from one to several hours existed and required visual interpolation. With the

exception of buoy 46042, which was out of service during January and February 1989, complete wind records for each cruise were obtained.

B. DATA PROCESSING

The raw CTD data, which was collected at 0.1 m intervals, was averaged in 2 meter bins using programs written by Mr. Paul Jessen, NPS Oceanography Dept. The data was then calibrated according to the procedures discussed in chapter III. Additional quality control consisted of searching the temperature and salinity information for vertical gradients in excess of $0.2^{\circ}\text{C m}^{-1}$ and 1.0 PSU m^{-1} , respectively. When these values were exceeded, the data was visually inspected, and if it was determined that the points were in error, the data was linearly interpolated (Jessen et al. 1989). Errors of this type are usually the result of the temporal mismatch in the response of the temperature and salinity sensors.

To allow for the computation of anomalies of temperature, salinity, and spiciness along a constant pressure surface, these data sets were interpolated to 2 dbar pressure levels. This interpolation of the original data sets, averaged to 2 meter bins, was necessary because this averaging did not always result in an incremental value of exactly 2 dbar. Density anomaly (γ) was computed using the algorithm found in Volume 4 of the International Oceanographic Tables (UNESCO, 1987). Spiciness, which is a state variable most sensitive to isopycnal variations, was computed using the algorithm developed by Flament (1986).

The wind data from buoys 46028 and 46042 were first transformed into a u, v coordinate system and then into an alongshore and across-shore coordinate system. The drag coefficient was calculated (Large and Pond 1981) as

$$C_D = 1.14 \times 10^{-3}, \quad |\vec{v}| \leq 10 \text{ m s}^{-1}$$

$$C_D = 0.49 \times 10^{-3} + (0.065 \times 10^{-3})(|\vec{v}|), \quad |\vec{v}| > 10 \text{ m s}^{-1}$$

The alongshore wind stress was computed as

$$\tau_{AL} = \rho_a C_D |\vec{v}| v_{AL}$$

where ρ_a is the density of air, $|\vec{v}|$ is the magnitude of the wind velocity, and v_{AL} is the alongshore component of the wind velocity.

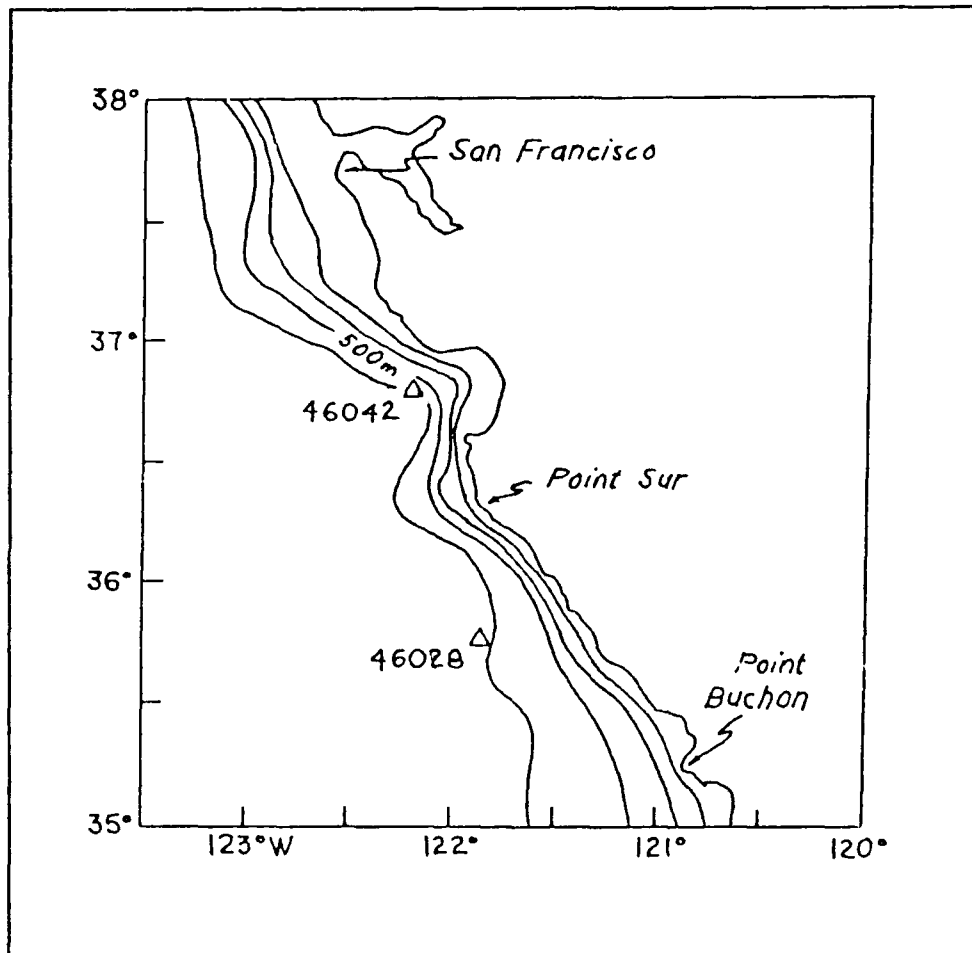


Figure 3. NOAA weather buoys used to calculate alongshore component of wind stress: Buoy 46042 is off Monterey Bay and buoy 46028 is off Cape San Martin. The 100, 200, 500, and 1000 m isobaths are also shown. (Adapted from: Chelton et al. 1988)

III. CALIBRATION PROCEDURE FOR HYDROGRAPHIC DATA

Prior to any type of formal scientific analysis, a data set should be subject to a rigorous calibration procedure to produce the most accurate results possible. This section discusses the methodologies used in both pre- and post- cruise conductivity, temperature and pressure calibrations, along with a more detailed discussion of the salinity calibration procedure used in the post processing of individual cruises using bottle data.

A. STANDARD PRE- AND POST- CRUISE CALIBRATION PROCEDURE

Prior to each cruise a series of calibrations were performed to ensure the accuracy of the CTD's conductivity, temperature and pressure sensors. In some instances, a similar series of calibrations was performed after the cruise had been completed. In general, however, the pre-cruise calibration for one cruise served as the post-cruise calibration for the previous cruise. All of the calibrations discussed in this section were carried out by NPS personnel.

The conductivity calibrations were carried out using either a Guildline Model 8400 Autosol or an AGE Instruments Model 2100 Minisal. Comparisons between the standard and the CTD sensor were made at several different conductivity levels. At each level, a number of samples were taken and averaged to yield a single conductivity value for the sensor. Based upon the standard and sensor readings, a regression analysis was used to obtain the coefficients necessary to correct the sensor to the standard. In all cases the best fit was a simple linear regression. Since salinity and conductivity work equally well as the

calibration parameter, salinity was chosen for convenience based upon the structure of NPS oceanographic data storage.

The temperature calibrations were carried out using Seabird temperature sensors as the reference standard. Three different sensors (SBE # 439, 626, and 664) were employed, most frequently SBE# 664. These sensors were calibrated by the manufacturer approximately every two years. In addition, there were several in-house calibrations performed between the manufacturers calibrations. In these latter calibrations, one Seabird sensor was calibrated against another for a quick comparative check on the accuracy. Although these in-house calibrations were not as rigorous as those performed by the manufacturer, they still allow for early detection of large drifts in these sensors. For each calibration, an insulated tub containing approximately 70 to 80 liters of fresh water was used. Comparisons were made between the reference standard and the CTD temperature sensor at 1°C increments from 0°C up through 30°C. At each temperature, a number of values were collected and averaged to yield a single value. These values were then used to determine the best fit to the reference standard, with the result again being a simple linear regression. The values of the temperature coefficients used for each cruise (Table 2) are in most cases the pre-cruise values, although in some instances, the post-cruise values were used. Where the difference between the pre- and post-cruise temperature calibrations approached or exceeded the accuracy of the instrument, the instrument and reference temperature values from each calibration were combined into one set for determination of the final coefficients.

The pressure calibrations were performed with a Chandler Engineering deadweight tester as the reference standard. Comparisons made between the

CTD's pressure sensor and the deadweight tester at various pressures yield results that are within the manufacturers specifications of 0.1% of full scale. In some instances, a slope of 1.0 was used while in others, a value of other than 1.0 was used (Table 2). In all cases, the pressure offset, which is this observed difference between the CTD pressure sensor reading and the actual pressure on deck at the start of a cast, was applied to the data set and serves as the pressure intercept.

Table 2. TEMPERATURE AND PRESSURE CALIBRATION COEFFICIENTS

Cruise	Temperature Slope	Temperature Intercept	Pressure Slope
STMAY 1988	0.998543	0.047536	1.000000
August 1988	0.998030	0.039016	0.999640
November 1988	0.999769	0.0097487	0.999950
February 1989	0.999080	0.002360	0.999638
STMAY 1989	0.999364	0.003435	1.000000
July 1989	0.999960	-0.001150	0.999393
November 1989	0.999950	0.001800	1.000150

B. POST-CRUISE SALINITY CALIBRATION PROCEDURE

The previous section dealt strictly with the calibration procedures that are conducted routinely at the beginning and end of each cruise. By themselves they are generally not sufficient to guarantee an accurate data set. In this section the

manner in which the bottle samples collected on each cruise were used to perform a calibration upon salinity is discussed.

At the end of each cruise, the bottle samples were analyzed using either the Guildline Model 8400 Autosol, which determines the conductivity ratio between the sample and the reference standard, or the AGE Instruments Model 2100 Minisal, which outputs the bottle salinity. The program used to compute salinity from conductivity, temperature and pressure, CONDCAL FORTRAN, was written by Mr. Jim Stockel and utilizes the algorithm of Lewis and Perkin (1981). CONDCAL corrects both the raw temperature and pressure for the pre/post cruise calibrations, including the pressure offset and produces a salinity value corresponding to the input conductivity value. In addition, this program will also compute both the true conductivity and salinity based upon the conductivity ratio, provided that the Autosol was used. Once the raw salinity was computed, it was subtracted from the bottle salinity, hereinafter referred to as true salinity, to obtain the salinity difference, used to determine how well the CTD salinities have been calibrated.

Before the calibration procedure could begin, it was necessary to separate those cruises on which the small Neil Brown CTD was used from those on which the large Neil Brown CTD was used. The reason for this separation was that the small CTD conductivity channel had a peculiar pressure dependence, which was very noticeable when salinity difference was plotted versus pressure (depth). The error between the true salinity value and that of the instrument became greater with increasing depth. The problem was traced to a bad conductivity cell, which was replaced prior to the November 1989 California Undercurrent Cruise. However, those cruises which used the small CTD prior to November

1989 were subject to this problem and therefore had to be calibrated separately. Because of this problem, three separate calibration procedures were used; one for the large CTD and one for the small CTD both before and after repair. Each procedure will be discussed at length in the following sections.

1. Calibration of Large Neil Brown CTD

A total of 105 bottles samples were collected at 83 CTD stations for STMAY 1988. These samples were collected on two separate legs, the first off Point Sur, and the second in Monterey Bay. With the exception of one station on each leg, there was only one bottle sample taken at the bottom of each station. A scattergram of the initial bottle/instrument differences (Figure 4) shows that some outliers existed and needed to be removed. The removal of these outliers is based upon the assumption that these differences are randomly distributed and should fluctuate very little with time and depth. These points are due to ship motion in high gradients, human error in copying numbers, etc. This statement also assumes that any temporal trends are small and approach the noise level of the instrument. For the large CTD, these appear to be valid assumptions.

The criteria chosen in most cases to eliminate outliers was a two standard deviation limit. At most, two passes were made through each data set. This choice was made arbitrarily for statistical consistency. After each pass a new standard deviation was computed and used as the criteria for the next pass. Points that fell outside of these limits were subject to removal if they appeared unrealistic with respect to the observed salinity difference pattern. If points were close to the limit they were retained for further analysis.

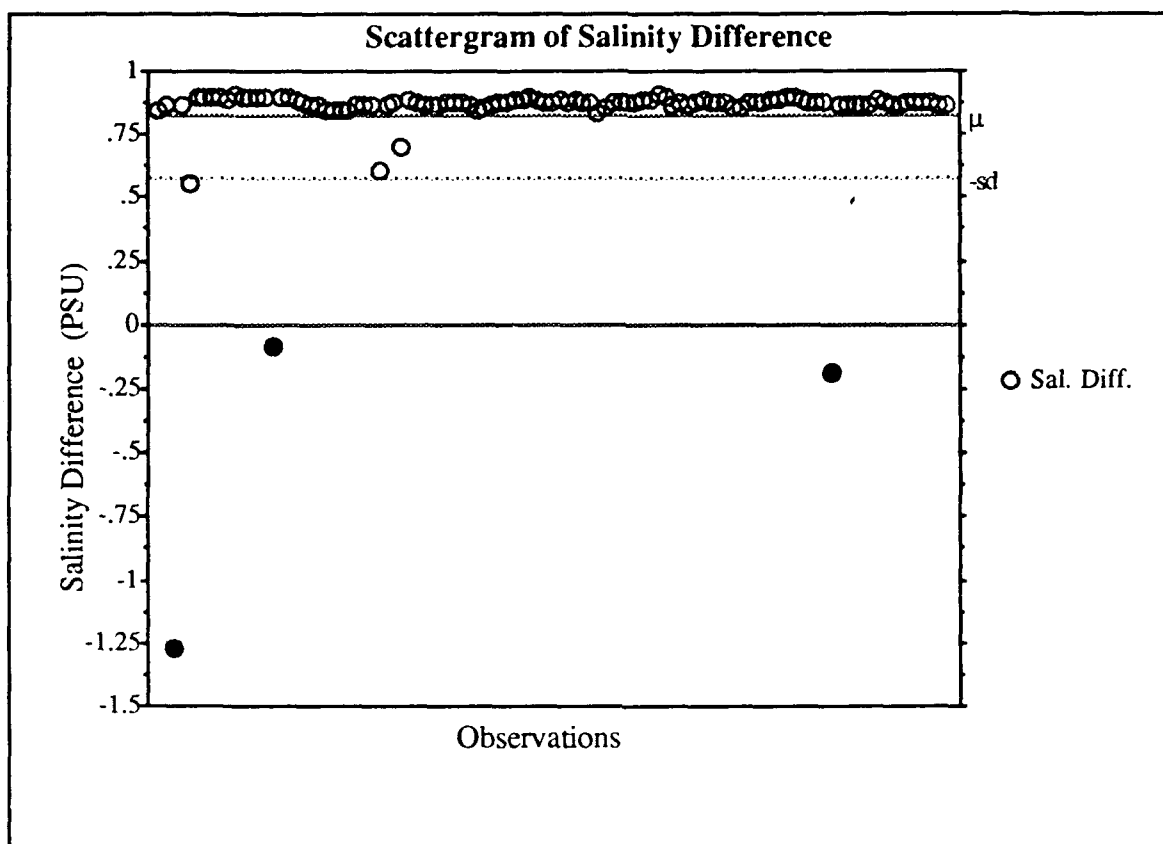


Figure 4. Scattergram of initial salinity difference for STMAY 1988: This plot results from subtracting the instrument salinity from the bottle salinity. No outliers have been removed. Positive values indicate the instrument is reading too low. The mean (μ) is 0.828 and the standard deviation (sd) is 0.253.

As a result of the first pass through this cruise data, three points were eliminated from further consideration. These are the highlighted points in Figure 4. The effect of removing these points can be seen in Figure 5, which also indicates the existence of additional outliers. Notice that the scale is not as coarse as that shown in Figure 4 due to the removal of these points. The scattergram shown in Figure 6 results from removing three more points, and is the data set used to calibrate the salinities for this cruise. Notice again the change to a finer scale with the removal of these points.

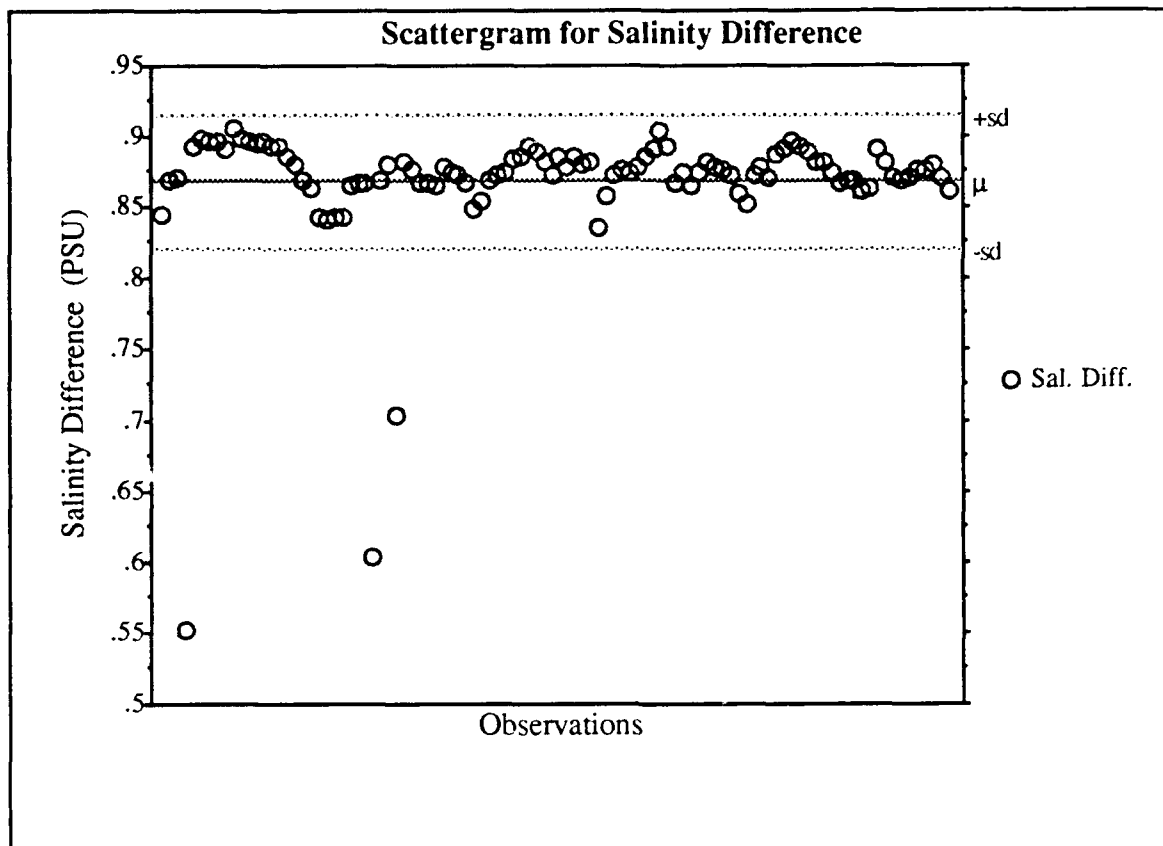


Figure 5. Scattergram of intermediate salinity difference for STMAY 1988: This plot results from removing three outliers. Points removed were the negative values shown in Figure 4. Positive values indicate the instrument is reading too low. The mean (μ) is 0.868 and the standard deviation (sd) is 0.047.

After this process was completed, a total of 99 data points remained for use in calibrating the instrument relative to the bottle samples. The best fit was linear (Figure 7) with a slope of 1.036714 and an intercept of -0.347450. The effect of this regression was to increase the instrument salinities, thereby removing an almost constant offset of 0.868 PSU. The resulting residual statistics had a mean of zero and a standard deviation of 0.007, with a minimum residual of -0.032 and a maximum of 0.016. Here the residual is computed as the fitted instrument salinity minus the raw instrument value. The standard

error of the residual mean was 0.001 and the correlation coefficient (r^2) was 0.999588. This latter statistic is an indicator of how much of the total variance can be explained by a simple linear regression. In this case it indicates a strong linear relationship.

The same calibration procedure was followed for each of the remaining cruises using the large CTD. The resulting calibration coefficients can be found in Table 3. In all cases, a linear fit was used in the final calibration of the instrument values. This choice was based upon the simple linear relation exhibited between the instrument and true salinity values. Calibration of the small CTD required considerably more effort and will be discussed in the next section.

2. Calibration of Small Neil Brown CTD before repair

The small CTD was observed to have an unusual pressure dependence as a result of a faulty conductivity cell which produced larger instrument errors as the ambient pressure was increased. As a result of this problem, the calibration procedure required a modification to remove this pressure effect. A second order polynomial fit was used in each case to model the pressure dependence. Fitted salinity differences were computed from these polynomials and added to the instrument salinities to remove the pressure effect. Once the pressure effect was removed, the calibration proceeded in a manner similar to those for the large CTD, and the procedure discussed has been applied to all small CTD cruises prior to November 1989.

The discussion of this procedure has been divided into two parts: removal of the pressure effect and final calibration of instrument salinity values.

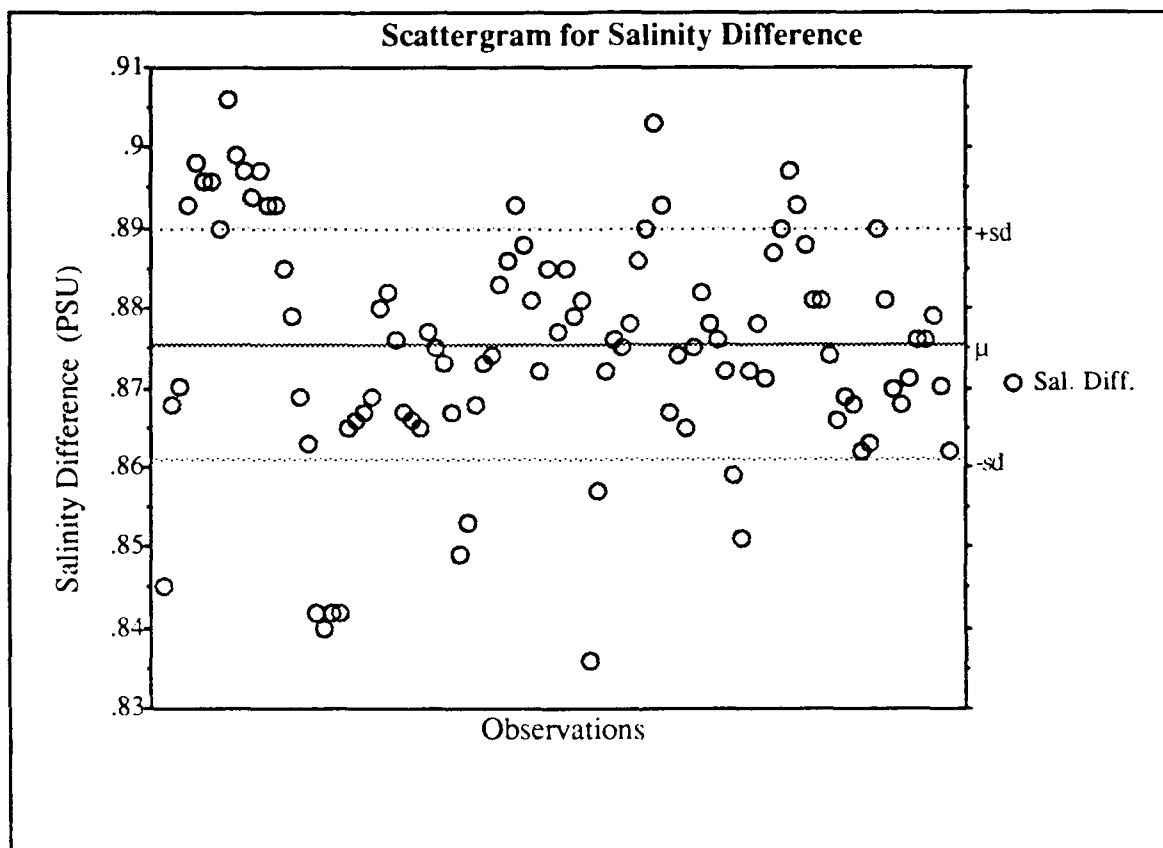


Figure 6. Scattergram of final salinity difference for STMAY 1988:
 This plot results from removing three more three outliers. Points removed were the values below 0.800 in Figure 5. Positive values indicate the instrument is reading too low. The mean (μ) is 0.875 and the standard deviation (sd) is 0.015.

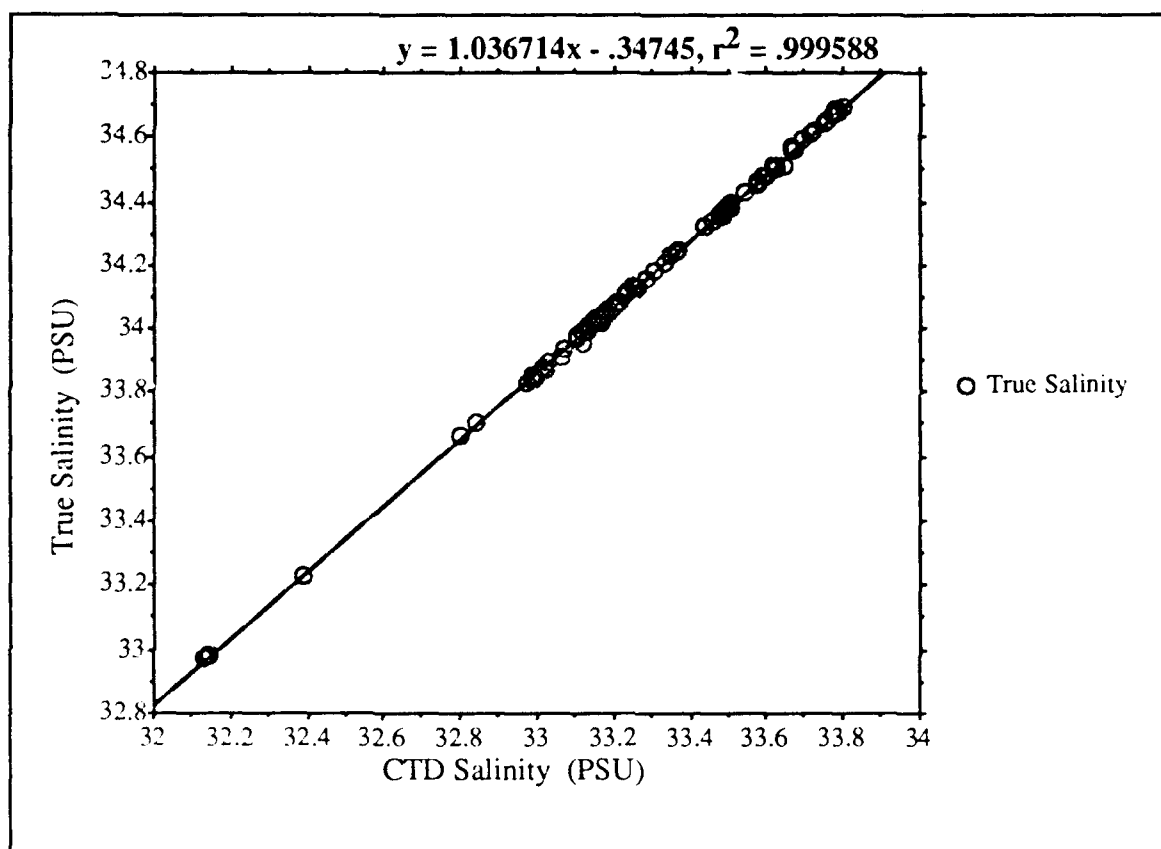


Figure 7. Linear Regression used to fit STMAY 1988 CTD salinities to bottle salinities: This plot results from regressing STMAY 1988 CTD salinities against corresponding bottle samples. The correlation coefficient (r^2) is 0.999588, which indicates that 99.9588% of the variance can be explained by a simple linear regression model.

Table 3. SALINITY CALIBRATION COEFFICIENTS FOR THE LARGE NEIL BROWN CTD: The standard deviation listed in this table is of the residuals after the calibration was applied. The number of points indicates the number of instrument/bottle pairs used in the analysis.

Cruise	Slope	Intercept	# of points	Standard Deviation
STMAY 1988	1.036714	-0.347450	99	± 0.007
August 1988	1.043071	-0.568235	45	± 0.006
STMAY 1989	1.005162	-0.167634	37	± 0.005
July 1989	1.002600	-0.140919	45	± 0.005

Removing this pressure effect proved to be a very difficult task and unfortunately residual statistics were not as good as in the case of the large CTD.

a. Pressure effect and its removal

To illustrate this process, the data from the February 1989 cruise will be discussed here at length. This particular cruise actually required two separate corrections to remove the pressure effect and was chosen for discussion for this reason. The pressure effect (Figure 3) had a parabolic shape, and in all but this particular case, a single quadratic polynomial fit was used to model and remove the pressure effect. During the course of this cruise the shape of the curve appeared to change. The resulting curve from stations 18 through 32 had considerably more curvature to it, unlike the curve from earlier stations. This is illustrated in Figure 8 where the lower set of points belong to stations 1 through 17, and the upper set to stations 18 through 32. Attempting to use this curve to correct the data prove unsatisfactory since predicted salinities were much too high in comparison to corresponding bottle salinity values. Using the deep T-S curves as a reference, the best results were obtained when stations 1 through 17

were calibrated independently, and stations 18 through 32 were calibrated using the polynomial computed from all 32 stations. Using bottle samples from all stations to calibrate those from stations 18 through 32, allowed the earlier bottles to influence the polynomial fit, which resulted in a shift of the computed curve closer to the characteristic shape exhibited by this instrument on this and other cruises using the small CTD.

The procedure described earlier for removing the pressure dependence, utilized pressure as the input variable into the quadratic polynomial to obtain a fitted value for the salinity difference. This fitted value was then added to the raw instrument salinity yielding a salinity value absent of the pressure effect. A new salinity difference was computed by subtracting this salinity from the true salinity and was used in subsequent steps of the calibration procedure. The effectiveness of this procedure on both data sets can be seen in Figure 9 which illustrates the salinity difference before and after removal of the pressure effect. The results show an improvement, however, they are not quite as good as those in the case of the large CTD, and in light of the problems discussed earlier, they have been taken to be the best obtainable.

b. Final adjustment of Small Neil Brown CTD salinities

The next step was to compare the pressure adjusted salinities to the true salinities and, if necessary, determine any further corrections. The procedure used for this was identical to that used with the large CTD, namely, examine a scattergram of the salinity differences to detect and remove any outliers, and then use a linear regression to fit the instrument salinities to the true values.

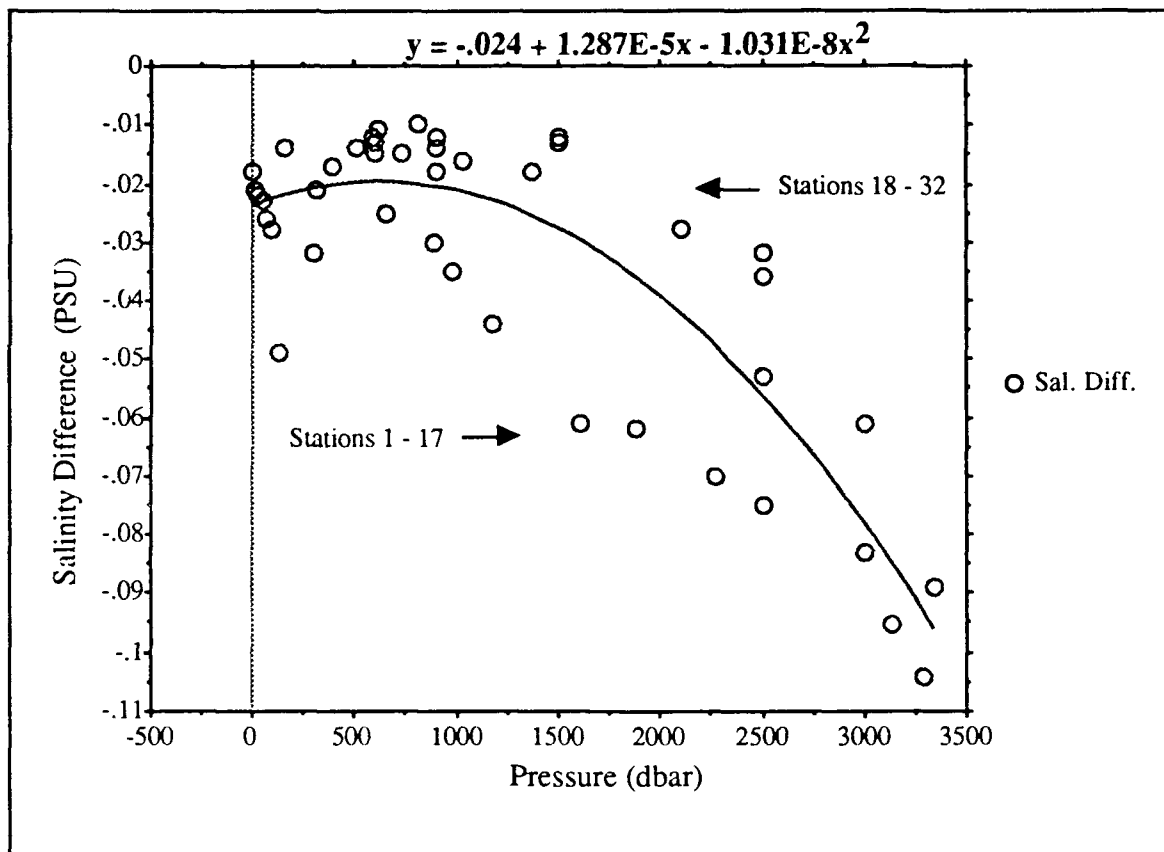


Figure 8. Pressure effect on small Neil Brown CTD (February 1989): This plot illustrates the pressure effect in terms of salinity difference. Negative values for salinity difference indicate the instrument is reading too high. Pressure is plotted in terms of corrected pressure based upon the pre-cruise calibration and pressure offset.

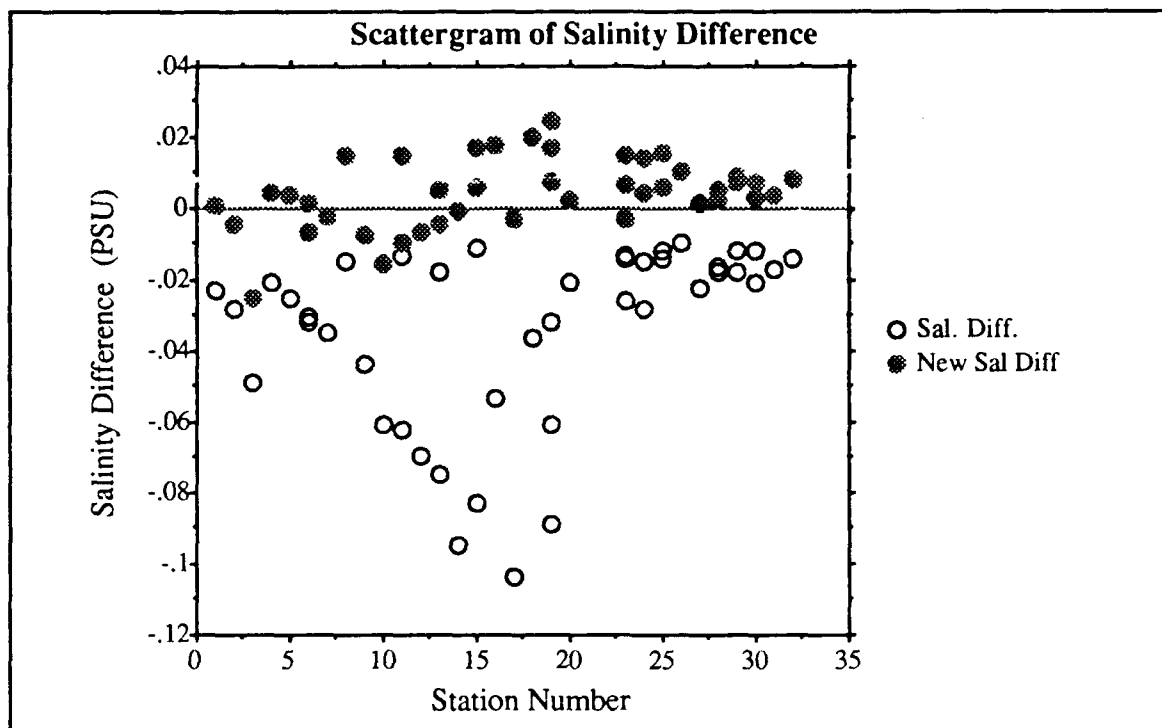


Figure 9. Comparison of salinity differences before and after removing pressure effect from CTD data (February 1989): This plot is results from removing the pressure dependence from the original salinity differences. The open circles represent salinity differences prior to removal, whereas the blackened circles represent the new salinity differences after the removal.

The final step in the calibration of the February 1989 cruise data was to perform a regression between instrument and true salinity. Again, two separate calibrations were used over the same data sets. In both cases, the chosen fit was linear (Figures 10a and 10b). Stations 0 through 17 were calibrated as one group, stations 18 through 32 using all stations. Station 0 was the first station occupied on this cruise, however no bottle samples were taken.

The net result of these calibrations were very small shifts in the instrument salinities which indicates that the pressure effect was the cause of

most of the observed difference. The choice of the linear fit was again based upon the linear appearance of the data.

The calibration of the November 1988 cruise required only a single calibration to remove the pressure effect. Upon examination of the resulting salinity differences, it was noticed that two distinct patterns existed (see Appendix A). Stations 1 through 17 were calibrated separately as one group, while stations 18 through 32 were calibrated as another. The coefficients used for this cruise as well as for February 1989 can be found in Tables 4 and 5.

3. Calibration of Small Neil Brown CTD after repair.

The cause of the pressure dependence associated with the small CTD was a faulty conductivity cell. Before the small CTD was used on the November 1989 cruise a new conductivity cell was installed by NPS personnel and the unit recalibrated. At this time a large portion of the pressure effect described above was removed. The calibration procedure used for the November 1989 cruise data was much simpler than earlier small CTD calibrations as a result of instrument modifications performed prior to the cruise. The initial scattergram of salinity difference versus pressure indicated that a simple two step linear pressure correction was required. In this case one correction was applied to pressures less than or equal to 1000 dbar, while the other was for pressure greater than 1000 dbar. To eliminate any discontinuities in the data both linear equations were constrained to yield identical results at the 1000 dbar level.

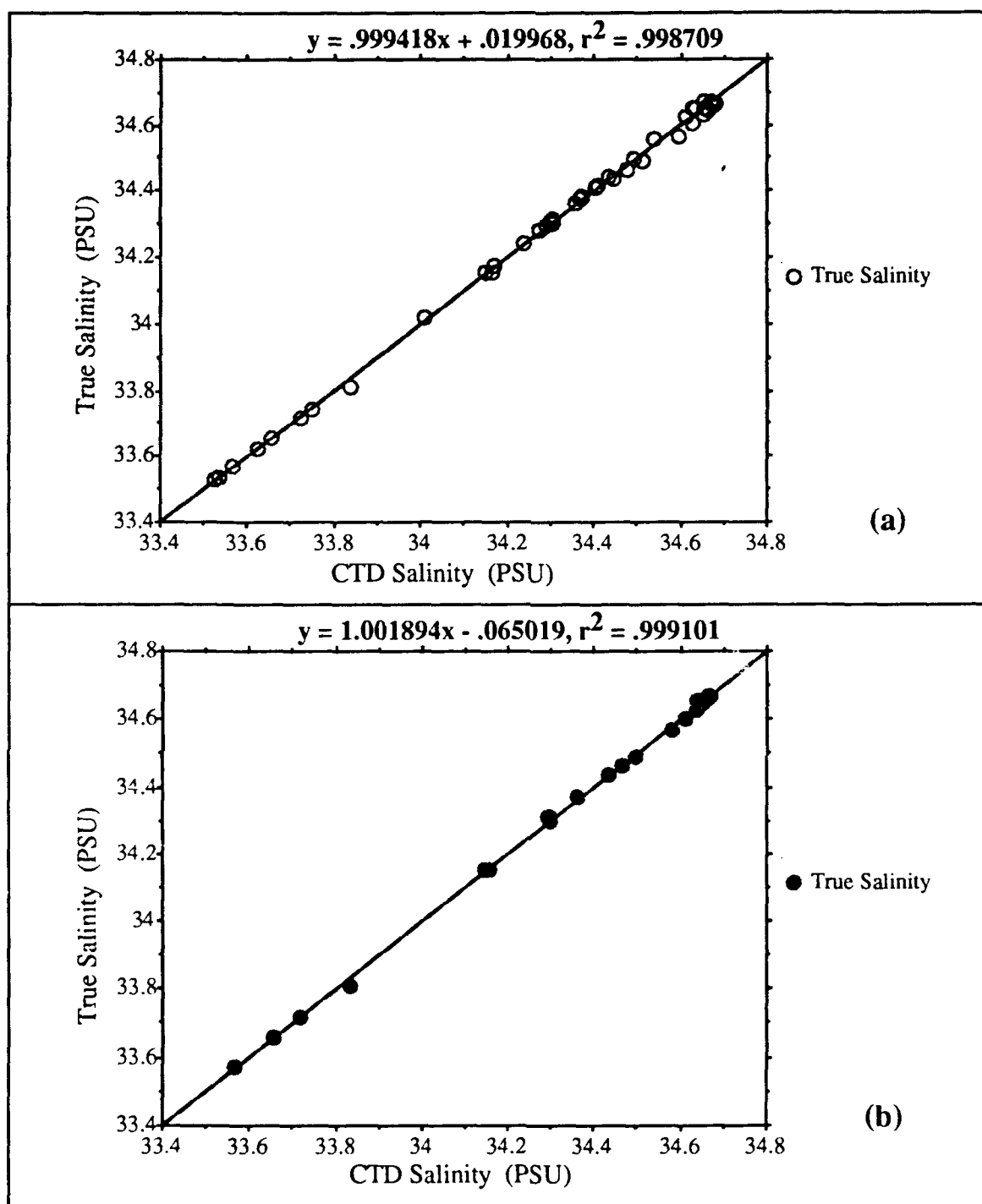


Figure 10. Linear Regression to fit February 1989 CTD salinities to bottle salinities: (a) represents the fit for stations 18-32, (b) represents the fit for stations 0-17. Correlation coefficients in both cases indicate that over 99% of the variance can be explained by a linear fit.

Table 4. CALIBRATION COEFFICIENTS FOR REMOVAL OF THE SMALL NEIL BROWN CTD PRESSURE DEPENDENCE: February 1989 has two separate corrections based upon station numbers. November 1989 has two corrections based upon depth range, where U = 0-1000 dbar, and L = 1000 dbar to maximum cast depth.

Cruise	$(a_2) \times 10^{-9}$	$(a_1) \times 10^{-6}$	(a_0)
November 1988	-4.385E-9	-8.975E-6	-0.015
February 1989 (0-17)	-5.889E-9	-4.171E-6	-0.023
February 1989 (18-32)	-1.031E-8	1.287E-5	-0.024
November 1989 - U	0.0	1.996E-5	0.028
November 1989 - L	0.0	1.921E-6	0.046

Table 5. SALINITY CALIBRATION COEFFICIENTS FOR THE SMALL NEIL BROWN CTD: The standard deviation listed in this table is of the residuals after the calibration has been applied. The number of points indicates the number of instrument/bottle pairs used in the analysis.

Cruise	Slope	Intercept	# of points	Standard Deviation
November 1988 1 - 17	1.007040	-0.246238	28	± 0.012
November 1988 18-32	1.002435	-0.076711	24	± 0.006
February 1989 0-17	1.001894	-0.065019	21	± 0.011
February 1989 18-32	0.999418	0.019968	43	± 0.013
November 1989	1.002761	-0.095870	74	± 0.005

Once the pressure effect was removed, a linear fit was used to perform the final step of the calibration. The coefficients used in this process are listed in Tables 4 and 5.

To verify the effectiveness of these calibrations, a deep water regime was chosen for Temperature-Salinity analysis. Deep water masses of the world oceans have been regarded as having relatively stable T-S properties, with those of the North Pacific being nearly homogeneous (Warren and Owen 1988). Any variations from a mean T-S curve are the result of geographic differences (Worthington 1981). The regime selected was between 2800 and 3300 dbar. This range was chosen to bracket the 3000 dbar level, however, the limits themselves were arbitrary. If the calibrations were successful, the deep TS curves for cruises along the POST would bear a strong resemblance to one another, and predicted salinity values would approach the true values within the accuracy of the instrument. After plotting these deep T-S curves (Appendix A) for each cruise, it was observed that in fact they all exhibited a similar pattern and were all within ± 0.005 PSU of each other. From these results, it appeared the calibration procedures were successful and no further corrections were necessary.

IV. ANALYSIS

A. DESCRIPTION OF WATER MASS CHARACTERISTICS

The waters off Point Sur are comprised of four major water mass types which exist in varying proportions, summarized in Table 6. The location and spatial extent of the water masses were defined using an analysis similar to Lynn and Simpson (1990). They analyzed the flow of the CUC off southern California using spiciness and spiciness anomaly as tracers to identify the various water masses present throughout the survey region. Spiciness (π , Flament 1986), is the state variable which is most sensitive to isopycnal thermocline variations and least correlated with the density field. Spiciness is useful for the description of interleaving and double diffusive processes which occur at the boundary between different water types. Waters which are warm and salty have positive π values while those which are cool and fresh have negative π values.

Table 6. WATER MASSES OF THE CALIFORNIA CURRENT SYSTEM: (Source: Simpson 1984)

Water Mass	T	S	O ₂	Nutrients
Surface Water Masses (0-200 m)				
Pacific Subarctic	Low	Low	High	High
North Pacific Central	High	High	Low	High
Coastally Upwelled	Low	High	Low	High
Subsurface water masses				
Equatorial Pacific	High	High	Low	High

Lynn and Simpson (1990) calculated spiciness *anomalies* as deviations from a mean T-S curve representative of local CC water. In this study, only profiles

free of interleaving processes below the surface layer (upper 50 m) were chosen for the average. Eight stations from the seven cruises (Figure 11) were chosen for this average (Figure 12) and were assumed representative of the offshore waters along the POST. Anomalies were computed along level surfaces rather than isopycnal surfaces for ease in computation. Anomalies computed along level surfaces only differed from those computed along isopycnal surfaces in the upper 50 m of the water column. Representative curves for Pacific Subarctic and Equatorial Pacific waters (Figure 12) illustrate that mixing has produced a profile which is nearly 50% Equatorial Pacific water between the 26.5 and 27.25 density surfaces (roughly 250-750 m depth) and predominantly subarctic above (Tibby 1941). Because the calculation of spiciness is a nonlinear process, the values of spiciness for each of the eight stations were computed and then averaged (rather than vice-versa). Due to the exclusion of stations where interleaving processes were present the average profile in the upper water column was dominated by those stations from the August 1988 cruise where temperature values in the upper water column were high.

1. Analysis of spiciness and spiciness anomaly

Waters of subarctic origin (low T and S) will be represented by negative π values in the Point Sur region while those of equatorial origin (high T and S) will be represented by positive π values. Due to the strong effects of surface heating, the study of spiciness within the upper 50 m was difficult and in some instances had to be neglected in subsequent analysis. The following discussion has been organized by cruises.

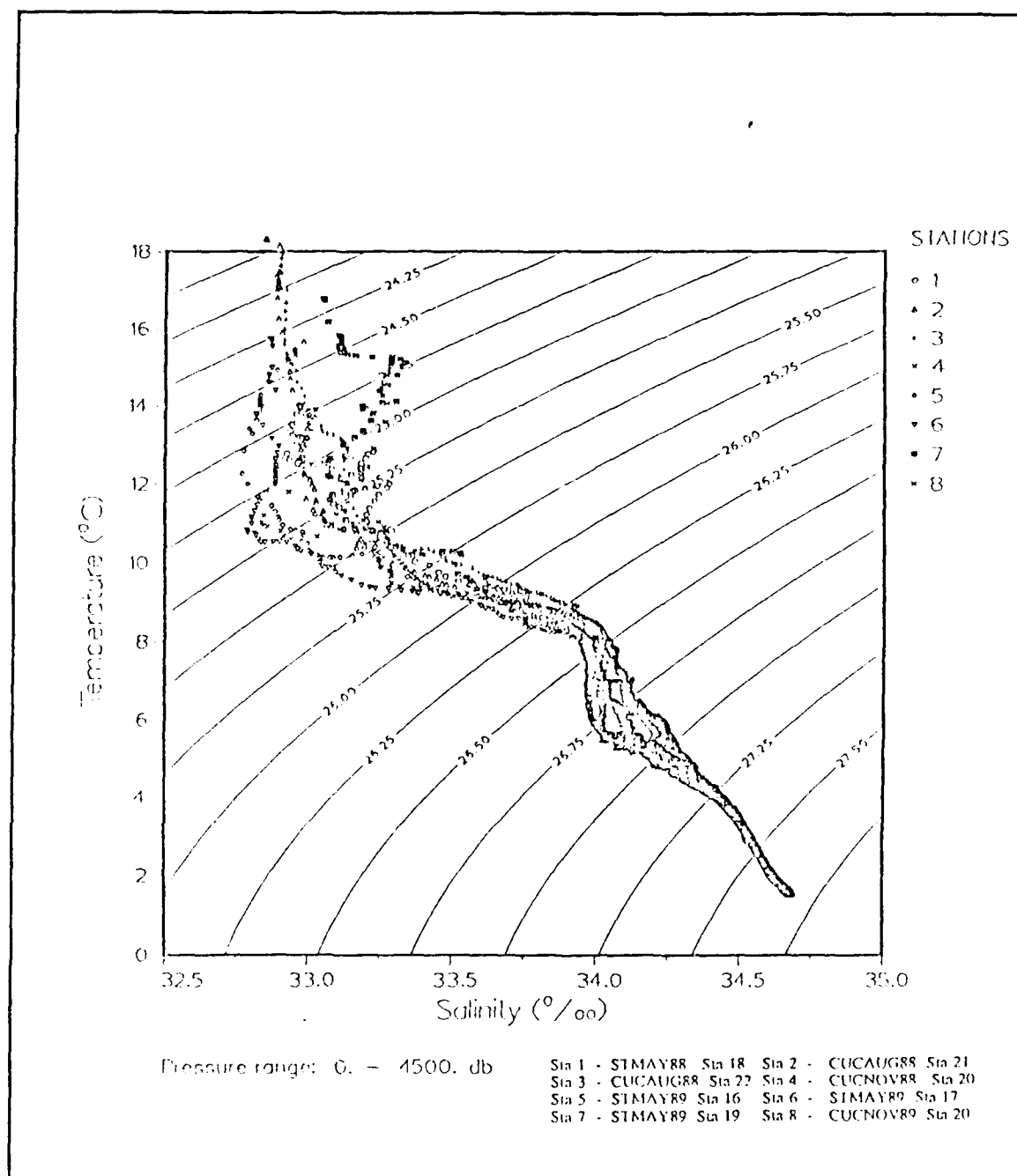


Figure 11. The eight T-S profiles used to obtain the average offshore profile. Points are plotted at 2 dbar intervals.

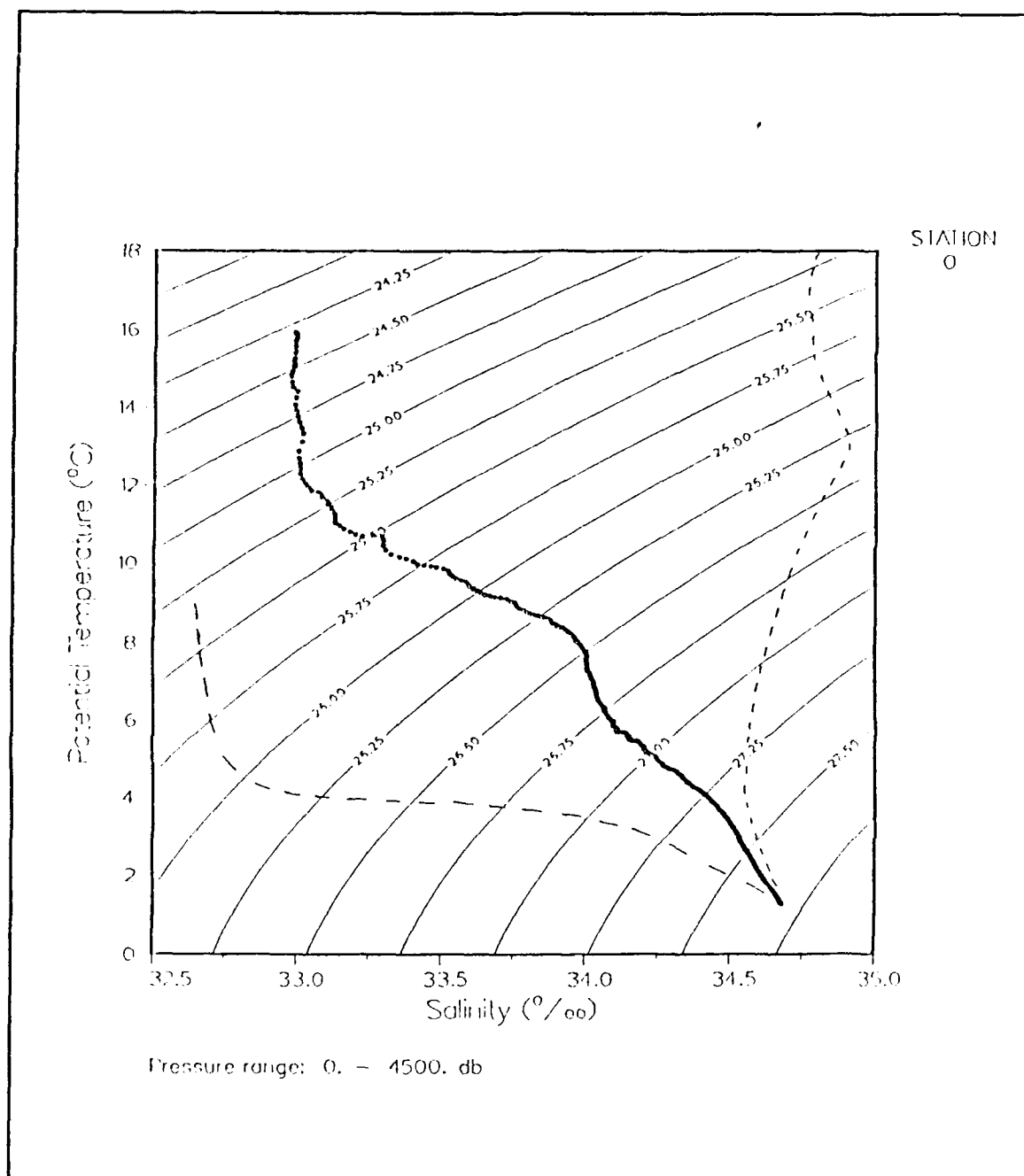


Figure 12. Average offshore T-S profile used in calculation of spiciness anomalies: Curves representative of Pacific Subarctic (long dash) and Equatorial Pacific (short dash) waters from Tibby (1941) are superimposed for comparison.

a. August 1988 Water Mass Analysis (seasonal normal)

Data from the August 1988 cruise has been chosen to illustrate the relation between the fields of temperature, salinity, and spiciness. Inspection of the T and S fields (Figures 13 and 14, respectively) reveals a deepening of the isotherms and a shallowing of the isohalines near the continental slope. This is characteristic of the CUC which carries warmer, saltier water poleward. The relatively cooler

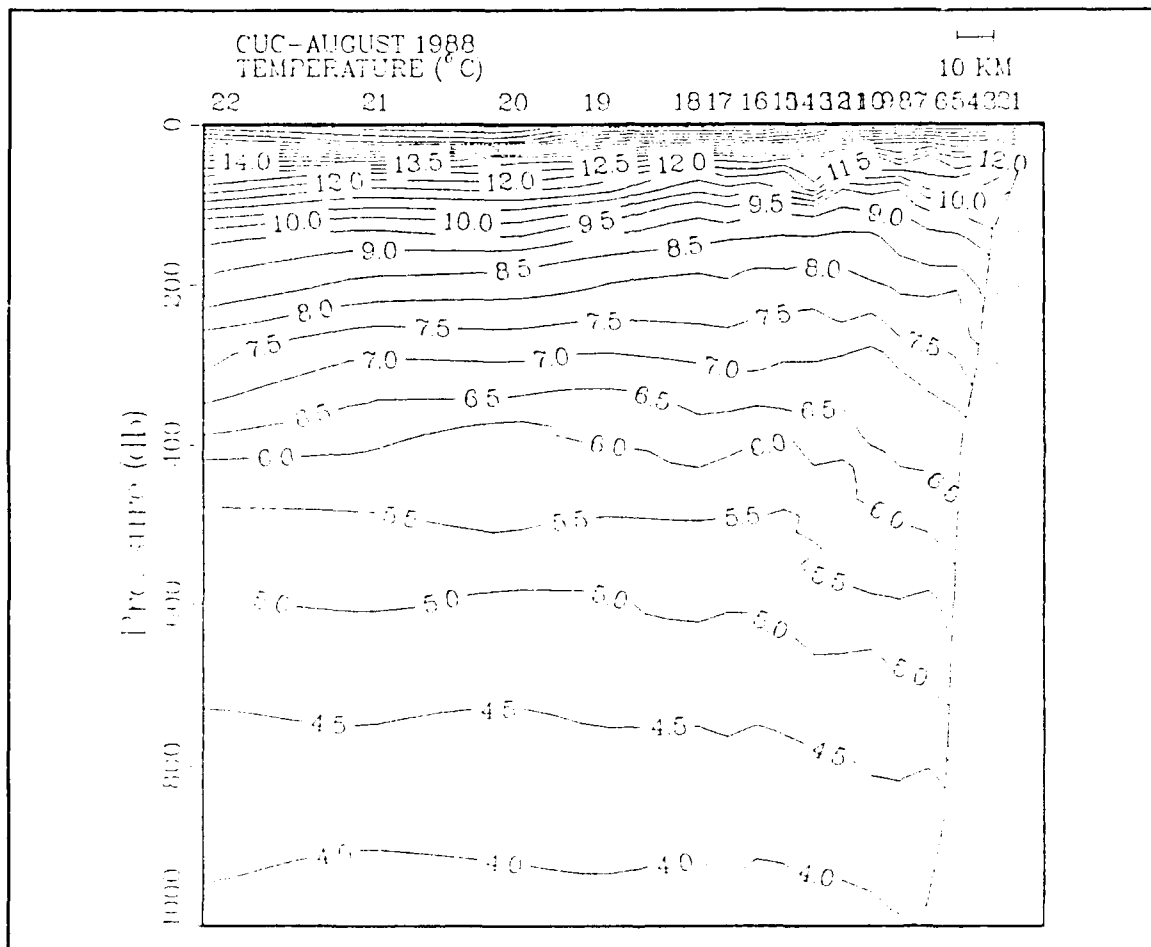


Figure 13. Vertical section of temperature for cruise CUC-August 1988:
The contour interval is 0.5°C.

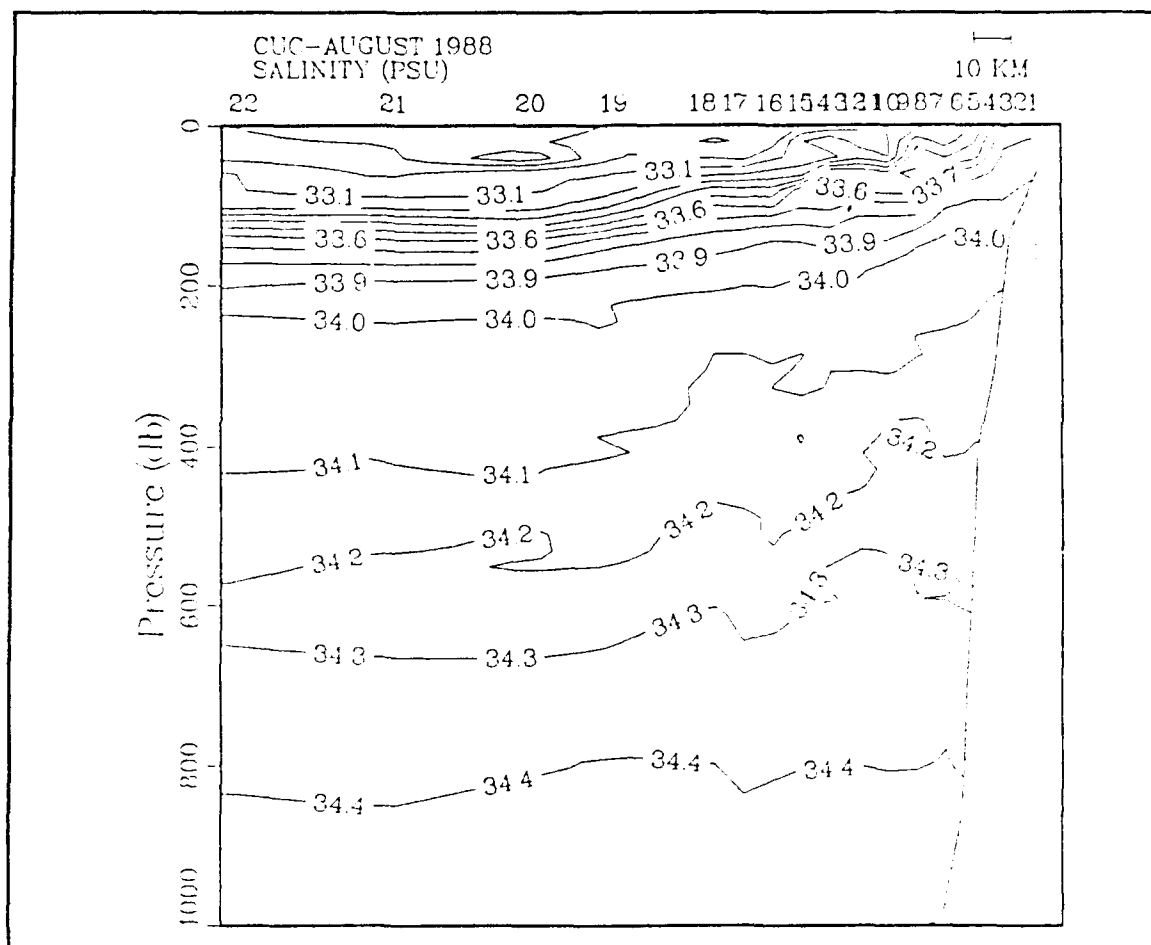


Figure 14. Vertical section of salinity for cruise CUC-August 1988:
The contour interval is 0.5 PSU.

and fresher waters of Subarctic origin associated with the CC can be seen offshore between stations 16 and 22 below 200 m. There is a subsurface salinity minimum (50 m depth), with values less than 32.8 PSU, located near station 20 associated with the core of the CC. These regions are reflected in the vertical sections of spiciness and spiciness anomaly (Figures 15 and 16, respectively). Comparison of Figures 15 and 16 reveals a positive shift in magnitude of roughly 0.2 units in spiciness anomaly. This results from the fact that anomalies

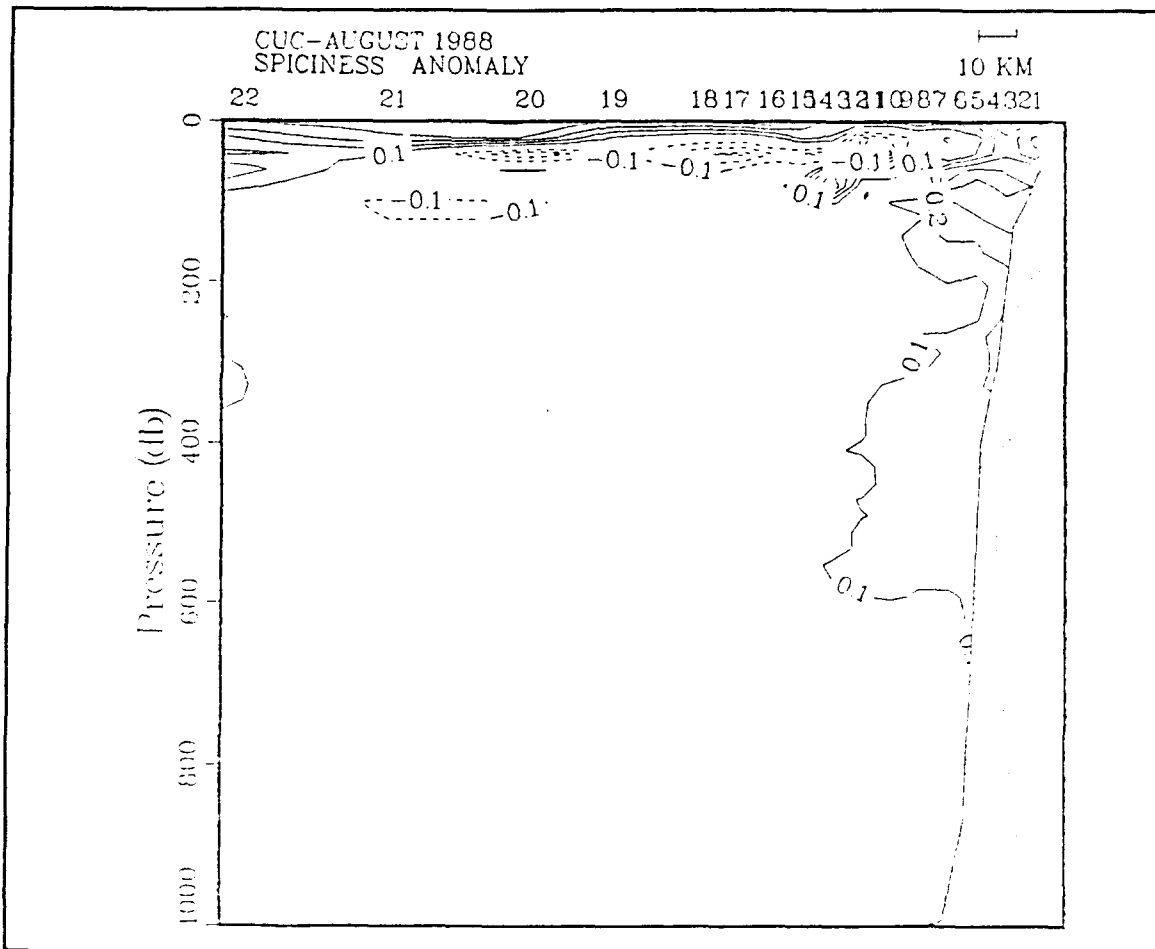


Figure 16. Vertical section of spiciness anomaly for cruise CUC-August 1988: The contour interval is 0.1 units.

This region of positive spiciness is associated with the warmer, more saline waters of the CUC, and lies next to the cooler waters of subarctic origin.

Vertical sections of spiciness anomaly offer a better depiction of the spatial extent of the CUC, and further discussion will be limited to spiciness anomaly although mention of spiciness will be made when necessary. The spiciness anomaly section for August 1988 (Figure 16) illustrates the same features discussed earlier, however, due to the shift in magnitude the region of positive spiciness anomaly now extends to a depth of almost 700 m along the continental slope. This agrees favorably with the position of the CUC seen in the August 1988 alongshore geostrophic velocity, discussed later in this Chapter. Downward sloping isotherms below 200 m at station 22 correspond to the region of positive spiciness anomaly seen in Figure 16 and are suggestive of intrusion of warm, salty water which entered the CC from the west.

b. May 1988 Water Mass Analysis (weak poleward flow)

A period of strong equatorward wind stress, at times in excess of 23 knots, preceded this cruise and persisted through its first two days. These equatorward winds produced upwelling of cold, saline water near the coast which was then transported offshore through Ekman dynamics. Surface fronts were observed in the vertical fields of T and S and corresponded to those seen in the density field (Figure 17).

The vertical section of spiciness anomaly (Figure 18) illustrates a similar pattern with positive spiciness anomaly values occurring within the upper 100-150 m and near zero anomalies (of Subarctic origin) below. The negative

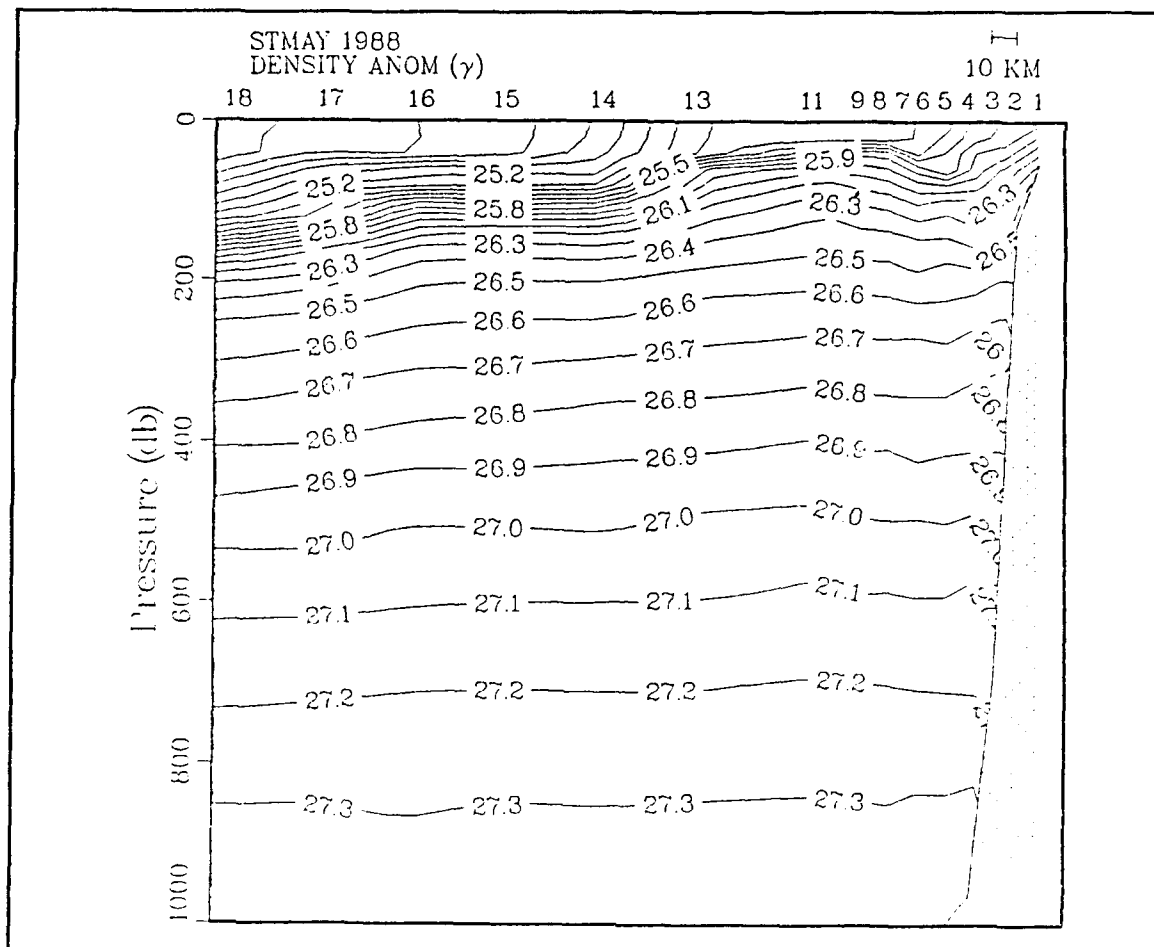


Figure 17. Vertical section of density anomaly for the May 1988 Student Cruise: The contour interval is 0.1 units.

values found near the surface reflect the difference from the average profile which, as mentioned earlier, was dominated by the August 1988 cruise. The region of positive spiciness anomaly located between 100 m and 150 m between stations 17 and 18 can again be explained as an intrusion of warm, salty water from the west. There is a region of positive spiciness anomaly found along the continental slope centered near 400 m between stations 2 and 8 which corresponds to an area of weak poleward flow associated with the CUC. The

relative weakness of this flow may be related to the strength of the equatorward winds.

c. November 1988 Water Mass Analysis (strong mesoscale feature)

This cruise differed from the rest in that it was dominated by a rather strong anticyclonic mesoscale feature. The depression in the isopycnals (Figure 19) between stations 4 and 14 have the characteristic appearance of a deep (greater than 700 m) warm-core mesoscale feature. This feature is also present in NOAA 9 AVHRR satellite imagery (Figure 20) taken three days after the occupation of POST stations. Breaker and Broenkow (1989) and Tracy (1990) discuss a recurring anticyclonic mesoscale eddy off Monterey Bay whose position varies in accordance with local forcing. It is hypothesized that the mesoscale feature observed during the November 1988 cruise is a southward displacement of this recurring anticyclonic eddy. Inshore of this feature the isopycnals (greater than 26.8) slope down toward the continental slope in accordance with the fields of temperature and salinity (not shown) due to the presence of the CUC.

A region of positive spiciness anomaly (subsurface maximum near 100 m) is associated with this mesoscale feature indicative of relatively warm, saline water characteristic of Equatorial Pacific origin (Figure 21). In their study of a mesoscale dipole eddy off southern California, Simpson and Lynn (1990) found that anticyclonic features were comprised of CUC water. Huyer et al. (1984) analyzed the T-S structure of a mesoscale feature off Oregon and concluded its core contained water of shelf-slope origin. The fact that larger

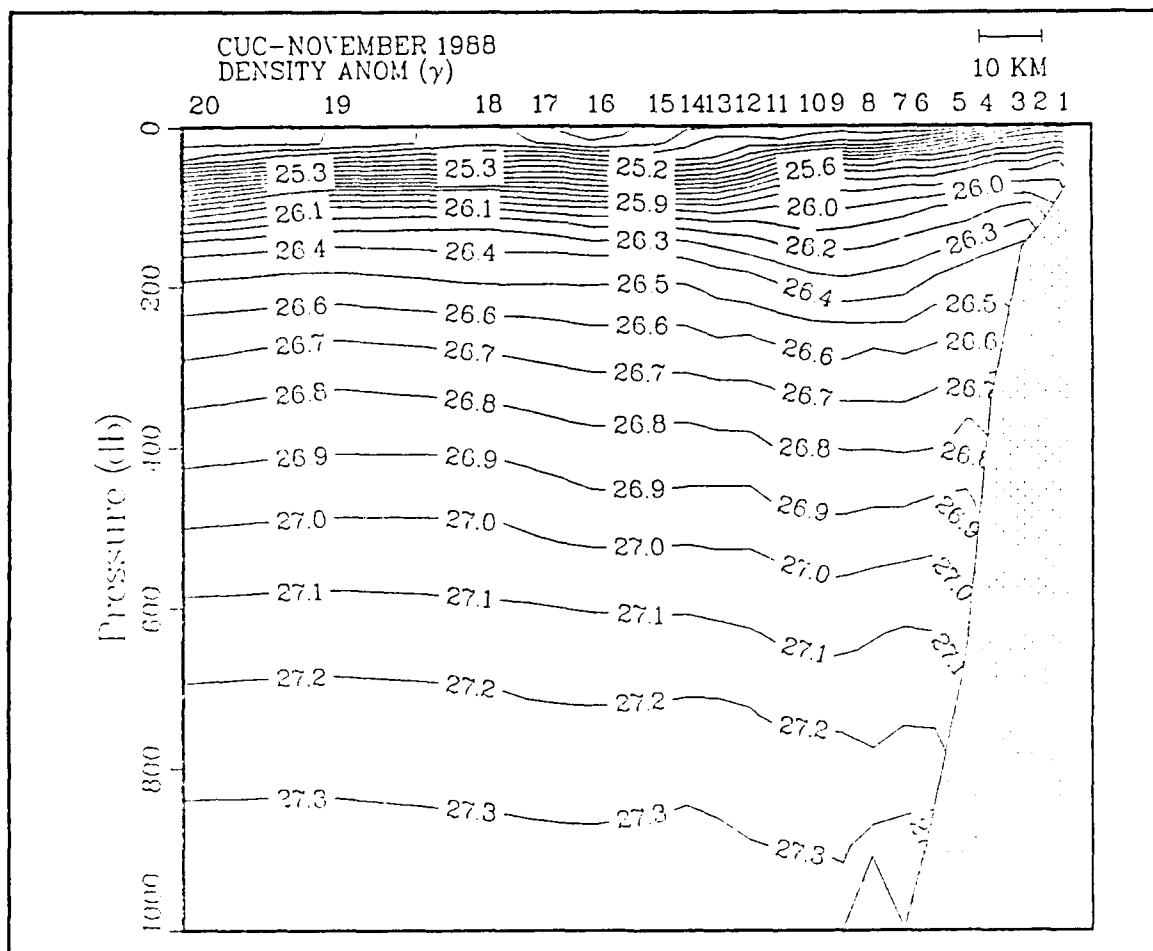


Figure 19. Vertical section of density anomaly for cruise CUC-November 1988: The contour interval is 0.1 kg m^{-3} .

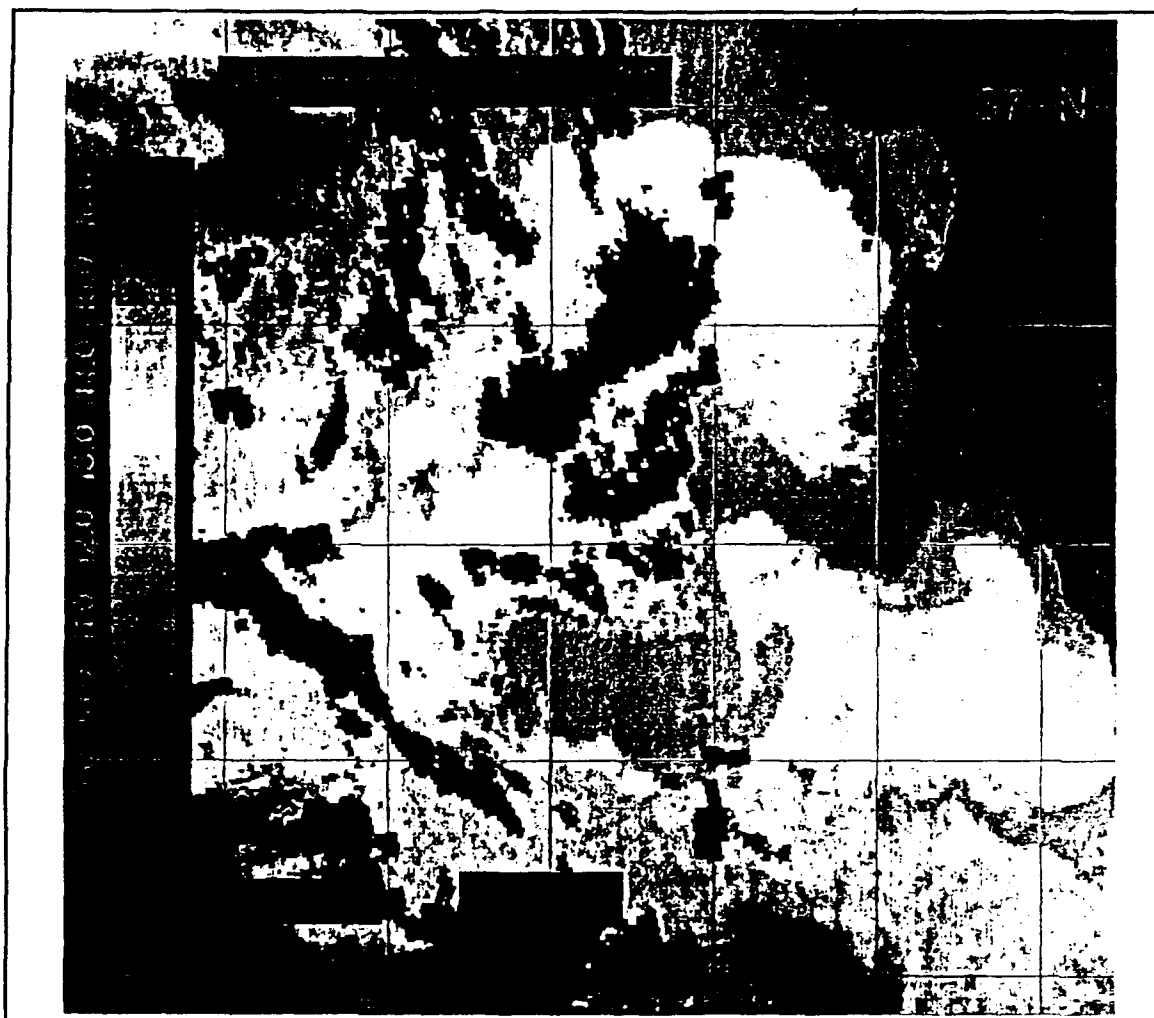


Figure 20. NOAA AVHRR satellite image from 0004 GMT, 21 November 1988: Darker shades along the coast and off Point Sur depict colder water. Lighter shades found off Monterey Bay, south of Point Sur, and in western half of the image depict warmer water. Note the presence of an anticyclonic feature between 122°- 123°W, and 36°-36.5°N. Grid spacing equals 30'.

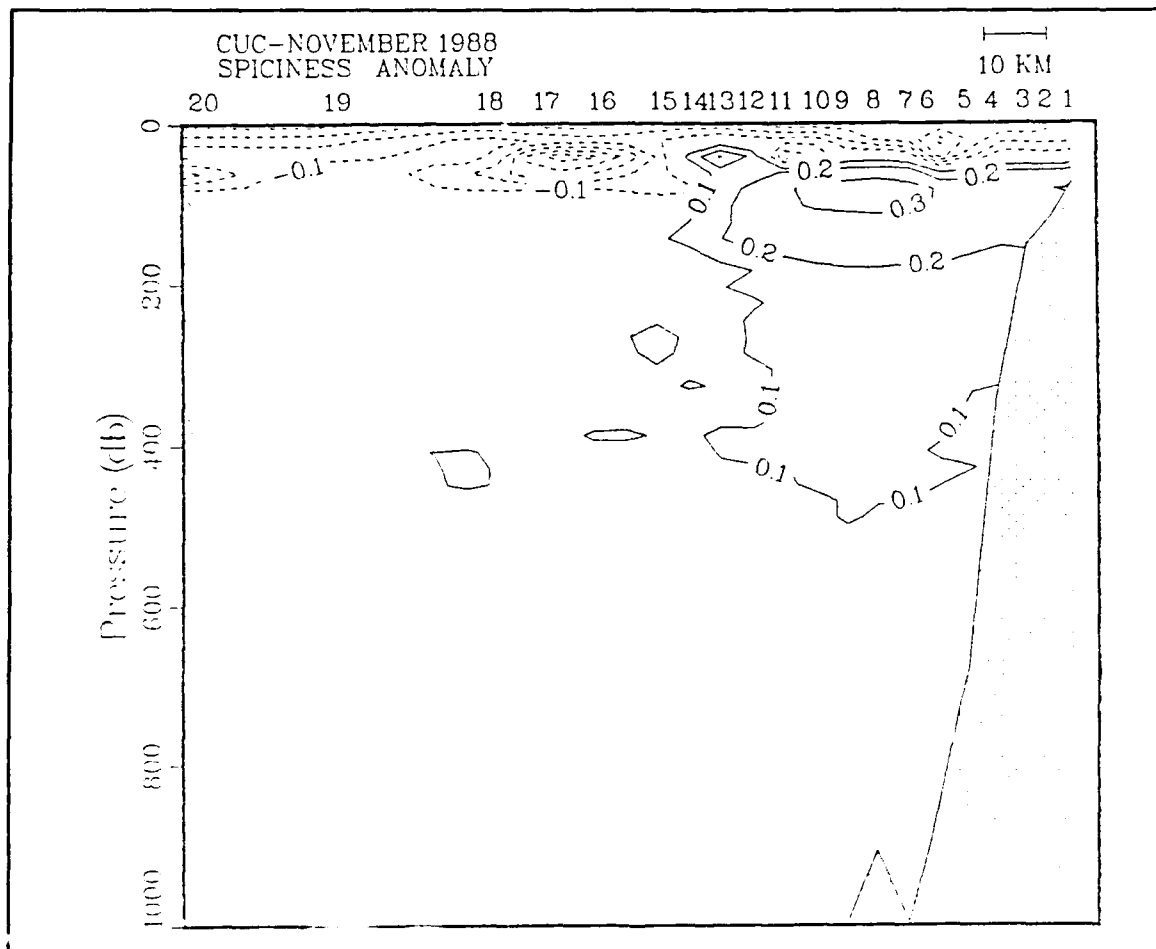


Figure 21. Vertical section of spiciness anomaly for cruise CUC-November 1988: The contour interval is 0.1 units.

d. February 1989 Water Mass Analysis (strong equatorward flow near coast)

Temperatures within the upper 100 m were nearly isothermal with values ranging between 10.0°C and 10.5°C. This agreed favorably with NOAA 11 AVHRR satellite imagery (Figure 22) for the cruise period which also depicts



Figure 22. NOAA AVHRR satellite image from 2058 GMT, 5 February 1989: Darker shades throughout the entire image depict colder water and near isothermal conditions. Grid spacing equals 30'. Note the nearly isothermal temperatures between 121.5°-122.5° W, and 36°-36.5° N.

an isothermal SST. Within 45 km of the coast, isotherms and isohalines (not shown) below 100 m exhibited slight downward tilting toward the continental slope. In the surface layer, a salinity minimum (less than 33.3 PSU) was located between stations 5 and 6, while offshore beyond station 14 surface salinity remained between 33.5 PSU and 33.6 PSU throughout the upper 50 to 75 m.

The spiciness anomaly (Figure 23) shows values greater than or equal to +0.1 over the range from 75 m to 500 m, while above 75 m negative

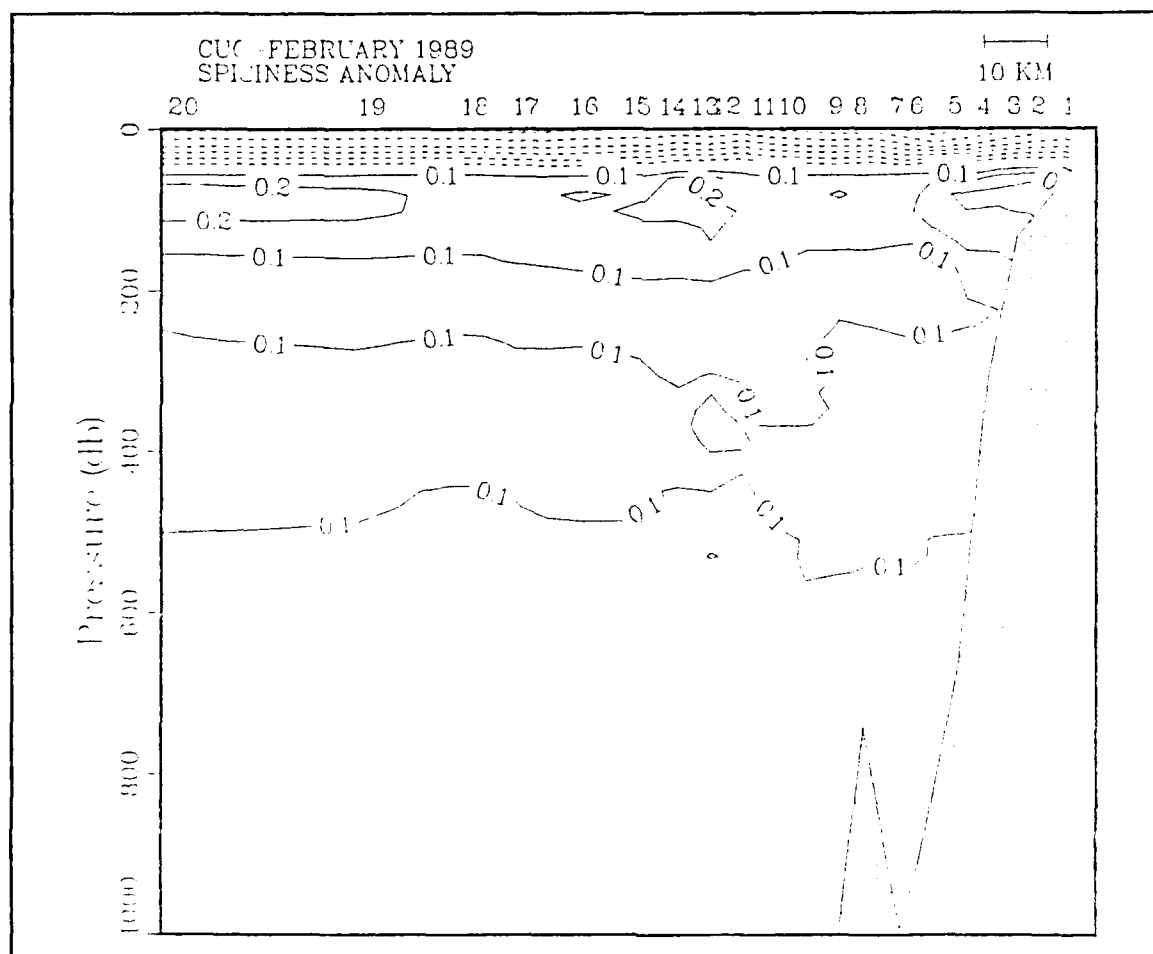


Figure 23. Vertical section of spiciness anomaly for cruise CUC-February 1989: The contour interval is 0.1 units.

values prevail. This indicates the waters below 75 m were relatively warmer, and saltier than the average offshore profile, and may result from the strong CUC which reached the surface (as the DC) during this time.

e. May 1989 Water Mass Analysis (poleward flow near coast)

A vertical section of salinity (Figure 24) depicts several dominant features. First, there are two low salinity cores (less than 32.9 PSU) between stations 12 and 13 and at station 17. Second, the strong halocline centered at 150 m offshore shoals to less than 50 m inshore. Last, there are large amplitude variations in the 34.1 and 34.2 isohalines. Along the continental slope, isotherms slope downward toward shore (not shown) and isohalines upward (Figure 24) toward shore indicating the water is warmer, and more saline than offshore. The depressions in the 34.1 isohaline and the low salinity cores correspond to regions of equatorward flow (shown later) and likely contain Pacific Subarctic water associated with the CC.

The cores of low salinity cause the regions of negative spiciness anomaly above 100 m depth (Figure 25). Below 200 m, waters with negative spiciness values of Subarctic origin appear as a blank region below an overlying region of positive anomaly values, comprised of two different water masses. The first occurs along the continental slope where values greater than +0.2 units are observed and values of +0.1 extend downward to 600 m. This region is associated with the Equatorial waters of the CUC. Offshore the +0.1 contour has a subsurface tongue-like appearance extending to approximately 240 km from shore at 150 m depth near stations 15 and 16. A subsurface maximum (greater than +0.2 units) is found between stations 11 and 12 corresponding to a

subsurface anticyclonic feature present in the density field (Figure 26). As in the case of the mesoscale feature observed in November 1988, it is hypothesized

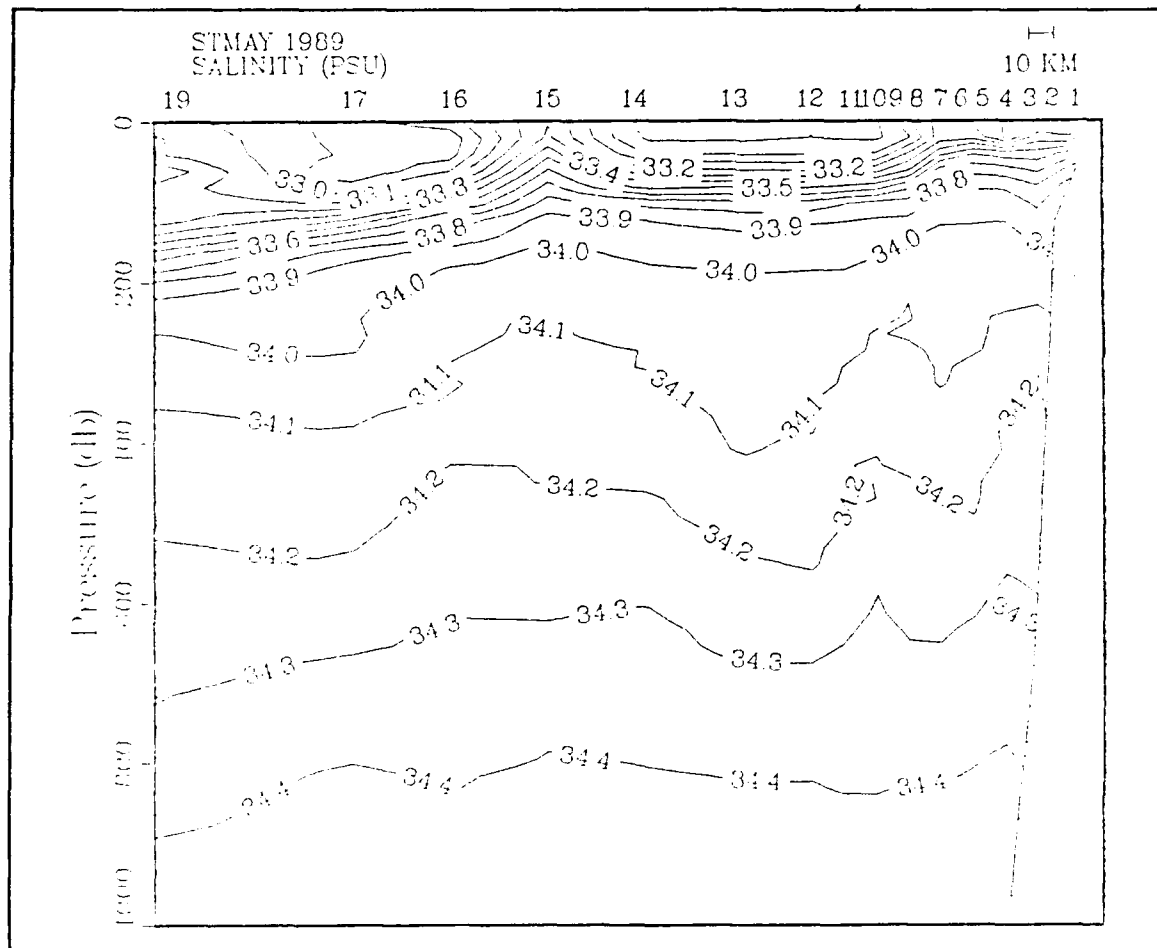


Figure 24. Vertical section of salinity for the May 1989 Student Cruise:
The contour interval is 0.1 PSU.

that these larger values offshore result from lateral entrainment and offshore advection of CUC water.

Further offshore near station 19 is another region of positive spiciness anomaly believed to result from the intrusion of warmer, saline water

from the west. This intrusion can be seen along the 24.75 isopycnal in the T-S curve for station 19 (Figure 11) and will be discussed further in Chapter V.

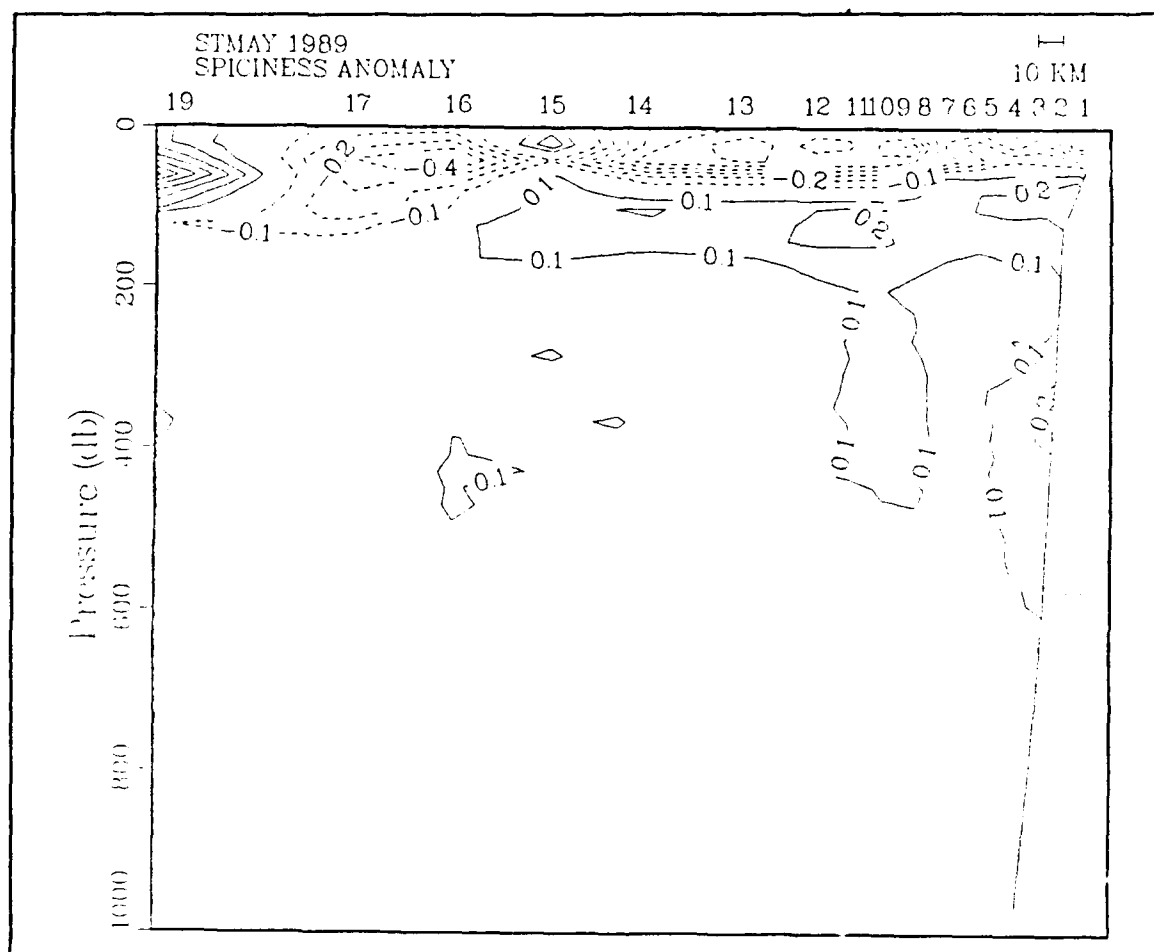


Figure 25. Vertical section of spiciness anomaly for the May 1989 Student Cruise: The contour interval is 0.1 units

f. July 1989 Water Mass Analysis (anomalous poleward flow)

The water mass structure shown in the vertical section of spiciness anomaly (Figure 27) is very different than August 1988 (Figure 16), one year

earlier. The section is almost completely dominated by positive values of spiciness anomaly, which extend to depths of 600 m in some locations. Prior to and during the cruise the winds at both buoy locations were equatorward

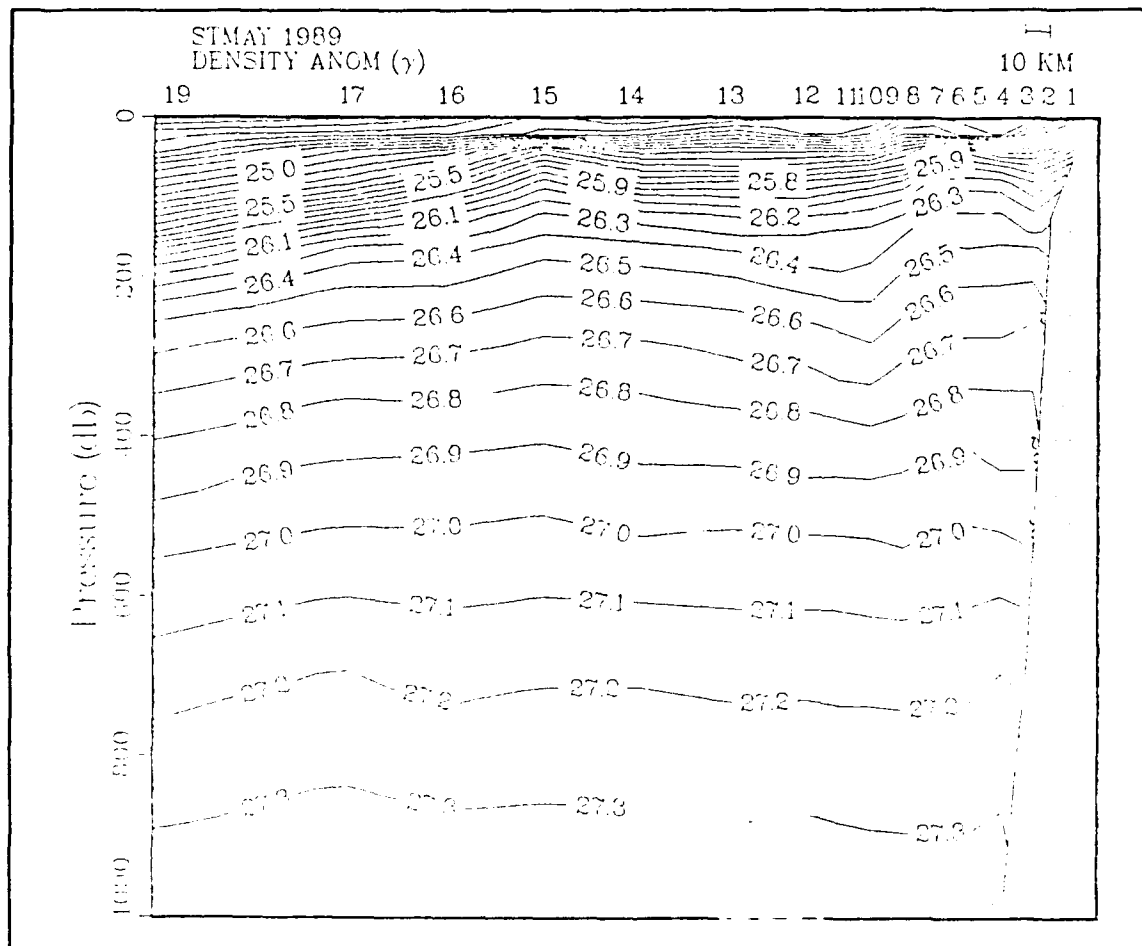


Figure 26. Vertical section of density anomaly for the May 1989 Student Cruise: The contour interval is 0.1 kg m^{-3} .

($\leq -1.0 \text{ dyne cm}^{-2}$), however, a substantial wind relaxation lasting 3 days preceded the cruise by two days. Remote forcing by this wind relaxation is believed to be one of the mechanisms involved in generating this anomalous field. Surface salinities along the section on this cruise (Figure 28) are approximately 0.6 PSU

greater than the August 1988 cruise. Further discussion of this relaxation and the associated poleward flow will be presented later in this Chapter.

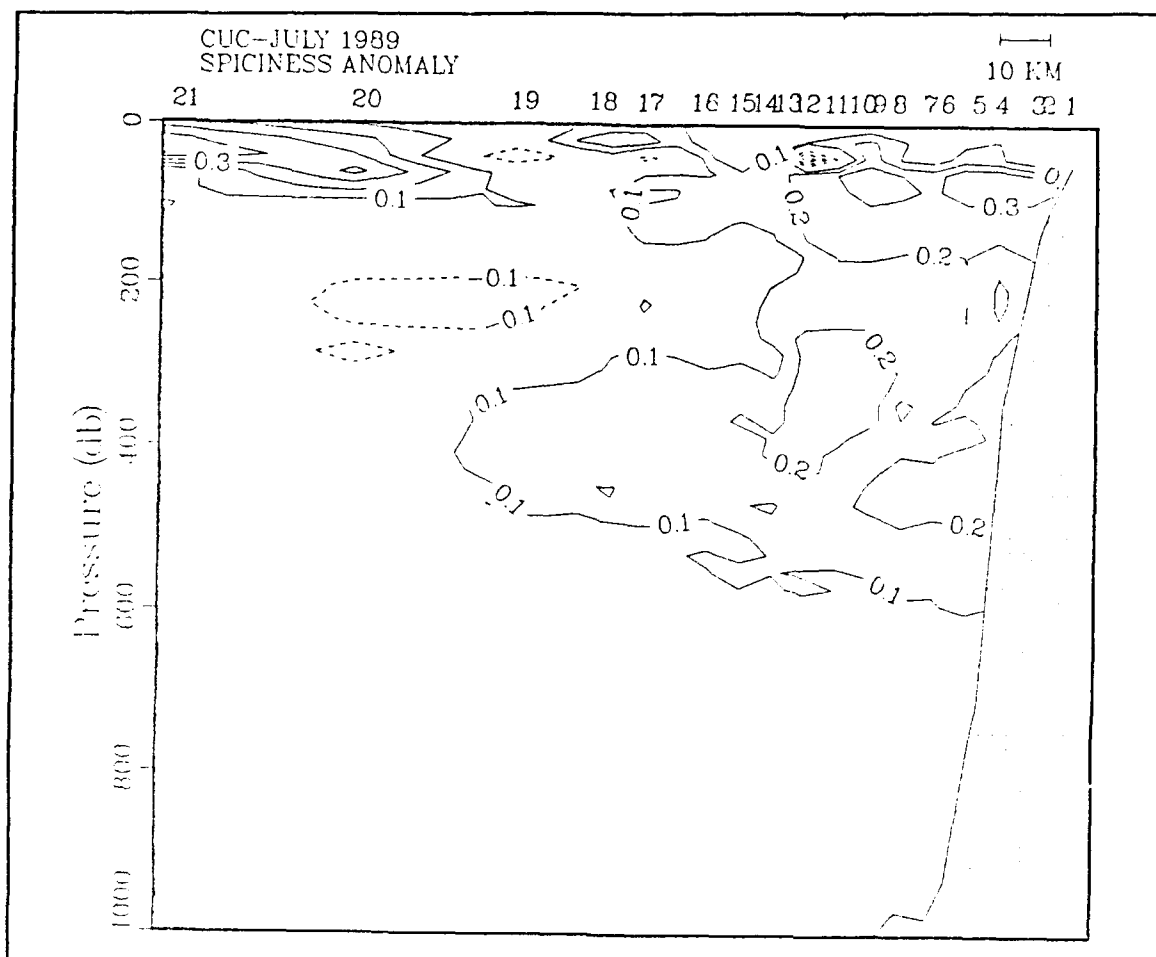


Figure 27. Vertical section of spiciness anomaly for cruise CUC-July 1989: The contour interval is 0.1 units.

T-S curves for stations 20 and 21 (not shown) reflect the intrusion of warmer, saline water along the 25.1 kg m^{-3} isopycnal surface. Water inshore of stations 18 and 19 are composed of Equatorial Pacific water advected northward with the observed strong poleward flow. The core of positive anomaly ($> +0.3$ units) is associated with the CUC which appears to have

surfaced during this cruise. Below 150 m there is a region of negative spiciness anomaly occurring between stations 18 and 22 believed to be of

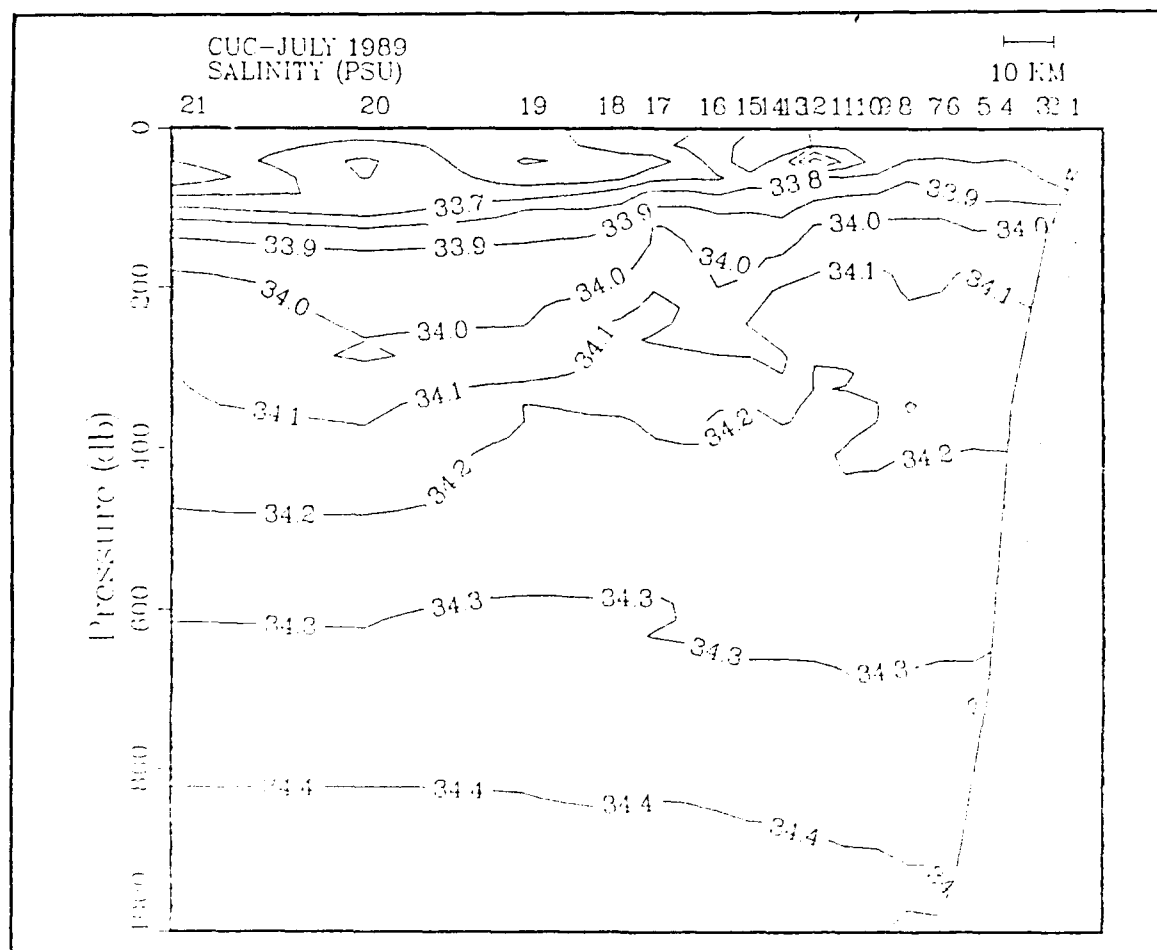


Figure 28. Vertical section of salinity for cruise CUC-July 1989:
The contour interval is 0.1 PSU.

Subarctic origin associated with the CC, even though it occurs in a region of poleward flow ($> 5 \text{ cm s}^{-1}$, shown later). Centered near a depth of 50 m between stations 17 and 19 are small areas of negative anomalies associated with CC water. Inshore between stations 11 and 13 is a core of negative anomaly values associated with a core of low salinity water (Figure 28). T-S curves for stations

11 through 13 (not shown) reflect the intrusion of cool, low salinity water along the 26.8 kg m^{-3} isopycnal surface (depth approximately 50 m), characteristic of Subarctic origin. This core lies within a region of poleward flow and is probably the northward transport of CC water associated with the observed wind relaxation.

g. November 1989 Water Mass Analysis (deep equatorward flow)

November 1989 was the final cruise included in this study and shows marked differences from the November 1988 cruise, one year earlier. Isopycnal surfaces below 250 m (Figure 29) have a domed appearance which extends over the entire transect. They are closest to the surface near station 19 and slope downward away from this station. Above 250 m, isopycnals between stations 21 and 22 begin to slope upward as they progress offshore, while those inshore of station 19 continue to slope up toward the coast until they reach stations 7 and 8 where they begin to slope down toward the continental slope. A sharp density front is located near station 17 and marks a transition region between equatorward flow inshore and poleward flow offshore (shown later). The corresponding vertical section of spiciness anomaly (Figure 30) shows several interesting features. First, the upper 100 m of the transect is characterized by a complex series of sign reversals in the anomaly field. Areas of subarctic waters are shown by the negative values, while those of southern origin are shown by positive values. Inshore the deeper signature of the CUC is seen, with a subsurface maximum ($> +0.3$ units) lying between stations 3 and 7 at a depth of approximately 110 m. Positive values extend downward to a depth of 500 m, which agrees favorably with the poleward flow of the CUC (shown

later). Second, a region of negative spiciness values within the interior of the transect, shown as the large blank area centered between stations 12 and 21

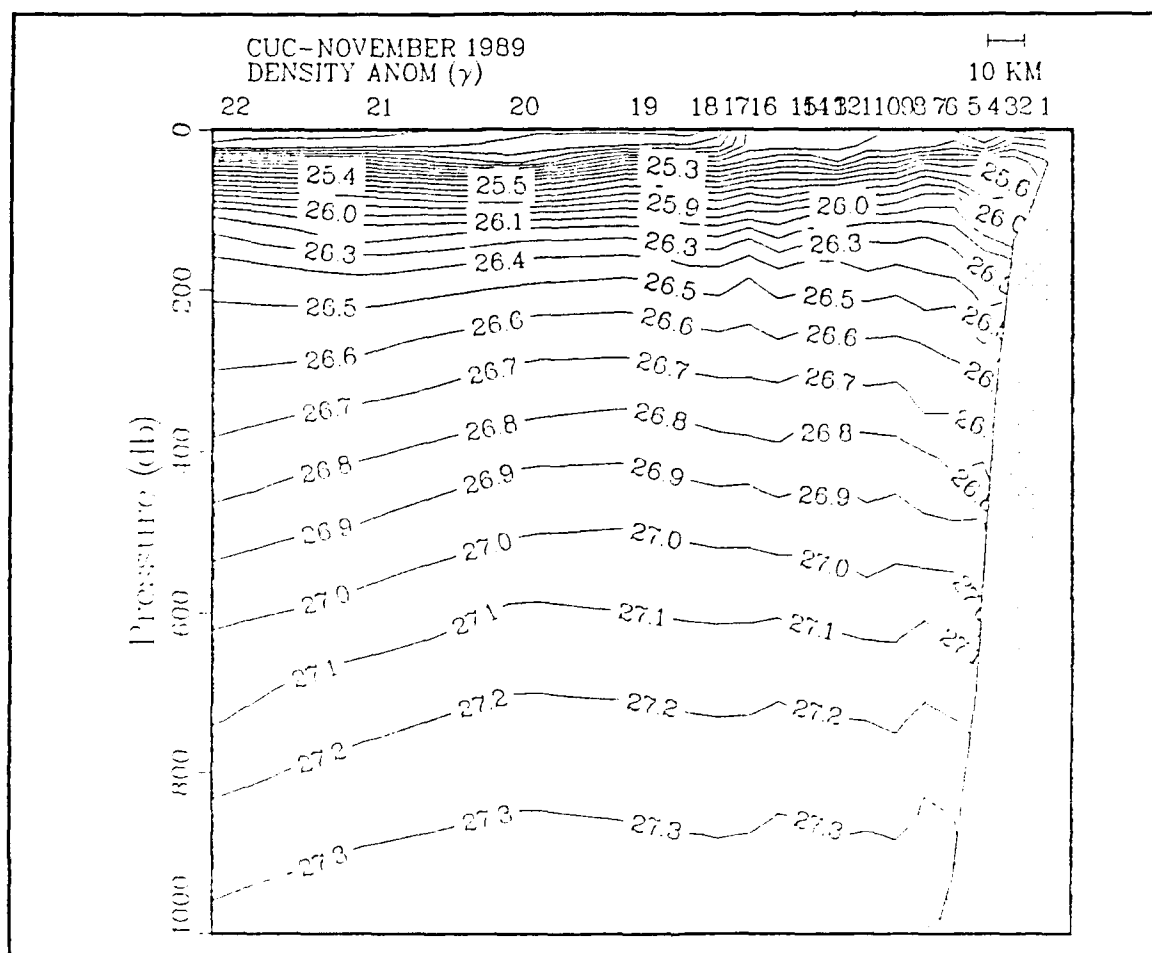


Figure 29. Vertical section of density anomaly for cruise CUC-November 1989: The contour interval is 0.1 kg m^{-3} .

(Figure 30). This region corresponds to the doming of the isotherms (not shown) and depression of the isohalines (Figure 31), which are reflected in the density field (Figure 29). Lastly, the extensive region of positive anomalies found between stations 21 and 22 below 100 m depth results from the downward sloping isotherms and sharply upward sloping isohalines resulting in water which

is warmer, and more saline than adjacent inshore waters. This water may either be a very strong and deep manifestation of North Pacific Central water entering the CCS from the west at depth, or an unusually strong recirculation of CUC water. North Pacific Central water has a salinity minimum of approximately 34.1 PSU between depths of 300 m to 800 m (Pickard and Emery 1982). The resulting slope of the isopycnals has produced extremely deep equatorward flow (flows $< -5.0 \text{ cm s}^{-1}$ at 700 m).

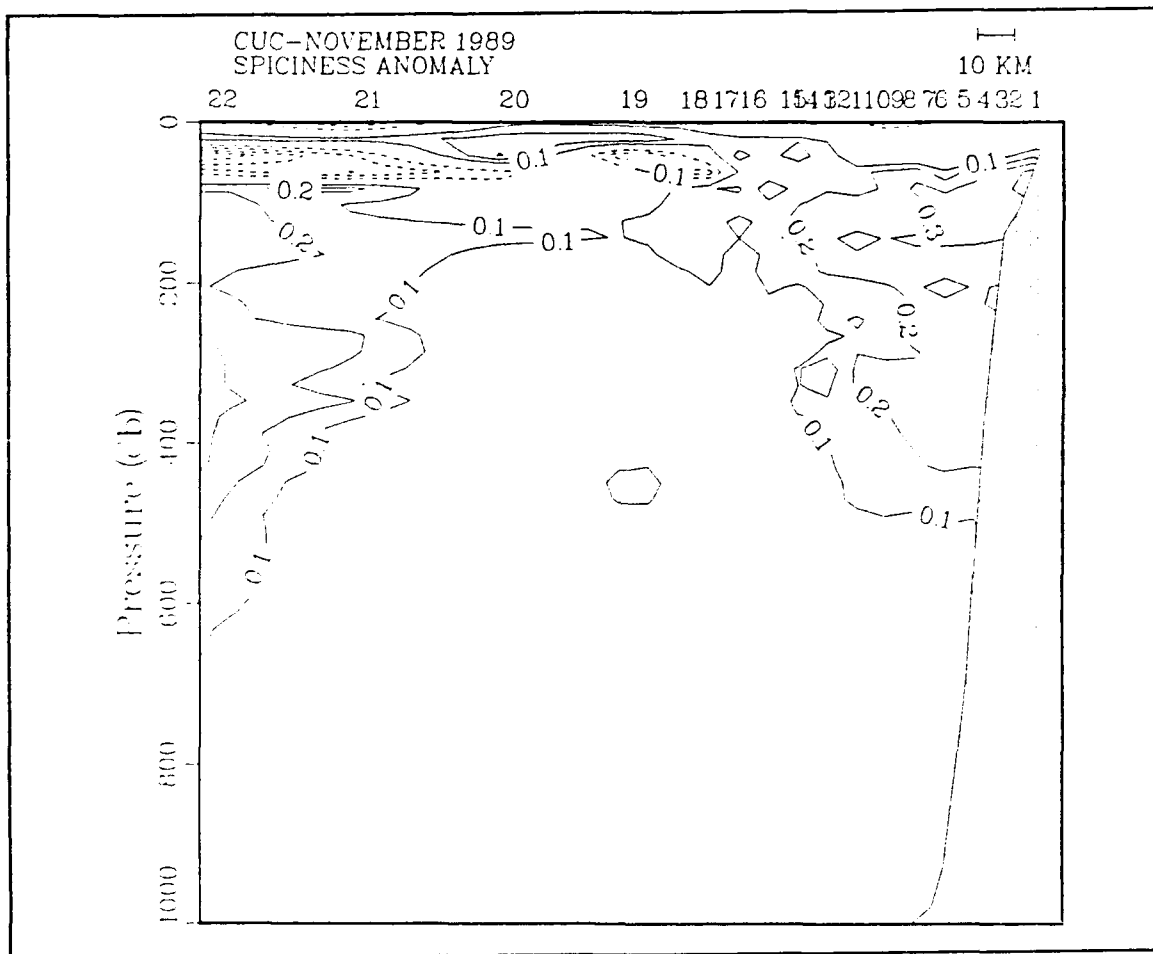


Figure 30. Vertical section of spiciness anomaly for cruise CUC-NOVEMBER 1989: The contour interval is 0.1 units.

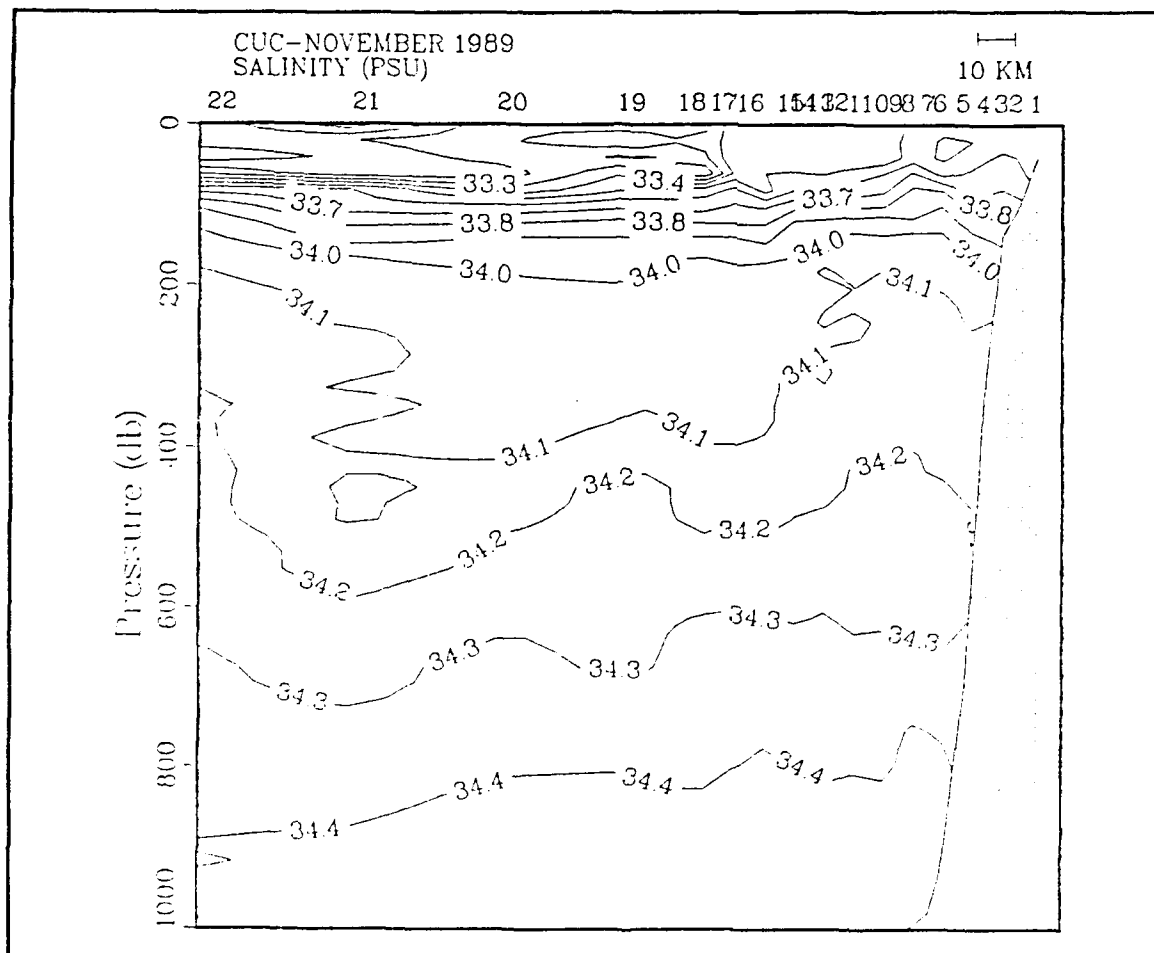


Figure 31. Vertical section of salinity for cruise CUC-November 1989:
The contour interval is 0.1 PSU.

B. DESCRIPTION OF ALONGSHORE GEOSTROPHIC FLOW

1. Geostrophy and its limitations

In the absence of wind stress and frictional forces, along with proper scaling considerations, the equations of motion (1a,b,c) can be reduced to (2a,b) in the horizontal and (2c) in the vertical. The former are commonly referred to as the geostrophic equations while the latter is known as the hydrostatic equation.

$$\frac{du}{dt} = -\frac{1}{\rho} \frac{\partial p}{\partial x} + fv + \frac{1}{\rho} \frac{\partial \tau_x}{\partial z} + F_x \quad (1a)$$

$$\frac{dv}{dt} = -\frac{1}{\rho} \frac{\partial p}{\partial y} - fu + \frac{1}{\rho} \frac{\partial \tau_y}{\partial z} + F_y \quad (1b)$$

$$\frac{dw}{dt} = -\frac{1}{\rho} \frac{\partial p}{\partial z} - g + F_z \quad (1c)$$

$$\frac{1}{\rho} \frac{\partial p}{\partial x} = fv \quad (2a)$$

$$\frac{1}{\rho} \frac{\partial p}{\partial y} = -fu \quad (2b)$$

$$\frac{1}{\rho} \frac{\partial p}{\partial z} = -g \quad (2c)$$

These equations are suitable for large scale ocean currents, where the flow is assumed to be steady and the primary balance is between the pressure gradient and Coriolis forces. This involves phenomena with length scales longer

than the first internal Rossby radius of deformation. To compute relative geostrophic velocities from an observed density field we need to redefine these equations in terms of density instead of pressure. This can be accomplished by taking the vertical derivatives of equations (2a,b) and the horizontal derivative of equation (2c). Combining these results we obtain what are commonly referred to as the "thermal wind" equations:

$$\frac{\partial v}{\partial z} = - \frac{g}{\rho f} \frac{\partial \rho}{\partial x} \quad (3a)$$

$$\frac{\partial u}{\partial z} = \frac{g}{\rho f} \frac{\partial \rho}{\partial y} \quad (3b)$$

From these two equations it is possible to compute the vertical shear of the geostrophic velocity provided the horizontal gradient of density is known. In practice, however, it is desirable to use a variation of these equations, which is based upon the geopotential distance between two pressure surfaces.

The "geostrophic method" as described by Pond and Pickard (1983) utilizes the temperature and salinity information collected at each station to compute the specific volume anomaly, δ . The specific volume anomaly is the sample specific volume, α , minus the specific volume of standard sea water ($\delta = \alpha_{s,t,p} - \alpha_{35,0,p}$). Using this quantity, the geostrophic shear (m s^{-1}) between two pressure surfaces can be computed from data at stations A and B as (Pond and Pickard 1983):

$$v_2 - v_1 = \frac{1}{L2\Omega\sin\phi} [\Delta D_B - \Delta D_A]$$

$$\text{where } \Delta D = \int_{p_1}^{p_2} \delta dp \quad (4)$$

is the dynamic height anomaly ($\text{m}^2 \text{s}^{-2}$) at each station, L the station spacing (meters), δ in $\text{m}^3 \text{kg}^{-1}$, and p in pascals.

The velocity resulting from this equation is the relative shear between two arbitrary isobaric surfaces. To convert this relative velocity to an absolute velocity we may consider two possibilities. First, a reference "level of no motion", $v_{\text{ref}} = 0$, can be assumed where the corresponding isopycnal surface between station pairs is assumed to be level. Second, additional information from a current meter, ADCP, or PEGASUS instrument can be used to prescribe a "level of known motion", where v_{ref} is not necessarily equal to zero. The geostrophic velocities discussed throughout the remainder of this paper have been computed using the assumption of a level of no motion at 1000 dbar based upon the PEGASUS observations of Rago and Collins (1989) along the POST from April 1988 to March 1989.

Before proceeding further it is appropriate to first discuss the limitations of (or errors in) the geostrophic method which arise due to the assumptions that have been made in its calculation. The geostrophic method has several disadvantages (Pond and Pickard 1983) which are as follows;

- it produces a relative current which itself is dependent upon the assumption of a level of no motion;

- a problem arises when the selected reference level reaches or becomes deeper than the ocean bottom which occurs as stations become close the shore;
- it is best suited for stations which are tens of kilometers apart where it will yield a mean velocity over that distance;
- friction, which has been neglected, may in fact be large near the bottom or in regions where there is strong shear;
- the equations do not apply near the equator ($\pm 0.5^\circ$) where the Coriolis parameter tends toward zero;
- internal waves and tides can disturb the mass field from its equilibrium state aliasing the data in an unknown way.

2. Calculation of alongshore geostrophic velocity

Geostrophic velocities have been computed based upon a reference level of 1000 dbar. The method used here to extrapolate nearshore is that utilized by Reid and Mantyla (1976), in which the value of dynamic heights have been linearly extrapolated horizontally along their last observed slope (Figure 32). This technique, though artificial, has been used by many investigators (Huyer 1980; Lynn and Simpson 1987; Lynn and Simpson 1989) in the calculation of alongshore geostrophic velocities and appears to be the preferred technique.

3. Estimation of error in dynamic height and geostrophic velocity

Besides the inherent limitations of geostrophy, the observations themselves often contain error, which has a direct effect on the final velocity field. Throughout this paper the term "error" refers to random error, and "bias" to systematic errors. Random error is equivalent to the precision of the quantity in question and is not a measure of accuracy. Accuracy includes both

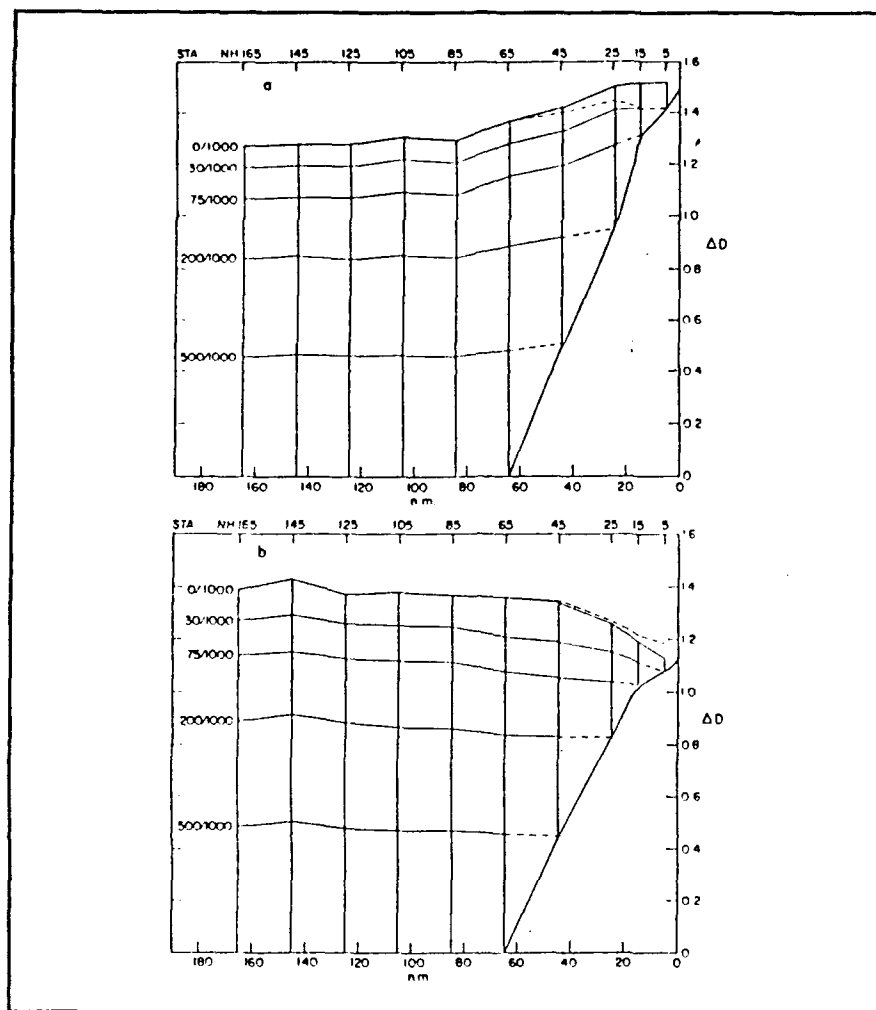


Figure 32. Extrapolation of dynamic height relative to 1000 decibars: This figure illustrates the technique of a linear extrapolation of the dynamic height field to estimate geostrophic currents when the bottom becomes shoaler than the reference level. The technique is based upon using the last observed slope of dynamic height to project what the inshore values might be if the bottom were replaced by a fictitious water column. The dashed line at the surface beginning at station 65 represents the sea surface value which would result if the dynamic heights were extended horizontally instead of along the last observed slope. (Source: Reid and Mantyla 1976)

random errors and bias. Random error is expressed as the standard deviation of the errors (σ), and σ^2 is the variance of the distribution.

Reid (1958) discusses several sources of error, which can effect the dynamic computations. When necessary this discussion has concentrated on the more modern instrumentation used today. Possible sources include;

- incorrect temperatures which arise from improper calibration of the CTD temperature sensor;
- incorrect salinities which arise from either contamination of water samples, operator error on the lab salinometer, or from errors in the calibration procedure;
- incorrect estimate of the pressure at which the readings and samples were taken due to improper calibration of the CTD pressure sensor;
- improper station location and spacing due to errors in navigation and vessel drift;
- errors in the mass field due to inadequate sampling which can result from irregularities in the horizontal and vertical mass structure, fluctuations of the field with time, and the fact that stations are not occupied simultaneously;
- and displacement of isopycnals due to internal waves.

Both Reid (1958) and Fofonoff (1985) discuss the effect that errors in the coefficients of the equation of state would have on the dynamical computations described earlier. Although different versions of this equation were used, both authors conclude that such errors are insignificant when compared to those which result from internal tides and measurement errors. For this reason the errors in the coefficients of the equation of state will be neglected in subsequent error analysis of geostrophic velocities.

To determine the effect of errors in the measurement of temperature, salinity and pressure on the computation of dynamic height and geostrophic velocity an analysis similar to that of Wooster and Taft (1958) and Johns (1984) has been performed. Briefly, this process consists of: 1) propagating the errors of T, S, and P through the equation of state to determine the corresponding error in the specific volume anomaly; 2) translating this into an error in dynamic height; and 3) using this value along with the error in station spacing to determine the error in geostrophic velocity. Each step in this procedure is described next in detail.

a. Determination of error in specific volume anomaly

To propagate the measurement errors into the specific volume anomaly it is necessary to differentiate the equation of state with respect to temperature, salinity and pressure. The equation of state used here is that found in UNESCO Technical Report #44 and Millero and Poisson (1981). Since analytic differentiation of this equation proves to be a difficult task, these derivatives have been computed numerically through finite differences.

Twenty values of temperature, salinity and pressure were randomly chosen from four separate cruises to use the maximum and minimum values of these variables. Keeping two of the three variables fixed the third was increased by either 0.005°C, 0.005 PSU, or 1% of depth. These values represent the accuracies of the Neil Brown CTD, and are subsequently used as estimates of the 1 σ random error in the measurements. The resulting values for these derivatives were;

$$\frac{\partial \delta}{\partial T} \approx 0.2 \times 10^{-6} \frac{\text{m}^3 \text{kg}^{-1}}{^\circ\text{C}}$$

$$\frac{\partial \delta}{\partial S} \approx -0.7 \times 10^{-6} \frac{\text{m}^3 \text{kg}^{-1}}{\text{PSU}}$$

$$\frac{\partial \delta}{\partial P} \approx 0.5 \times 10^{-10} \frac{\text{m}^3 \text{kg}^{-1}}{\text{dbar}}$$

It is clear that the dominant terms are those associated with temperature and salinity which are four orders of magnitude larger than the pressure term.

Using these values it is possible to compute the corresponding error in the specific volume anomaly in a manner similar to that of Wooster and Taft (1958). If it is assumed that the measurements are statistically independent the following expression for the variance of specific volume anomaly (σ_δ^2) can be utilized;

$$\sigma_\delta^2 = \left(\frac{\partial \delta}{\partial T}\right)^2 \sigma_T^2 + \left(\frac{\partial \delta}{\partial S}\right)^2 \sigma_S^2 + \left(\frac{\partial \delta}{\partial P}\right)^2 \sigma_P^2 \quad (5)$$

Substitution of these derivatives along with the estimated precision of the Neil Brown CTD into this equation yields a variance of $1.325 \times 10^{-17} (\text{m}^3 \text{kg}^{-1})^2$ which corresponds to an error of $\pm 3.64 \times 10^{-9} \text{m}^3 \text{kg}^{-1}$. The value used for σ_P^2 was 2 dbar. Development of this equation is based upon the principles outlined in Appendix B. The equation used by Wooster and Taft (1958) in their analysis included an additional term;

$$\sigma_\delta^2 = \sigma_c^2 + \left(\frac{\partial \delta}{\partial z}\right)^2 \sigma_z^2 \quad (6)$$

where the first term represents the variance of the measurement errors, analogous to the equation shown earlier, and the second term represents the variance of depth errors. They find that below the surface layer this second term is much smaller than the first, even if large vertical gradients are present at depth, and can therefore be neglected in the computation of dynamic height errors. Further, they indicate that the first term is dominated by salinity, which agrees with the results of this analysis. For the bulk of this analysis this term has been neglected, however it will be included when the effects of internal tides are examined.

b. Determination of error in dynamic height

The next step is to translate the error in the specific volume anomaly into an error in dynamic height. In the process of determining the derivative of δ with respect to temperature, salinity and pressure, it was found that the measurement errors did not vary significantly with these variables. As a result, the calculation of the error in dynamic height will depend on the number of levels used in the integration. In calculating the geostrophic velocities, a layer thickness of 20 dbar has been used. Since the data has been averaged into 2 dbar bins, the error in dynamic height must first be computed within this layer, and then carried from the reference level to the surface and bottom. The variance in dynamic height within a 20 dbar layer has been computed from the following equation;

$$\sigma_{\Delta D_{20}}^2 = \sigma_{\delta}^2 \sum_{i=1}^{10} (\Delta P_i)^2 = (\sigma_{\delta}^2)(10)(2 \times 10^4 \text{ Pa}) \quad (7)$$

where pressure has units of Pascals ($\text{kg m s}^{-2} \text{m}^{-2}$). Using the value obtained earlier for the error in specific volume anomaly, the resulting error in dynamic height for a 20 dbar layer becomes $\pm 0.00023 \text{ m}^2 \text{ s}^{-2}$. Since the error is the same at each station in the pair the value used to calculate the error in the geostrophic velocity is simply the square-root of the sum of the squares which is $\pm 0.00033 \text{ m}^2 \text{ s}^{-2}$.

To obtain the random error at any surface relative to 1000 dbar, multiply this value by the square-root of the number of layers. For the sea surface relative to 1000 dbar (50 layers) a random error in dynamic height of $\pm 0.0023 \text{ m}^2 \text{ s}^{-2}$ or ± 0.00023 dynamic meters is estimated as error in height difference between two stations. The smallness of this result can be attributed to good measurements and to the fact that the data was continuous which allowed for the use of small layers in the computational process. This in turn allowed for a better estimate of the integral in equation (4).

This value is similar to that obtained by Johns (1984), ± 0.0006 dynamic meters relative to 2000 dbar, where the small size results from the fact that the measurements were assumed to be free of any biases. As she points out, this value is very small and probably underestimates the total (random plus bias) error in the dynamic height. To obtain a more realistic result she allows for a bias of $\pm 0.0025 \text{ }^\circ\text{C}$ and $\pm 0.0025 \text{ PSU}$ in the measurements of temperature and salinity and obtains a value of ± 0.004 dynamic meters.

Application of biases in the temperature and salinity measurements will certainly have an effect on the value of dynamic height and will be important when considering plots of dynamic topography. However, in the computation of geostrophic velocities it is the difference in dynamic heights

between two stations which is important and a fixed bias will tend to cancel out. For this reason no bias has been introduced into this analysis.

c. Determination of error in geostrophic velocity

To obtain an equation for the error in geostrophic velocity take the total derivative of;

$$v_g = \frac{1}{fL} (\Delta D_B - \Delta D_A) + v_{ref} \quad (8)$$

and the square-root of the sum the squares of the components to obtain (assuming errors in L , v_{ref} , and ΔD are statistically independent);

$$\sigma_{v_g} = \sqrt{\left(\frac{\sigma_{\Delta D}}{fL}\right)^2 + \left(\sigma_L \frac{v_g}{L}\right)^2 + (\sigma_{v_{ref}})^2} \quad (9)$$

where L is in meters, v_g is in $m s^{-1}$, $\sigma_{\Delta D}$ is in $m^2 s^{-2}$, and σ_L is in meters (Appendix B). These three terms represent the error in the dynamic height, the error in station spacing and the error in the velocity at the reference level, respectively. Prior to computing error estimates for geostrophic velocities, the error in station spacing must first be determined.

Unlike previous error quantities which do not vary significantly from cruise to cruise, the error in station spacing must be calculated separately for each cruise. The two sources of error in station spacing are navigational errors and vessel drift. The navigation error is insignificant compared to the vessel drift which depends upon weather conditions and speed of surface currents. The navigation system used to position the vessel was LORAN-C,

which for the coastal waters in the vicinity of Point Sur has an absolute accuracy of about 0.25 nautical miles (Bowditch 1984). Most of this error is a spatially coherent bias which cancels upon differencing station positions to determine the station spacing. The remaining random error in station spacing is on the order of approximately ± 25 m (K.J. Schnebele, pers. comm.) in this region of the coast. This is a very small and essentially negligible in the geostrophic calculations. Therefore it is necessary to compute the differential drift between all applicable stations pairs for each cruise to determine an appropriate value for σ_L to be used in the geostrophic velocity error calculations.

From the starting and ending positions for each cast, the component of the change in station spacing which lies along the POST has been calculated for each pair. If at both stations the vessel drifted in the same direction the values were subtracted, while if the drift was in opposite directions the values were added. Since continuous data was collected on the downcast the maximum uncertainty in the spacing is one half this distance. This assumes that the ship drifted one-half the total distance during the data collection process and is valid for all casts, except those where numerous bottle samples were collected on the upcast. In these instances the actual drift would be less than one-half so that this procedure would tend to produce more conservative results. If it is also assumed that the drift of the instrument on the downcast was linear with time the error is zero at the surface and reaches the maximum uncertainty at the bottom.

Based upon the uniform probability distribution an rms value was determined by dividing the maximum uncertainty by 2 times the square-root of 3 (Appendix B). This value was then divided by the station spacing to obtain the dimensionless parameter, σ_L / L , needed for the calculation of the error in

velocity. For each cruise an average value has been obtained, along with the maximum and minimum values (Table 7).

The third term in this equation represents the uncertainty of the flow at the reference level. Based upon PEGASUS observations of Rago and Collins (1989), the flow at 1000 dbar is near zero $\pm 0.02 \text{ ms}^{-1}$. Where the bottom depth at a station was less than the reference level extrapolation of dynamic height was required. Since this extrapolation was linear, the deepest velocity in the extrapolated pair was equal to the velocity of the adjacent offshore pair at the same depth. Therefore the random error at the deepest common depth of the next inshore station pair is equal to the value of σ_{vg} of the adjacent offshore station pair.

Table 7. NORMALIZED ALONGTRACK DIFFERENTIAL DRIFT OF THE VESSEL: These values represent the rms differential drift normalized by the spacing between station pairs (σ_L / L). Drift refers to a distance rather than a measure of current speed.

Cruise	Average	Maximum	Minimum
STMAY 1988	0.0088	0.025	0.0001
August 1988	0.0157	0.059	0.0004
November 1988	0.0207	0.062	0.001
February 1989	0.0155	0.055	0.000
STMAY 1989	0.0114	0.022	0.001
July 1989	0.0154	0.041	0.0003
November 1989	0.0170	0.044	0.002

Using the maximum value for σ_L / L from (Table 7), the value for σ_{AD} determined earlier, and the appropriate value for the Coriolis parameter, f , which for this latitude is 8.6408×10^{-5} , the worst case error in the geostrophic velocity can now be determined. The November 1988 cruise had the highest values for both σ_L / L (0.062) and geostrophic velocities (45 to 55 cm s^{-1}) and was used for a test case to determine the magnitude of the resulting errors in geostrophic velocities. The errors were $\pm 2.0 \text{ cm s}^{-1}$ at the reference level and increased to a maximum near the surface or where the geostrophic currents were largest and at the deepest depth below the reference level. For this particular cruise the largest errors were on the order of approximately 3.5 to 4.0 cm s^{-1} , which occurred in the areas of the greatest geostrophic velocities. Based upon these results it appears that the worst case error in station spacing contributes to an error of approximately $\pm 1.5 - 2.0 \text{ cm s}^{-1}$. The errors for other cruises were much smaller, consisting primarily of the $\pm 2.0 \text{ cm s}^{-1}$ error in the reference level velocity.

d. Effect of internal tides on errors in dynamic height

Baroclinic tides result from the interaction of barotropic tides with variable bottom topography associated with coastal regions. Vertical particle displacements of 10 to 100 meters and horizontal velocities of 0.10 to 1.0 m/sec can result from internal tides (Wiseman et.al. 1983). Observations of internal tides over six days off Point Sur, California in October 1950 (Reid 1956), show wave amplitudes greater than 30 feet (9.1 m).

To examine the effect of internal tides on dynamic height and geostrophic velocities it is necessary to return to equation (6) (Wooster and Taft 1958) and include the second term. The first part of this term represents a

typical vertical gradient of the specific volume anomaly, δ , while the second part represents the variance associated with the sinusoidal internal wave. A typical value for the gradient of specific volume anomaly, $6.92381 \times 10^{-9} \text{ kg m}^{-3} / \text{m}^{-1}$, was obtained by observing the change of δ over a 20 meter distance in the vicinity of the thermocline for the May 1988 student cruise. For an internal tide wave with amplitude 10 m the variance becomes 50 m^2 . Combining these values with the value of the first term and following the same procedure, a value of $\pm 0.0031 \text{ m}^2 \text{ s}^{-2}$ is obtained for the random error in dynamic height of a 20 dbar layer at each station. Notice that this value is an order of magnitude larger than that obtained without the inclusion of an internal tide. It should be kept in mind that this value occurs in the thermocline region where the value of the specific volume anomaly changes most rapidly. Above and below this region the rate of change and thus the effect of the internal tide is much smaller.

Defant (1950) discusses the difficulties associated with internal tides and the resulting periodic fluctuations in the mass field. From observations off southern California, he found that internal tides can cause disturbances of up to 8 dynamic centimeters. He also discusses a method for removing the effect of the diurnal or semidiurnal tides through careful preparation of the sampling scheme. This procedure although capable of removing a desired tidal frequency is not very practical from an operational point of view. In addition, the period of the local internal tide is not known in most cases and is therefore extremely difficult if not impossible to account for or remove its effects on the mass field. As a result the reader should be aware that internal tides do exist and will have an effect on the observed mass field and resulting dynamic topography, however,

without actual measurements of these tides their effects cannot be isolated and/or removed.

4. Analysis of alongshore geostrophic velocity

A description of alongshore geostrophic velocities for each of the seven cruises is presented. With the exception of the November 1989 California undercurrent cruise a reference level of 1000 dbar appeared justified. Comparisons with earlier studies off Point Sur and discussion of possible dynamics involved follow in Chapter V. Observations are presented by cruises following a format similar to the water mass analysis.

a. August 1988 alongshore geostrophic velocities (seasonal normal)

For the two week period leading up to the cruise, the alongshore component of surface wind stress (Figure 33) was essentially zero with a brief period of equatorward stress on July 29th. Stations along the POST were occupied before any significant equatorward component in the wind stress developed. The vertical section of alongshore geostrophic velocity (Figure 34) depicts equatorward surface flow between stations 9 and 22 associated with the CC. The core ($v < -20.0 \text{ cm s}^{-1}$) located near station 19 is displaced 30 km inshore of the salinity minimum ($< 32.8 \text{ PSU}$, Figure 14). The region between stations 19 and 21 may coincide with the core of the CC, which carries low salinity water southward and may occur in bands defined by one or two pairs of stations separated by up to 75-150 km (Lynn and Simpson 1987). Subsurface poleward flow was observed predominantly inshore of station 15. The CUC is represented by two cores of poleward flow located at stations 3 and 9, between

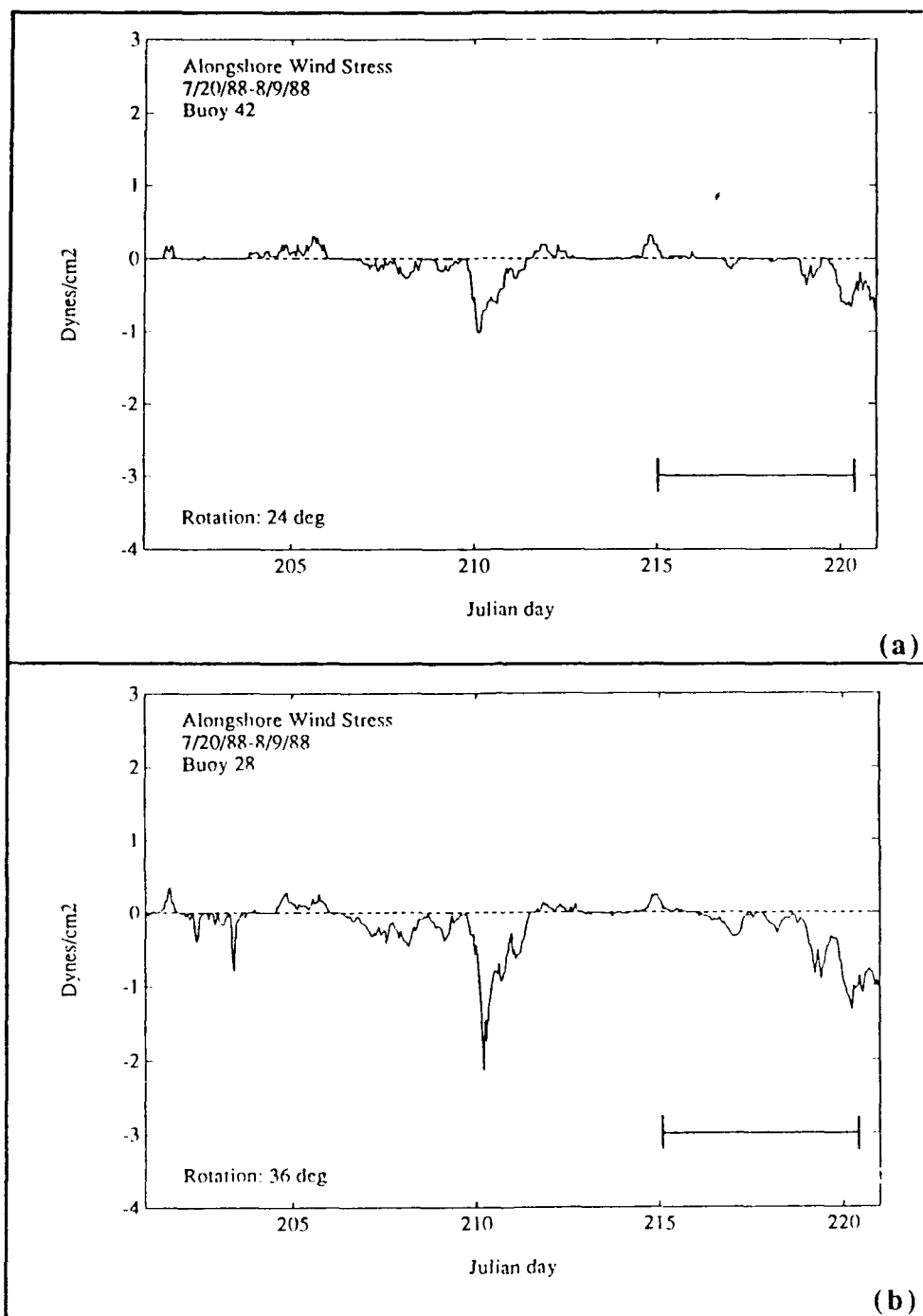


Figure 33. Alongshore component of wind stress during cruise CUC-August 1988: (a) Wind stress data from buoy 46042, Monterey Bay; (b) Wind stress data from buoy 46028, Cape San Martin. The cruise period is indicated by the solid horizontal line (8/3 = JD 215; 8/8 = JD 220).

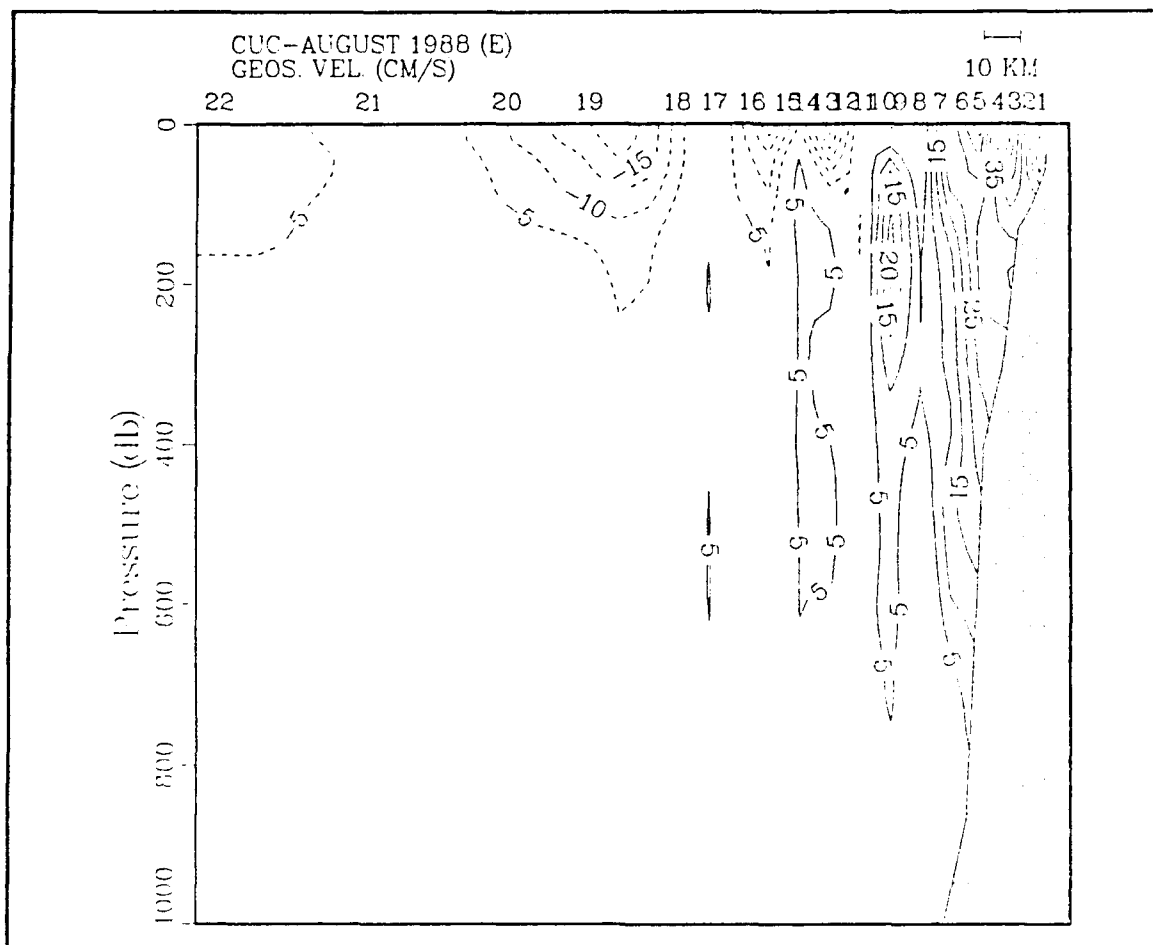


Figure 34. Vertical section (0-1000 dbar) of alongshore geostrophic velocity for cruise CUC-August 1988: The contour interval is 5.0 cm s^{-1} . Dashed lines equatorward and solid lines are poleward.

12 and 42 km of the coast at a depth of 190 m. Velocities in excess of 20 cm s^{-1} were observed in the core offshore, while inshore they exceeded 35 cm s^{-1} . The position of these cores agreed favorably with the region of positive spiciness anomaly shown in Figure 16.

Strong poleward flow ($v > 60 \text{ cm s}^{-1}$) at the surface was observed within 20 km of the coast. Such inshore countercurrents may be driven by a residual pressure gradient, causing a northward acceleration during wind

relaxations, however the dynamics involved are not clearly understood (Huyer et al. 1989). Wickham (1975) observed drifts in excess of 50 cm s^{-1} using subsurface drouges (at 50 m depth) deployed in August 1972 between Point Sur and Cypress Point, which he attributed to non-geostrophic components in the flow field. The 33.4-33.7 PSU isohalines surfaced between stations 3 and 5 (Figure 14) depicting a frontal structure not present in the temperature field. This developed after an upwelling event and surface heating erased the temperature signal. It is not clear how this frontal structure of salinity is related to the strong poleward flow observed between these stations.

b. May 1988 alongshore geostrophic velocities (weak poleward flow)

This cruise was preceded by a period of strong equatorward winds, at times in excess of 23 knots. The resulting alongshore component of surface wind stress (Figure 35) reached or exceeded $-2.0 \text{ dyne cm}^{-2}$ and persisted through the first two days of the cruise. A vertical section of alongshore geostrophic velocity from 0-1000 dbar (Figure 36) depicts equatorward flow above 200 m over most of the POST, expected with strong equatorward winds. An equatorward surface jet ($v < -25.0 \text{ cm s}^{-1}$) is present between stations 3 and 4, while velocities in excess of 35 cm s^{-1} are seen inshore at station 1. These features are characteristic of coastal upwelling which produces an equatorward jet in response to strong horizontal density gradients resulting from the raising of isopycnals near the coast (Huyer 1983). Upward sloping isopycnals and horizontal density fronts are seen in the vertical section of density (Figure 17) and correspond to the regions of intense equatorward flow (Figure 36).

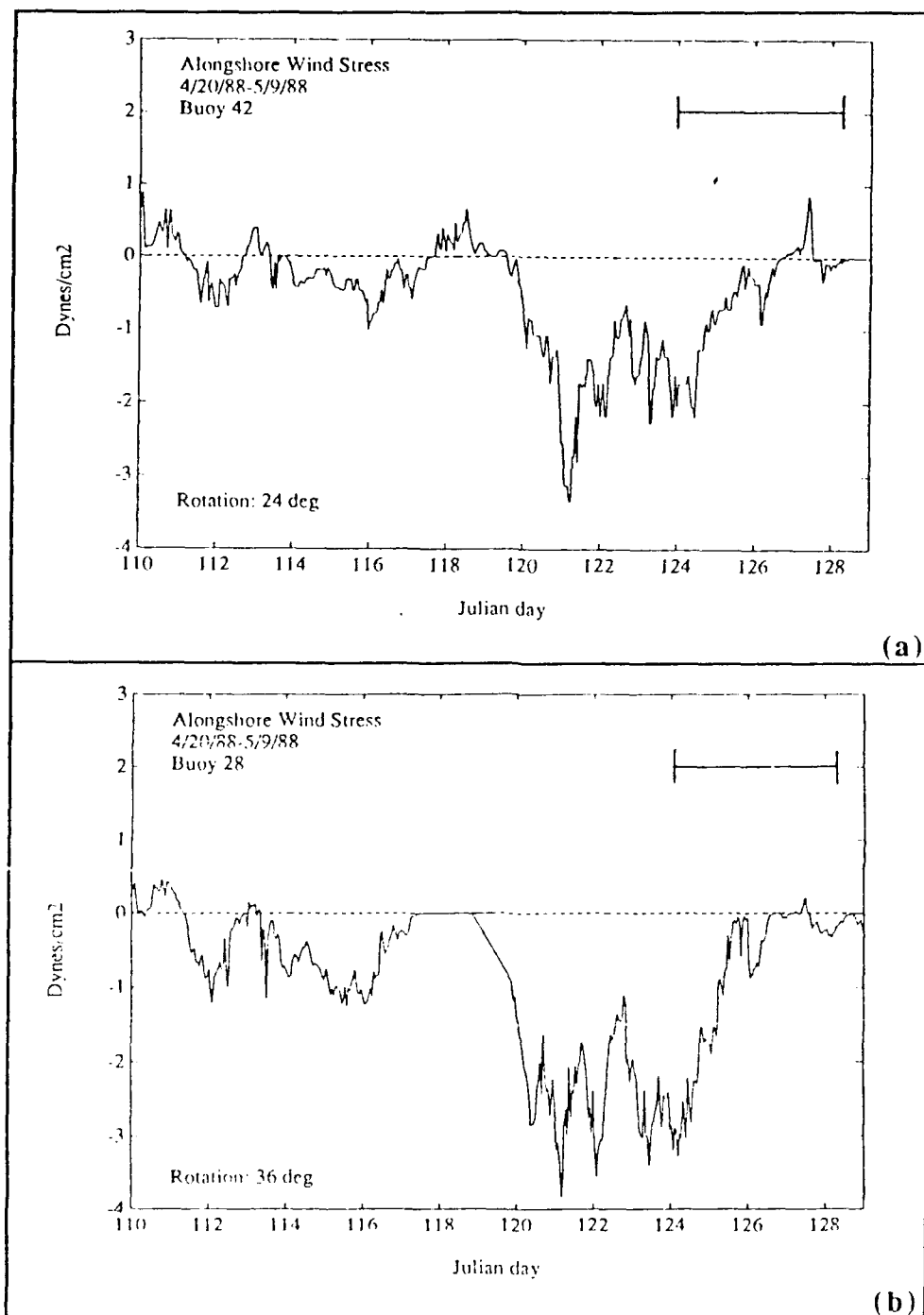


Figure 35. Alongshore component of wind stress during the May 1988 Student Cruise: (a) Wind stress data from buoy 46042, Monterey Bay; (b) Wind stress data from buoy 46028, Cape San Martin. The cruise period is indicated by the solid horizontal line (5/4 = JD 124; 5/8 = JD 128).

A secondary subsurface core of equatorward flow ($v < -10.0 \text{ cm s}^{-1}$) was observed below station 5, with velocities of -5.0 cm s^{-1} reaching 750 m. This deep equatorward flow is too deep for direct wind forcing and its cause is unknown.

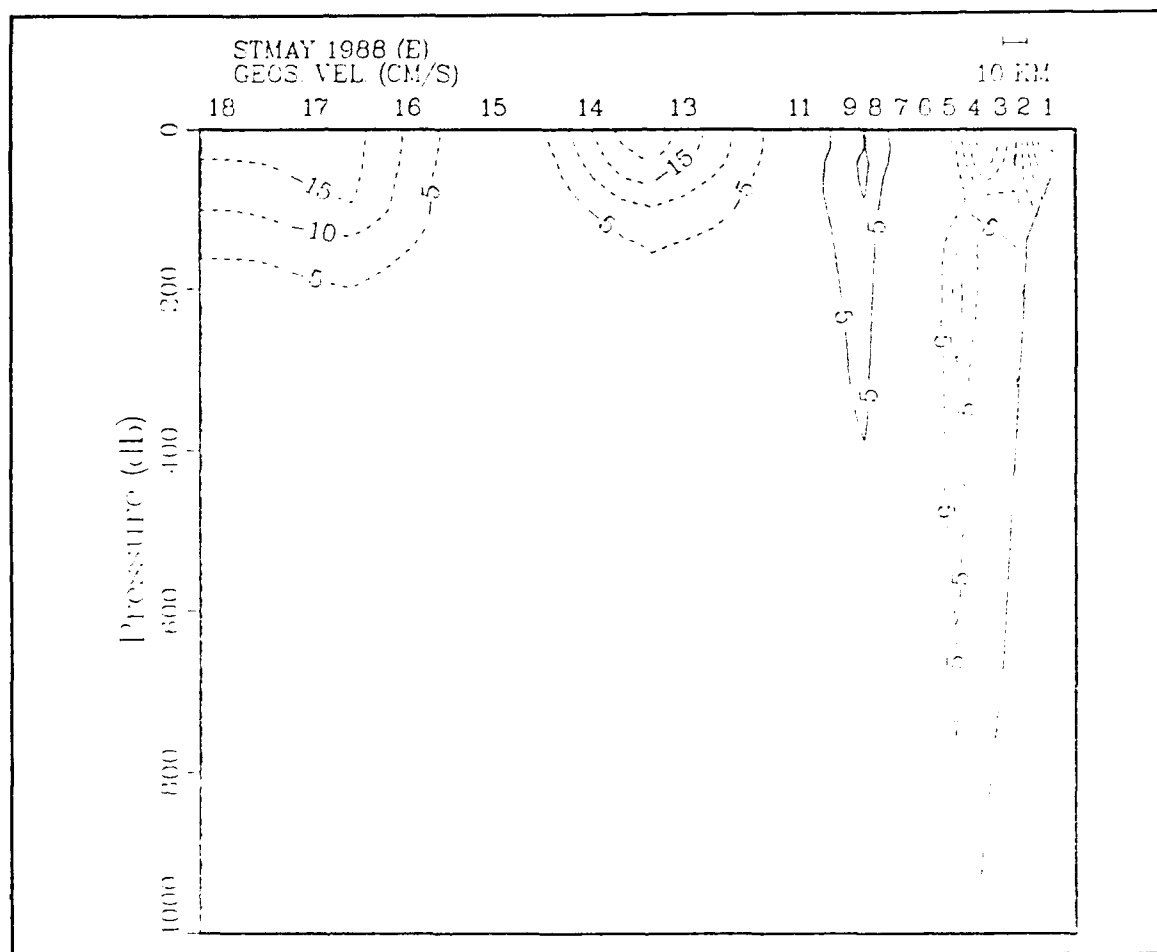


Figure 36. Vertical section (0-1000 dbar) of alongshore geostrophic velocity for the May 1988 Student Cruise: The contour interval is 5.0 cm s^{-1} . Dashed lines are equatorward and solid lines are poleward.

Weak poleward flow was observed below 200 m inshore of station 4 with a maximum of 4.5 cm s^{-1} near 460 m. Due to the contouring interval this

region is not depicted in Figure 34. The location of this poleward flow is indicative of the CUC which historically lies below the surface at this time of year. Its anomalously weak magnitude ($< 5 \text{ cm s}^{-1}$) may result from the intense equatorward winds which preceded this cruise. Poleward flow ($> 5.0 \text{ cm s}^{-1}$) was also observed between stations 7 and 11 with very weak equatorward flow in the upper 50 m between station 8 and 9.

c. November 1988 alongshore geostrophic velocities (strong mesoscale feature)

The water mass analysis showed that an anticyclonic mesoscale eddy was the dominant feature on this cruise, which is related to the geostrophic velocities (Figure 37). Poleward velocities in excess of 55 cm s^{-1} occur at station 11 near 110 m depth. A second subsurface maximum occurs at station 13 with velocities in excess of 40 cm s^{-1} .

Inshore of station 5, the CUC was observed at the surface and along the continental slope, with a core depth of 460 m. It appears the mesoscale eddy has limited the horizontal extent of the undercurrent to within 10 km of the slope. The location of the CUC in Figure 37 coincides with the downward sloping isopycnals shown in Figure 19 which result from the warmer, more saline waters of the CUC. The positive values of spiciness anomaly which occur within the mesoscale feature are likely the result of lateral entrainment of CUC water as discussed earlier.

Poleward flow was observed from station 16 to the midpoint between stations 18 and 19. From earlier analysis of the water mass structure, it was found that throughout this region the water was of subarctic origin. It is

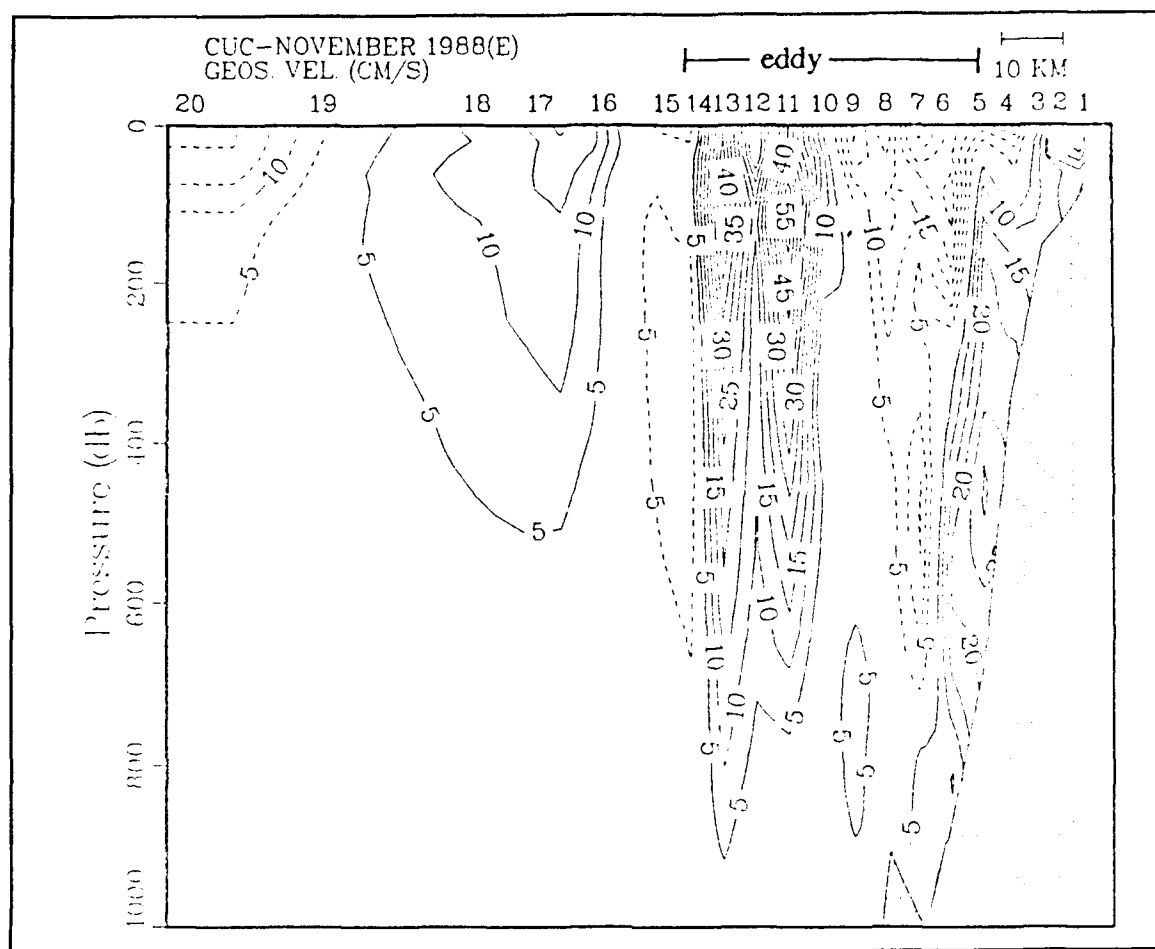


Figure 37. Vertical section (0-1000 dbar) of alongshore geostrophic velocity for cruise CUC-November 1988: The contour interval is 5.0 cm s^{-1} . Dashed lines are equatorward and solid lines are poleward.

possible that wind relaxations prior to and during the cruise (Figure 38) was the mechanism behind this poleward flow, and poleward advection of subarctic water, normally associated with equatorward flow. Offshore of this poleward flow was the equatorward flowing CC, with velocities less than -20.0 cm s^{-1} .

d. February 1989 alongshore geostrophic velocities (strong equatorward flow near coast)

Wind data for this cruise could only be obtained from the Cape San Martin buoy, since the Monterey Bay buoy was inoperative during the last half of January and all of February. The record from buoy 46028 (Figure 39) shows two strong equatorward wind events preceding the cruise by several days, and a weaker one just prior to the start of the cruise. A relaxation period of little or no wind occurred four days before the start of the cruise and another at the start of the cruise. By February 4th the winds were once again equatorward for two days, switching to poleward as time progressed.

The vertical section of alongshore geostrophic velocity (Figure 40) shows the CUC at the surface between station 5 and 11 extending to a depth of 600 m. It has a subsurface core ($v > 35.0 \text{ cm s}^{-1}$) lying near a depth of 100 m, 15 km from the coast. Offshore of the CUC, the flow is generally equatorward with large areas of weak flow between 0.0 and -5.0 cm s^{-1} . Correlation of wind records between buoys 46028 and 46042 for each cruise show stronger equatorward wind events at buoy 46028 to the south and stronger poleward wind events at buoy 46042 to the north. If it is assumed a similar pattern existed on this cruise, the equatorward wind event just prior to the cruise may have been stronger than represented in Figure 39. The poleward flow observed between stations 5 and 11 would then be the result of the relaxation of the equatorward winds. This may also account for the stronger flow of the CUC.

Inshore of station 5 is a region of strong equatorward flow ($v < -40.0 \text{ cm s}^{-1}$). A salinity minimum ($S < 33.3 \text{ PSU}$) existed between stations 5 and

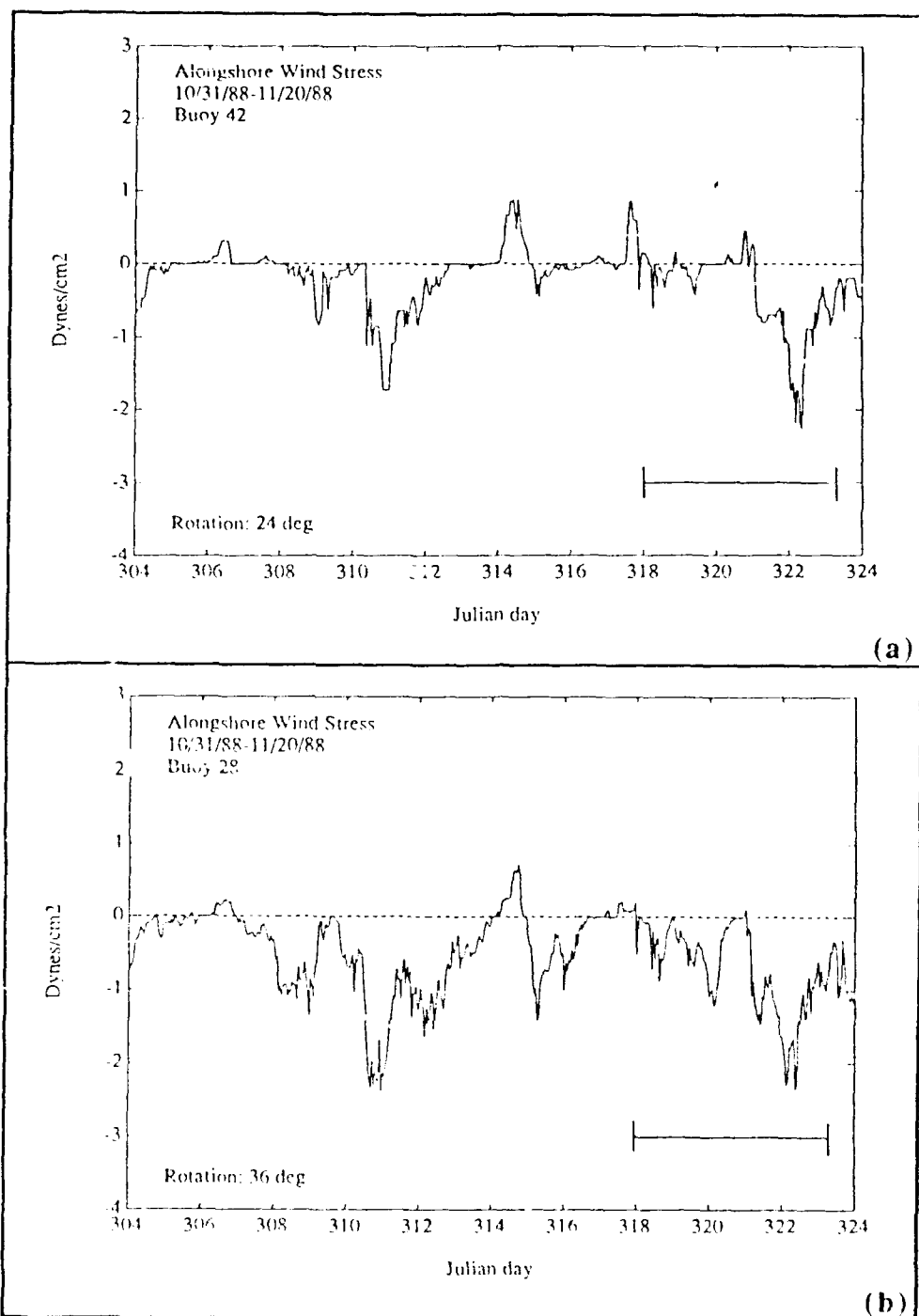


Figure 38. Alongshore component of wind stress during cruise CUC-November 1988: (a) Wind stress data from buoy 46042, Monterey Bay; (b) Wind stress data from buoy 46028, Cape San Martin. The cruise period is indicated by the solid horizontal line (11/14 = JD 318; 11/19 = JD 323).

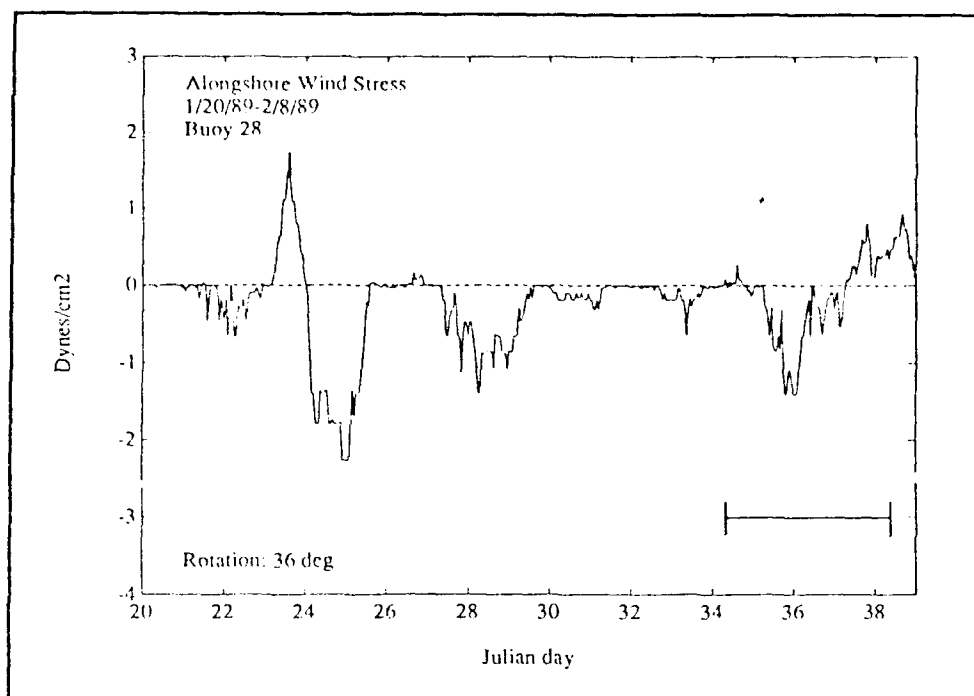


Figure 39. Alongshore component of wind stress during cruise CUC-February 1989: Wind stress data from buoy 46028, Cape San Martin. The cruise period is indicated by the solid horizontal line (2/3 = JD 34; 2/7 = JD 38).

6 corresponding to the density minimum shown in Figure 41. The upward sloping isopycnals near the coast suggest that the salinity minimum may be the mechanism behind the strong equatorward flow inshore of the CUC. The salinity minimum may be the result of ambient surface water trapped between previously upwelled water and higher salinity water near the coast.

e. May 1989 alongshore geostrophic velocities (poleward flow near coast)

The alongshore component of wind stress was between -1.0 to -2.0 dyne cm^{-2} three days prior to this cruise and continued through the first two days of the cruise (Figure 42). A pattern of poleward and equatorward flows is depicted in the alongshore geostrophic velocities (Figure 43). The most intense

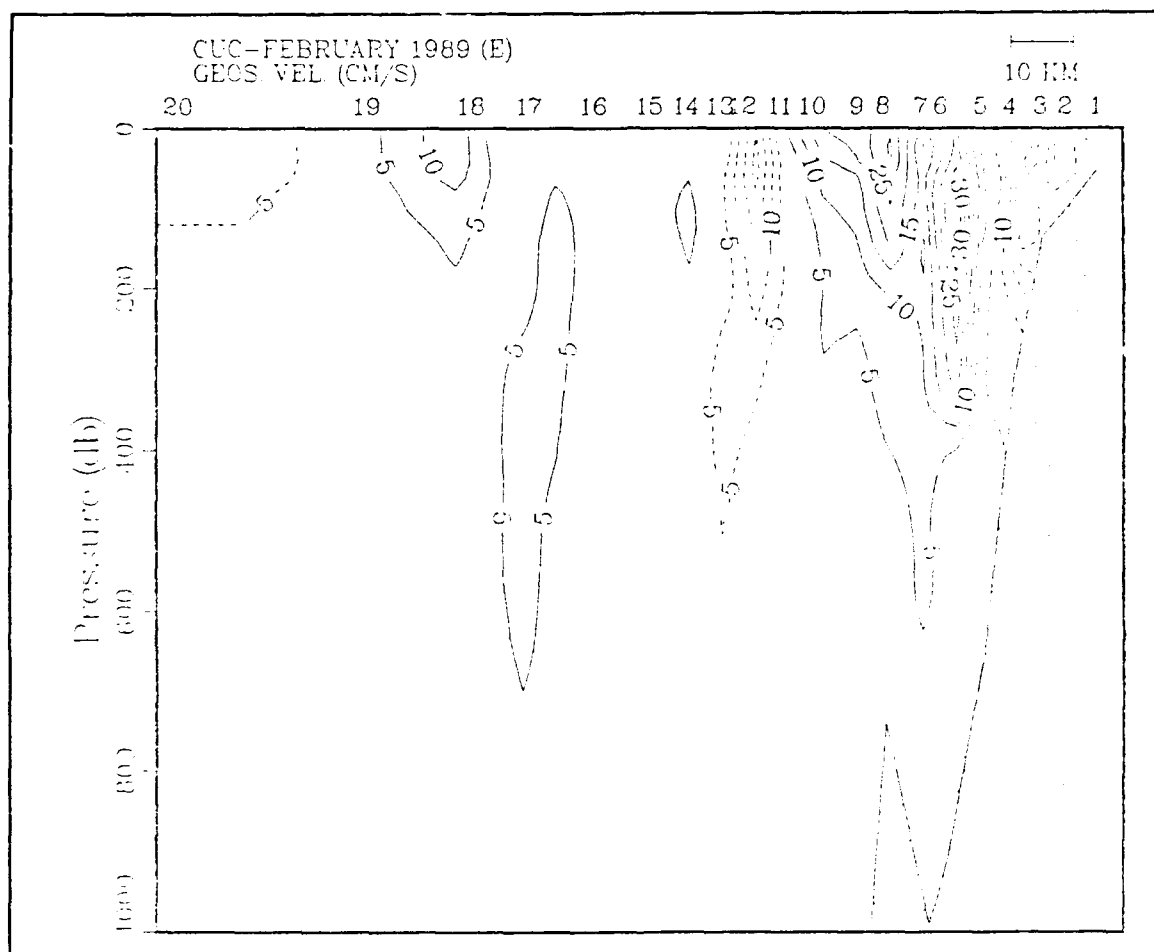


Figure 40. Vertical section (0-1000 dbar) of alongshore geostrophic velocity for cruise CUC-February 1989: The contour interval is 5.0 cm s^{-1} . Dashed lines are equatorward and solid lines are poleward.

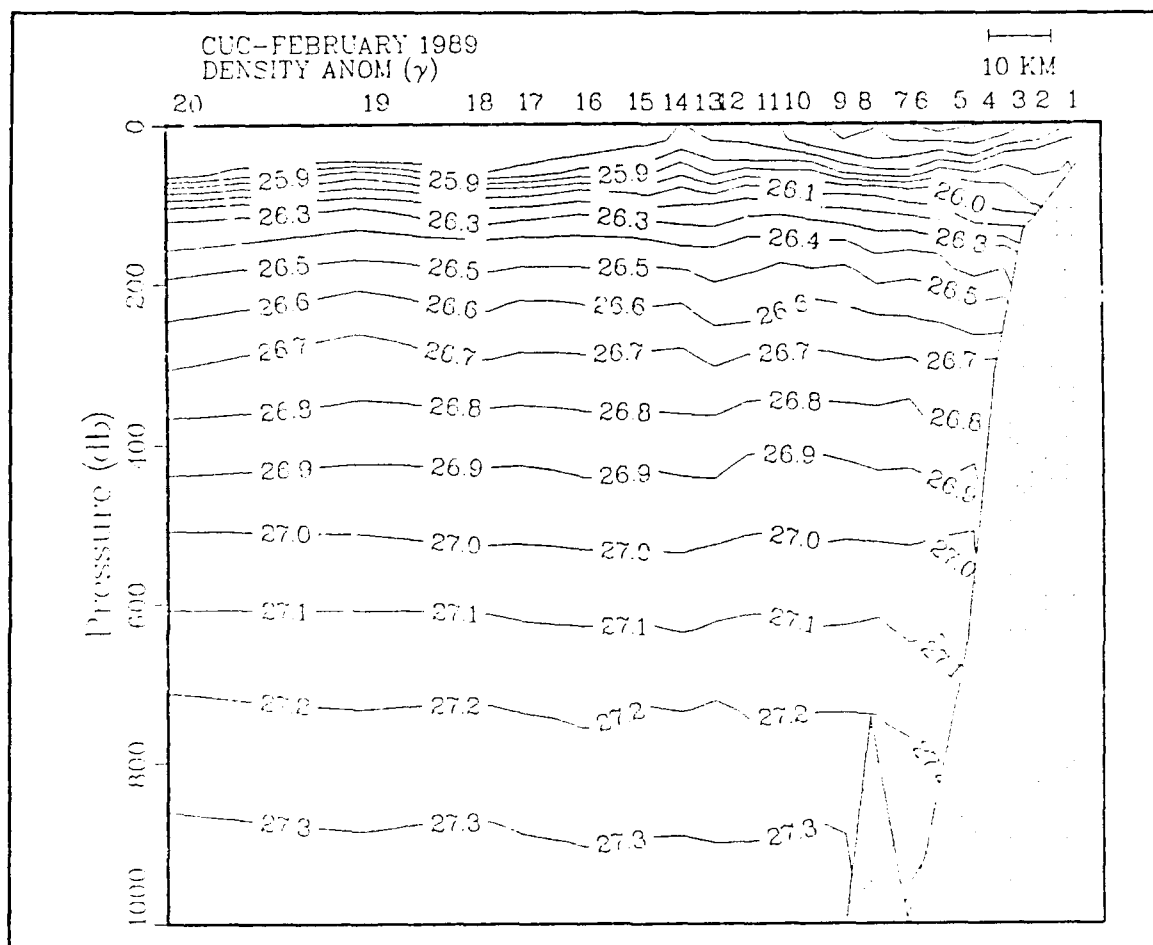


Figure 41. Vertical section of density anomaly for cruise CUC-February 1989: The contour interval is 0.1 kg m^{-3} .

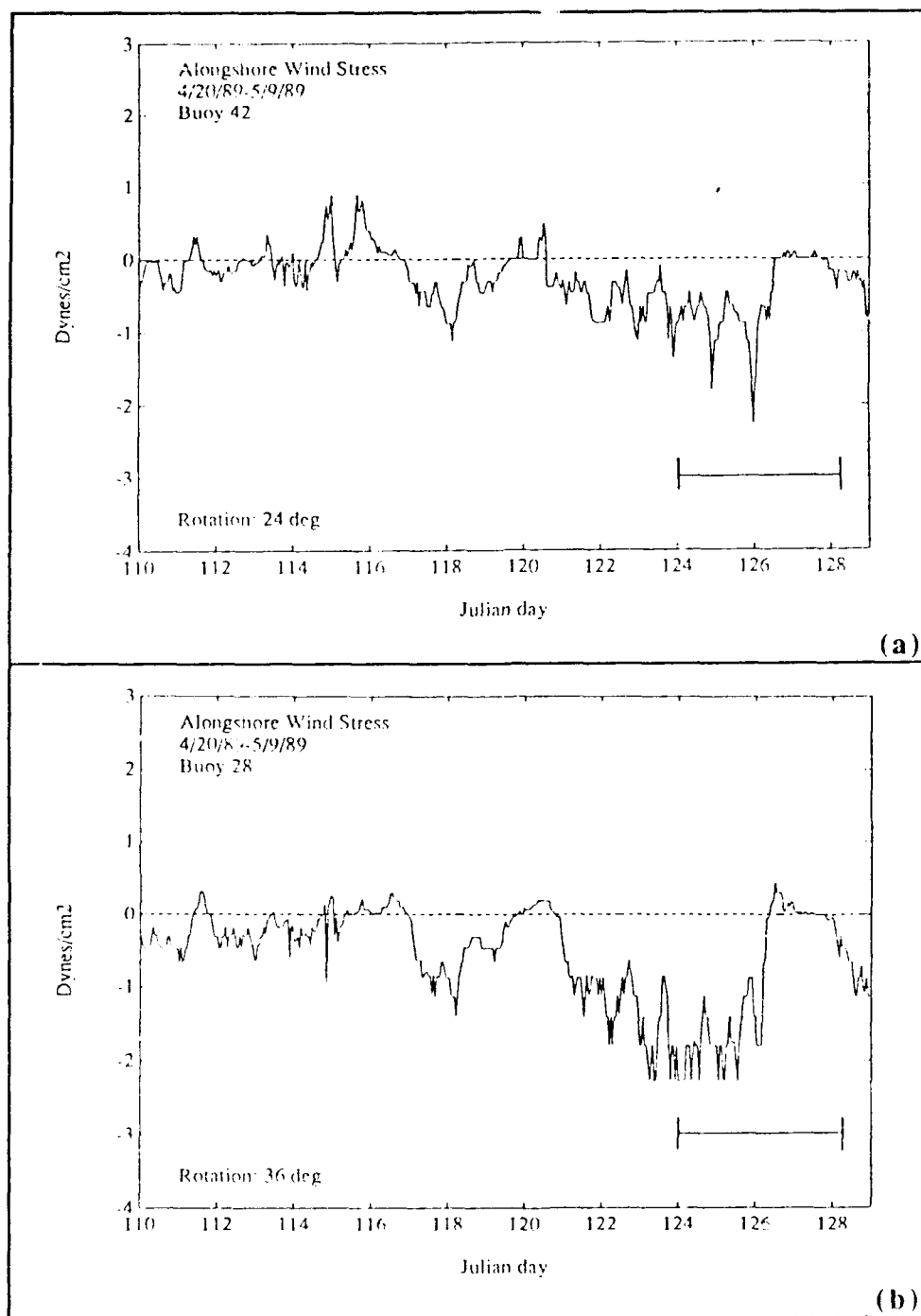


Figure 42. Alongshore component of wind stress during the May 1989 Student Cruise: (a) Wind stress data from buoy 46042, Monterey Bay; (b) Wind stress data from buoy 46028, Cape San Martin. The cruise period is indicated by the solid horizontal line (5/4 = JD 124; 5/8 = JD 128).

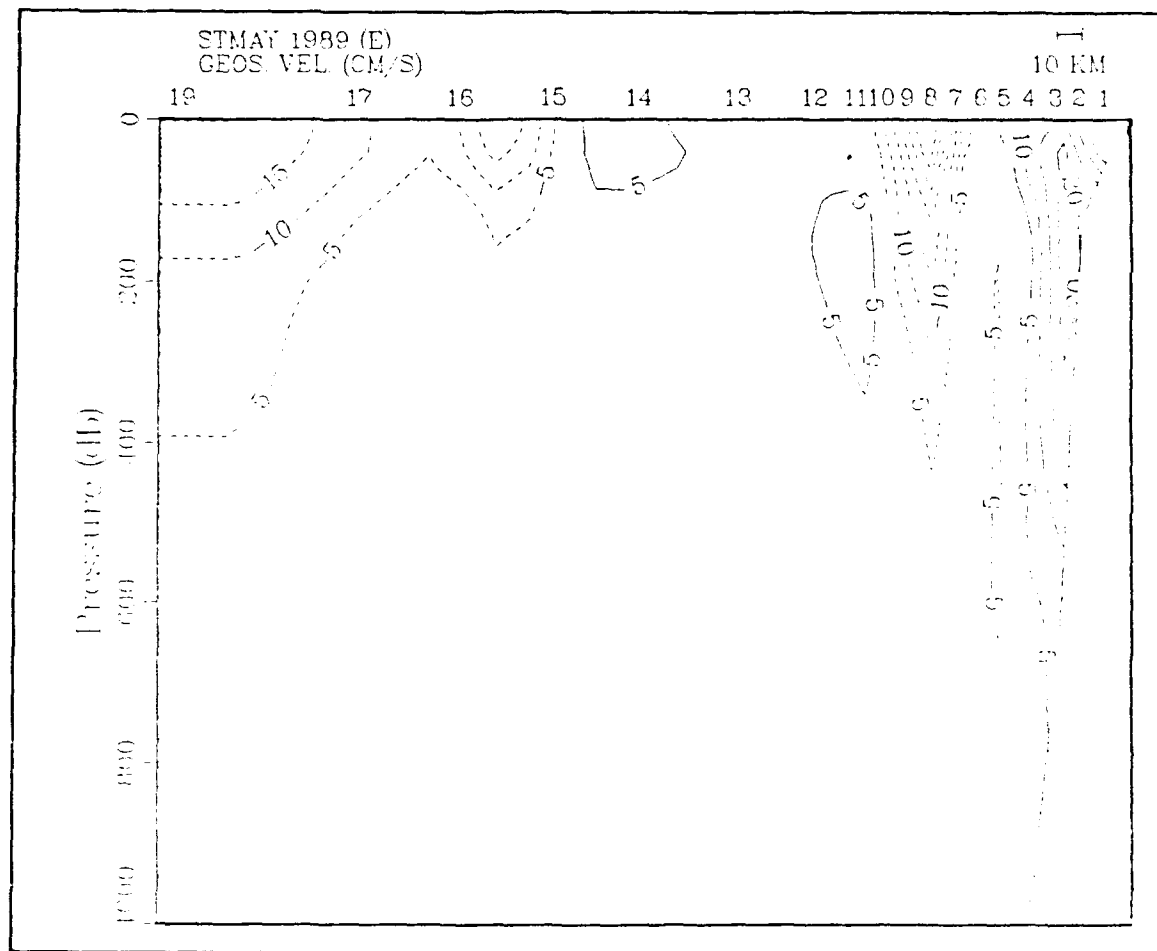


Figure 43. Vertical section (0-1000 dbar) of alongshore geostrophic velocity for the May 1989 student cruise: The contour interval is 5.0 cm s^{-1} . Dashed lines are equatorward and solid lines are poleward.

flows occur where surface density fronts are present, stations 7 through 11 and 14 through 16. A surface equatorward jet (core $v < -40.0 \text{ cm s}^{-1}$, $v < -20.0 \text{ cm s}^{-1}$ at 150 m) is coincident with the density front between stations 7 through 11 (Figure 26). The deeper structure penetrating to a depth of approximately 450 m coincides with the depression of the isopycnals below 200 m (Figure 26). The surface jet is a characteristic feature of an upwelling regime (Huyer 1983). An equatorward ($v < -15.0 \text{ cm s}^{-1}$) jet and weaker poleward jet ($v > 5.0 \text{ cm s}^{-1}$)

coincide with the frontal zone between station 14 and 16. This entire region is believed to be associated with the CC, with poleward flow resulting from the isopycnal slopes (downward toward the coast).

Inshore of station 5 is a region of poleward flow which extends from the surface to a depth of 750 m along the continental slope. In the presence of upwelling favorable winds the CUC is expected to lie at depth along the continental slope with no surface signature (Chelton 1984). However, due to the presence of a salinity minimum near the surface (Figure 24) between stations 3 and 5, poleward flow extends to the surface. Based upon the distribution of salinity, the CUC is believed to lie beneath and is dynamically distinct from the poleward flow at the surface. Isohalines at depth slope upward toward the continental slope characteristic of the more saline waters of the undercurrent, while those at the surface illustrate the presence of a salinity minimum. Surface temperatures between station 4 and 6 were greater than 13°C, making this intrusion warmer and less saline than surrounding waters. This warm region is also reflected in SST from NOAA 11 AVHRR satellite imagery (Figure 44). The upper water column undergoes geostrophic adjustment resulting in near surface poleward flow. The low salinity water may well be ambient surface water trapped between freshly upwelled water inshore and a previously existing front offshore from the equatorward wind event and relaxation six days prior to the cruise.

f. July 1989 alongshore geostrophic velocities (anomalous poleward flow)

Winds for the 14 day period leading up to this cruise were predominantly equatorward with a substantial wind relaxation lasting approximately three days

just two days before the cruise. Winds during the cruise were equatorward at both buoy locations with alongshore wind stress between $-0.75 \text{ dyne cm}^{-2}$ at buoy 46042 and $-2.5 \text{ dyne cm}^{-2}$ at buoy 46028 (Figure 45). The vertical section of alongshore geostrophic velocity (Figure 46) is dominated by poleward flow along most of the transect. Weak equatorward flow ($v > -5.0 \text{ cm s}^{-1}$) is found at the surface offshore of station 17 and the -5.0 cm s^{-1} contour becomes visible near the surface at station 21. There is weak equatorward flow between stations 1 and 2 and 8 and 9 in response to equatorward winds however it is minor compared to the poleward flow.

The strong poleward flow throughout the section is believed to result from the substantial wind relaxation which preceded this cruise. When equatorward winds relax, a residual alongshore pressure gradient can produce a northward acceleration. The wind records indicate that the relaxation at the southern buoy was of longer duration than to the north. In their study of variability along the California shelf induced by local and remote winds during the Coastal Ocean Dynamics Experiment (CODE), Davis and Bogden (1989) discuss a length scale of 500 km associated with remote forcing. Without wind records from buoys farther south it can only be hypothesized that this poleward flow was in response to a large scale wind relaxation which might have occurred previously over the entire central and southern California region. The CUC was observed to occupy the region of the continental slope between 200 m and 600 m, with a core depth of 400 m. Above the CUC, poleward flow is believed to be associated with the wind relaxation discussed earlier. The weaker equatorward flow offshore may be the oceanic response to the dominant equatorward winds.

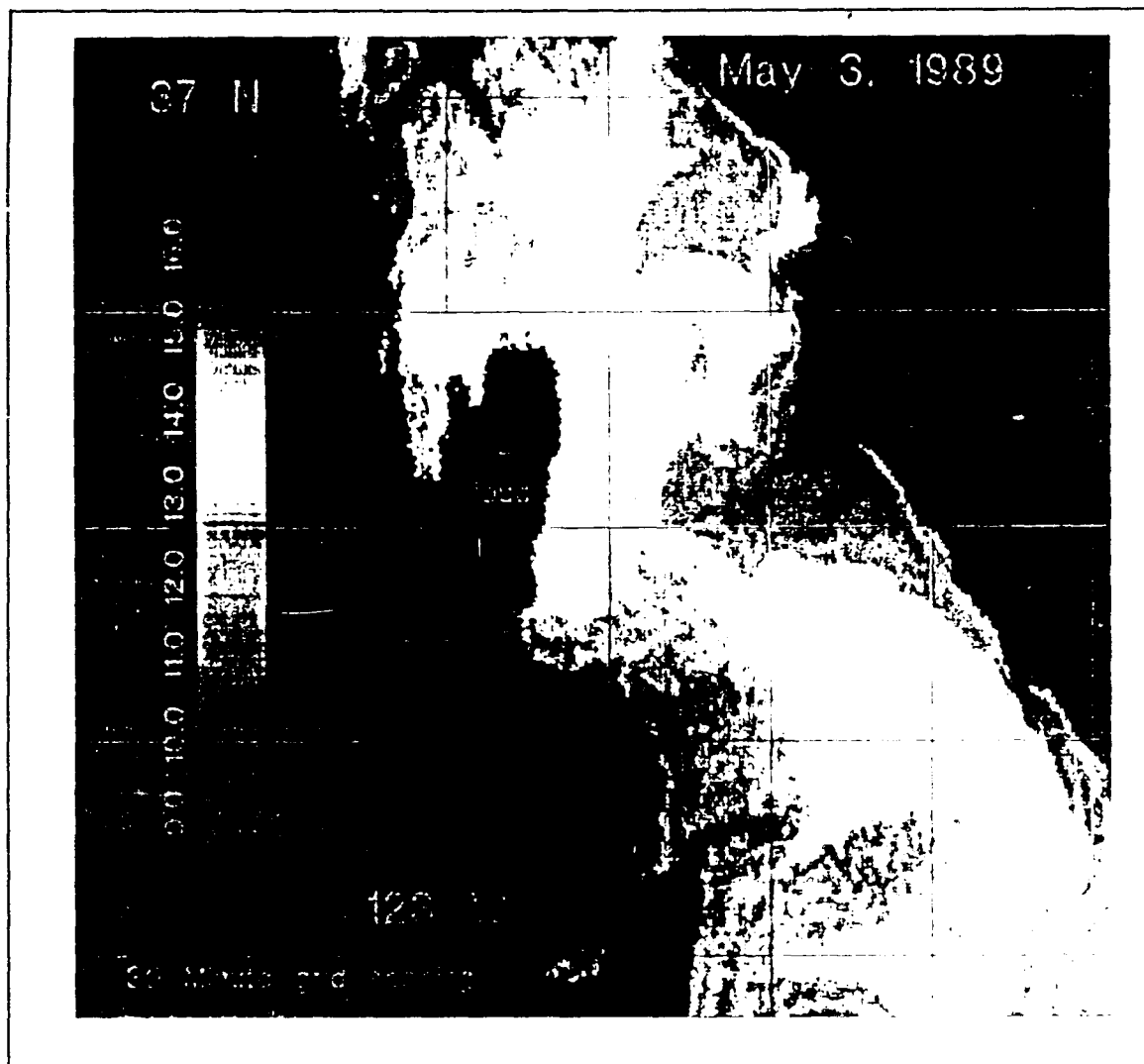


Figure 44. NOAA AVHRR satellite image from 2044 GMT, 3 May 1989: Darker shades near the coast depict colder, more recently upwelled waters. Lighter shades found offshore depict warmer water. SST increases toward the offshore corner of the image. Grid spacing equals 30'. Note the warm region between 122.25°-123.00° W, and 35.75°-36.50° N.

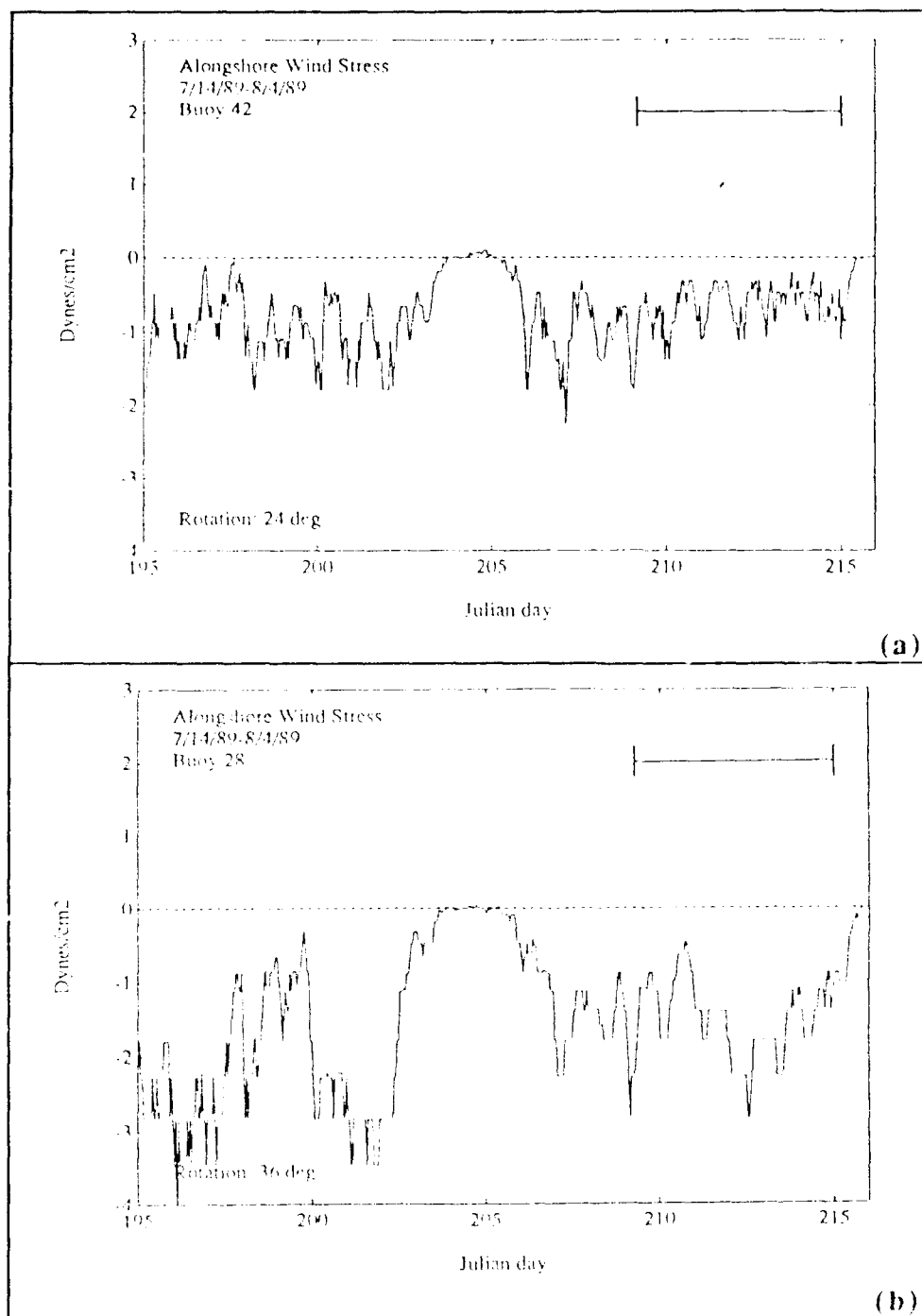


Figure 45. Alongshore component of wind stress during cruise CUC-July 1989: (a) Wind stress data from buoy 46042, Monterey Bay; (b) Wind stress data from buoy 46028, Cape San Martin. The cruise period is indicated by the solid horizontal line (7/28 = JD 209; 8/3 = JD 215).

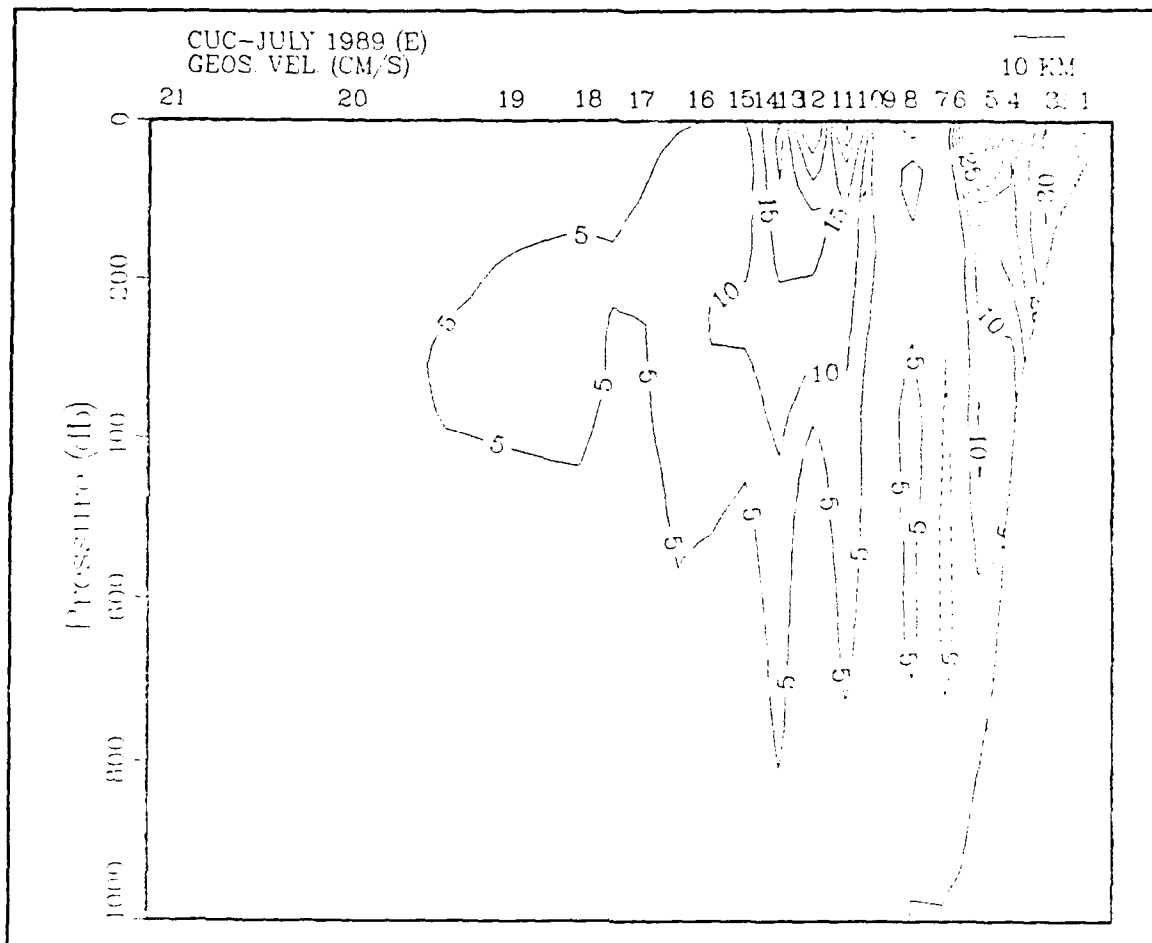


Figure 46. Vertical section (0-1000 dbar) of alongshore geostrophic velocity for cruise CUC-July 1989: The contour interval is 5.0 cm s^{-1} . Dashed lines are equatorward and solid lines are poleward.

This would explain why the poleward flow becomes both deeper and weaker offshore as flow conditions begin to return to normal. Comparisons with similar observations from July 1981 and 1984 (Chelton et al. 1988) follow in Chapter V.

g. November 1989 alongshore geostrophic velocities (deep equatorward flow)

The alongshore component of surface stress (Figure 47) shows a series of equatorward wind events and relaxations prior to and during this

cruise. In opposition to the earlier cruises where the equatorward winds were stronger at the southern buoy, the Monterey Bay buoy reflects greater values of equatorward stress than the Cape San Martin buoy. Unlike the previous six cruises, the choice of 1000 dbar as a level of no motion appears to be in error on this cruise. Focussing on the upper 1000 m (Figure 48), the CC, normally found within the upper 300 m (Lynn and Simpson 1987), has considerable vertical extent. Inshore of station 19 the flow pattern becomes more complicated. The complex pattern shown in Figure 48 may be in response to the rapidly changing wind field during the cruise. From water mass analysis, there was significant intrusion of either North Pacific Central water at depth or an unusually strong recirculation of CUC water between stations 20 and 22, which forced a large area of equatorward flow (Figure 48) extending to depths of more than 700 m near stations 20-22, and poleward flow greater than 5.0 cm s^{-1} extending from 1800 m to the bottom (Figure 49). Deep poleward flow of this magnitude is unlikely and suggests that on this cruise 2000 dbar may have been a better choice for the LNM.

The CUC is observed at the surface between stations 4 and 10, with a subsurface maximum ($v > 35 \text{ cm s}^{-1}$) at a depth of 70 m. Inshore of this is a region of weaker equatorward flow within 15 km of the coast believed to result from the equatorward winds present at the start of the cruise. The poleward flow and strong horizontal velocity gradient seen near station 18 and 19 correspond to the isopycnal slopes (downward toward the coast) and surface front seen in Figure 29.

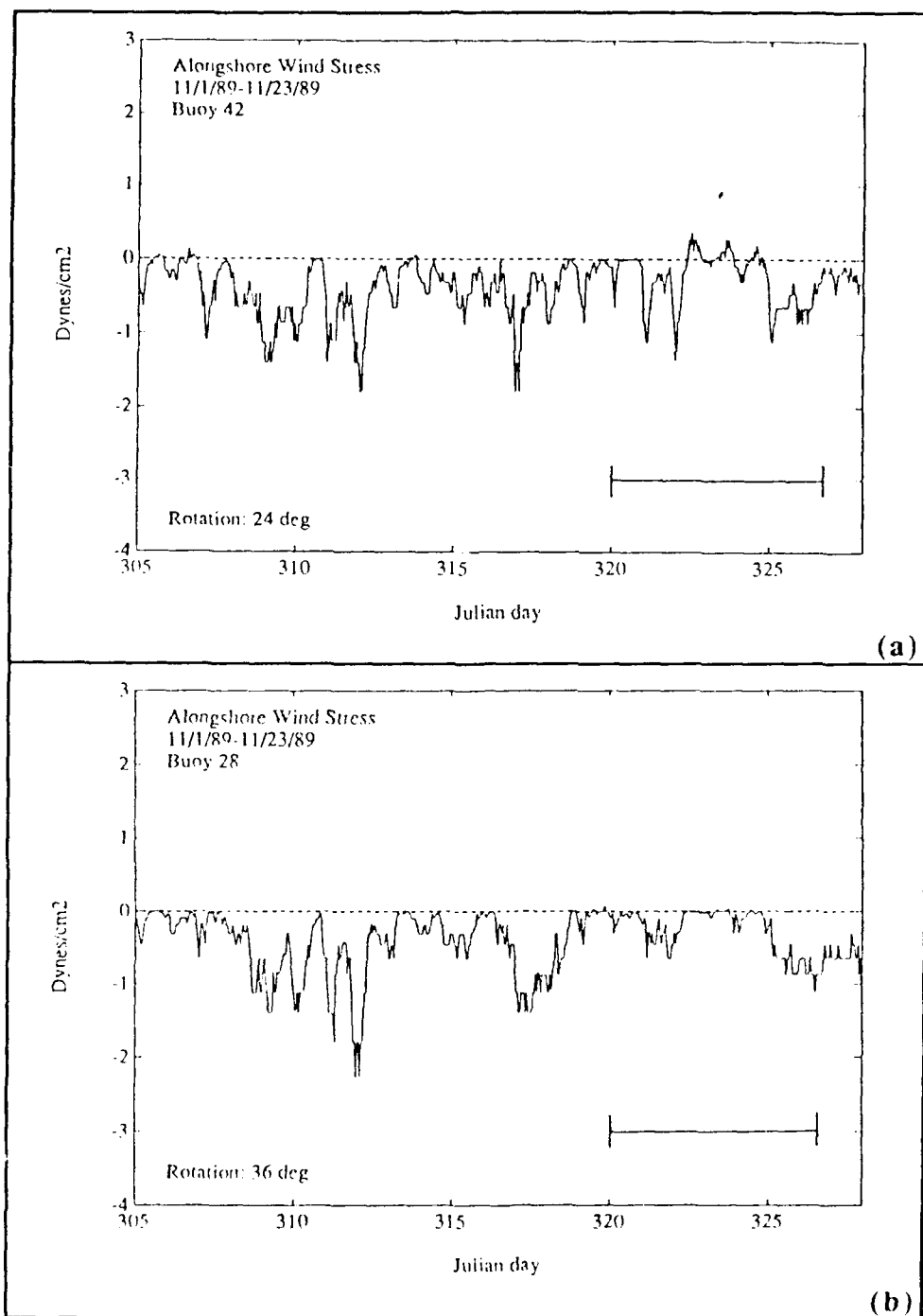


Figure 47. Alongshore component of wind stress during cruise CUC-November 1989: (a) Wind stress data from buoy 46042, Monterey Bay; (b) Wind stress data from buoy 46028, Cape San Martin. The cruise period is indicated by the solid horizontal line (11/15 = JD 320; 11/22 = JD 327).

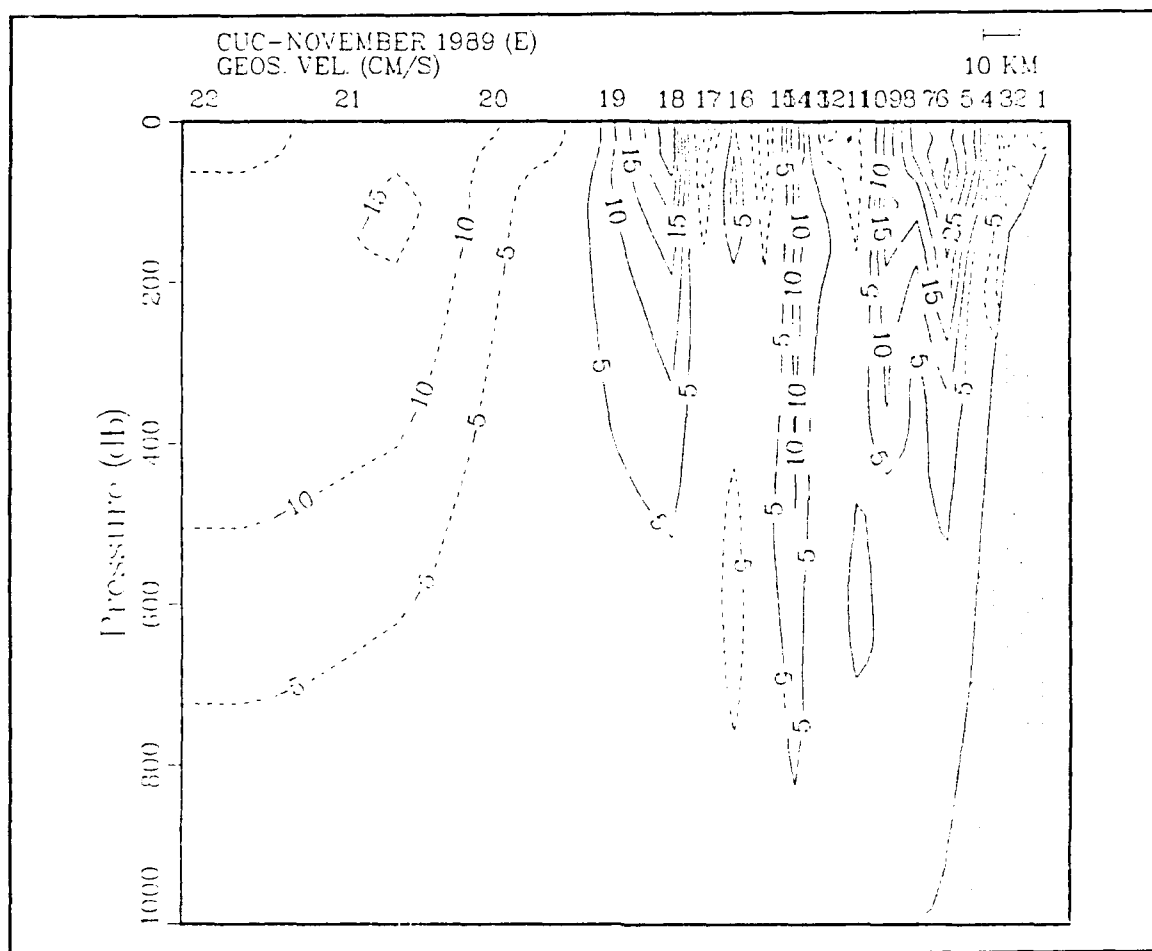


Figure 48. Vertical section (0-1000 dbar) of alongshore geostrophic velocity for cruise CUC-November 1989: The contour interval is 5.0 cm s^{-1} . Dashed lines are equatorward and solid lines are poleward.

Another interesting feature found in all the sections (Figure 49, for example) is the deep banding of the velocity structure which occurs below the reference level between stations 9 and 18. This banding was first noticed by Berryman (1989) in his study of currents off Point Sur during February 1989. The topography in this area is complicated by the presence of the southern extension of the Monterey canyon which is responsible for the steepness of the

continental slope in this area. This banded structure is believed to be the result of high frequency motions interacting with the steep canyon topography. The flow is not in geostrophic balance as the magnitude of flow sometimes reached or exceeded 40 cm s^{-1} (November 1988, not shown). The magnitudes of these flows are far greater than those resulting from error in the calculations supporting the idea that a high frequency motion exists, disturbing the mass field to produce this banded structure, which requires further investigation.

For the sake of uniformity, the reference level was left at 1000 dbar for comparison with earlier cruises. By using a deeper level one would expect to see an increase in the magnitude of the values shown in Figure 48 and the elimination of the deep poleward flow seen in Figure 49.

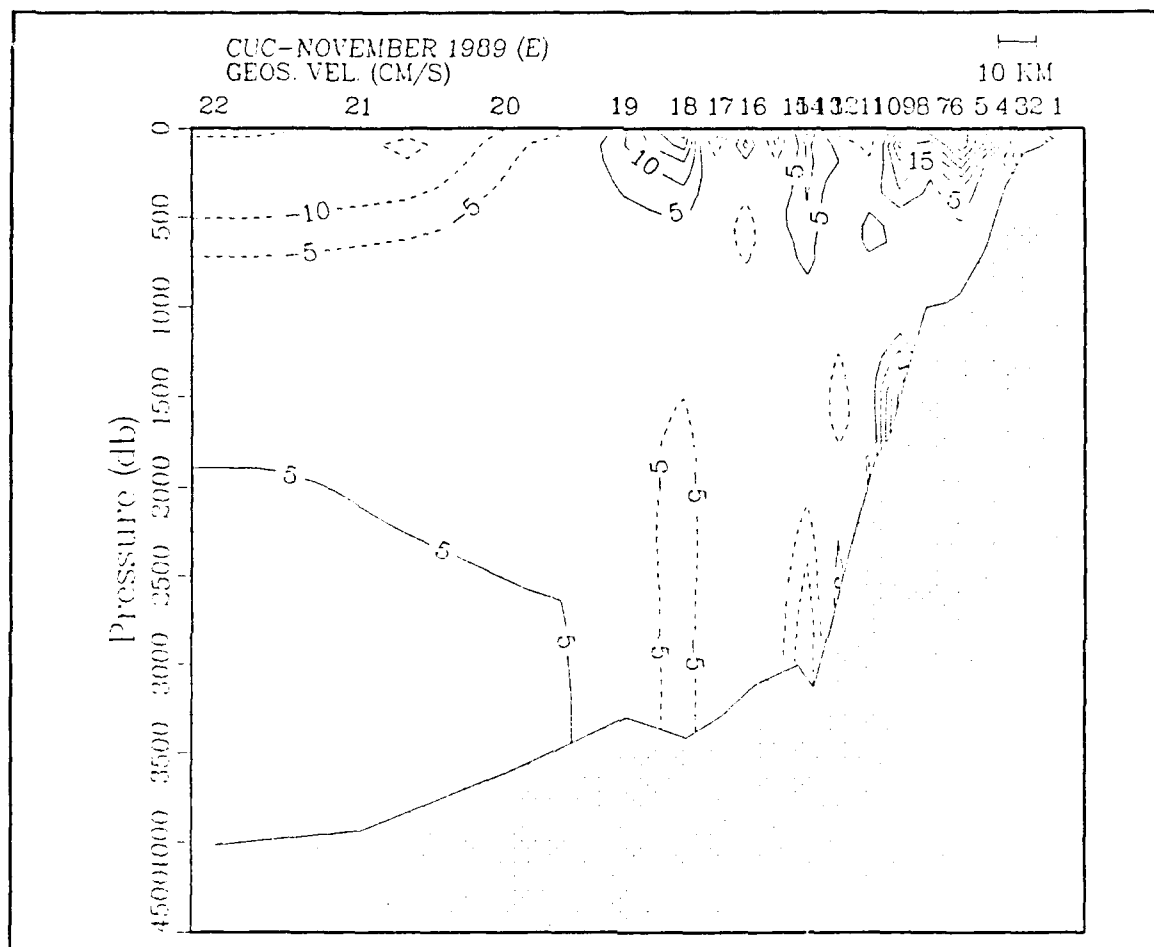


Figure 49. Vertical section (0-4500 dbar) of alongshore geostrophic velocity for cruise CUC-November 1989: The contour interval is 5.0 cm s^{-1} . Dashed lines are equatorward and solid lines are poleward.

V. DISCUSSION

This Chapter focuses on similarities and differences between the observations of this study and those of earlier studies conducted off Point Sur, California, with emphasis placed on the possible dynamics of the flow. As previously mentioned, most of the earlier studies off Point Sur utilized many years of hydrographic data collected in connection with the CalCOFI program, and our observed differences may in most cases lie within the standard deviations from their seasonal averages.

A. WATER MASS CHARACTERISTICS

The water masses present off Point Sur as indicated by the spiciness anomaly appear to be consistent with those discussed by Lynn and Simpson (1987) based on the CalCOFI data set. The core of the CC is characterized by relatively low temperature and low salinity. The western boundary of the CC as defined by Lynn and Simpson (1987) is a salinity frontal structure which lies between the southern extension of the Subarctic Frontal Zone and waters of the eastern North Pacific. Along CalCOFI line 70 (Figure 50), the mean salinity for July along the surface where $\sigma_t = 25.0$ shows a minimum of less than 33.0 PSU between 124° and 125° W. Observations from May 1988 and November 1988 (not shown) also reveal salinities less 33.0 PSU near the surface in the CC, while during May 1989 (Figure 24) and November 1989 (not shown), values less than 32.9 PSU were observed. Salinity values less than 32.8 PSU were observed in the CC during August 1988 (Figure 14). The Coastal Transition Zone (CTZ) sampling grid covers a section of the northern California coast approximately 200 km in

length, including Point Arena and Point Reyes, and extends to about 200 km offshore (Huyer et al. 1990). Surface salinities found in the offshore region of the CTZ sampling grid in the summer of 1988 were commonly less than 33.0 PSU with a low salinity core ($S < 32.6$ PSU) extending offshore from Point Arena coincident with a strong baroclinic jet (Huyer et al. 1990). During the survey period a sharp meander developed in this jet. The lower salinity values

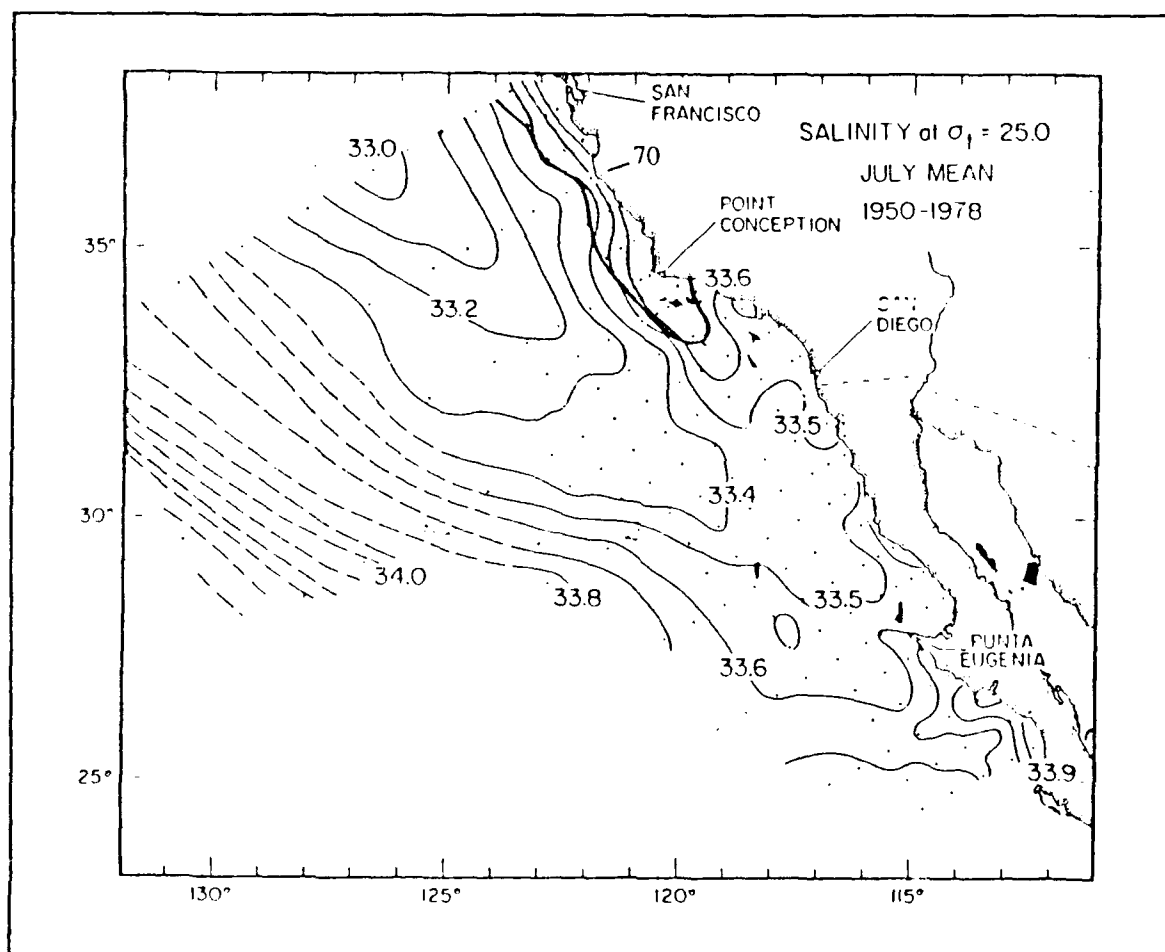


Figure 50. Mean salinity on the surface where $\sigma_t = 25.0$ for July:
 The data presented here comes from the CalCOFI data set.
 The bold line represents the intersection of this density surface
 and the sea surface. The density is less inshore of the bold line.
 Contour interval is 0.1 PSU. (Source: Lynn and Simpson 1987)

observed along the POST are characteristic of waters farther to the north and may result from the southern transport of fresher water through energetic jets and meanders present within the transition zone as described by Lynn and Simpson (1987) and the Coastal Transition Zone Experiment.

Unusually high surface salinities (>33.5 PSU) were observed during the July 1989 cruise, nearly 0.6 PSU higher than the August 1988 cruise. Chelton et al. (1988) also found anomalously high salinity values off Point Sur in July 1981 and July 1984. Salinities at the 10 m level for both these periods (Figure 51) show intrusions of higher salinity water from the south in opposition to the surface equatorward winds, suggestive of remote forcing from the south. The vertical sections of salinity from August 1988 (Figure 14) and July 1989 (Figure 28), illustrate that the surface values were much higher in 1989 and appear to mimic the conditions observed by Chelton et al. (1988).

The deep intrusion of warm, salty water and accompanying deep equatorward flow in November 1989 is a significant deviation from the normal seasonal picture of this area. Below 200 m over the entire POST the isopycnals (Figure 29) have a domed appearance centered at station 19 and slope downward both offshore and inshore. This doming of the isopycnal surfaces is common during winter off the California coast (Reid 1973). The intrusion of the warmer, more saline water may represent either North Pacific Central water which usually lies farther offshore (128° W at this latitude, Lynn and Simpson 1987) or an unusually strong recirculation of CUC water. Similar but weaker intrusions were also observed in August 1988, May 1989, and July 1989 and may again result from either of these sources. To determine the exact cause a more intensive T-S analysis is required.

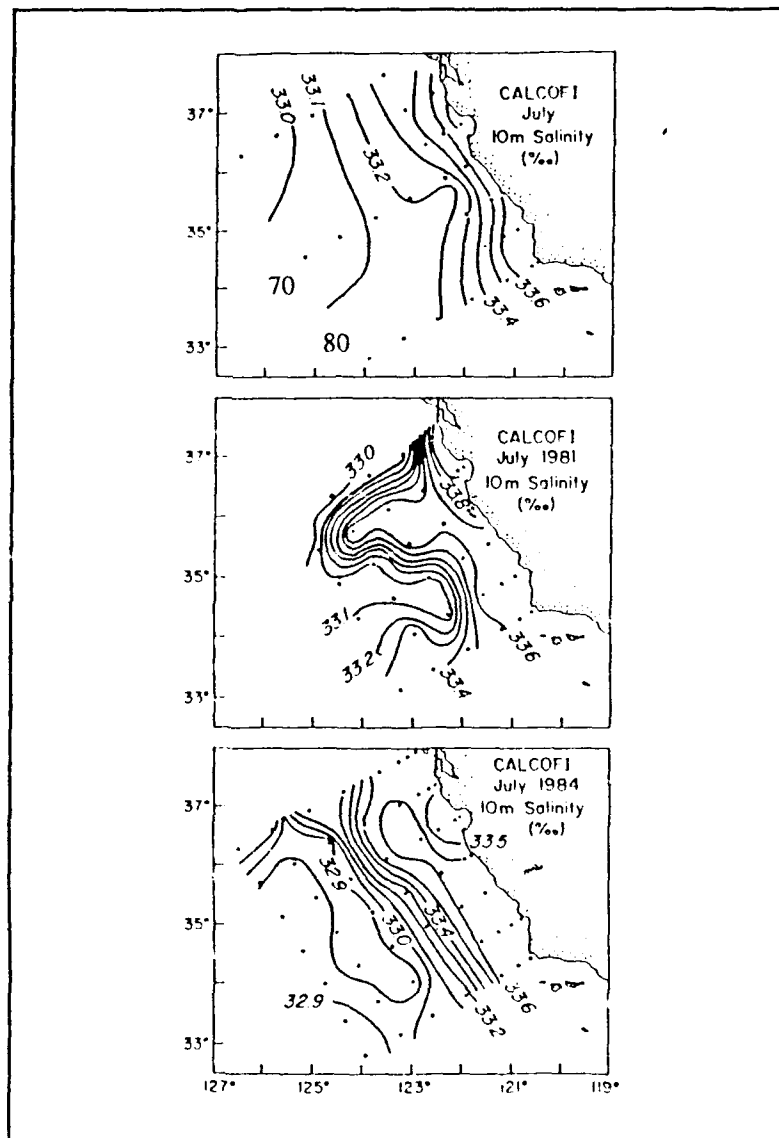


Figure 51. Horizontal sections of salinity at 10 m depth from CalCOFI data: The top section illustrates the July seasonal average; the center section illustrates the conditions for July 1981; the bottom section illustrates the conditions for July 1984. (Source: Chelton et al. 1988)

B. ALONGSHORE GEOSTROPHIC VELOCITIES

In his study of alongshore geostrophic velocities along the central California coast, Chelton (1984) used 23 years of hydrographic data along CalCOFI lines 70

and 80, off Point Sur and Point Conception, respectively, to establish the seasonal variability of alongshore geostrophic currents across these sections. His analysis was restricted to stations where the bottom depth exceeded 500 m, which was roughly within 15 km of the coast off Point Sur. These historical data (Figure 52) reveal the CC within the upper 200 m flowing equatorward with its core located between 100 and 200 km off the coast. There are two maxima during the year, between February and March and July through September where the velocities exceed -9.0 cm s^{-1} . A narrow second maximum occurs near the coast during March-April and July-September with velocities exceeding -7.5 cm s^{-1} and -5.0 cm s^{-1} , respectively. Chelton (1984) indicates this narrow jet may be even more intense over the continental shelf. This banded flow structure was also observed by Lynn and Simpson (1987), who found that equatorward flow in excess of -4 cm s^{-1} rarely occurred. The CUC off Point Sur (Figure 52) appears to be confined to the continental slope within 75-100 km of the coast, with no nearshore poleward flow at depth in March through May. Poleward flow extends to the surface from October through February (the Davidson Current?) with a maximum surface velocity of 14.0 cm s^{-1} in December, and is subsurface throughout the remainder of the year. Chelton points out that while seasonal poleward flow is small near 500 dbar, it may not necessarily be zero suggesting the use of 500 dbar as the LNM may be in error. Based upon the observations of our study the use of 500 dbar as the LNM is clearly in error. Equatorward flow associated with the CC was observed below 500 dbar on several occasions and the nearshore poleward flow of CUC was found as deep as 600 m in some cases.

Peak velocities of the CC and CUC along the POST typically exceeded those observed during CalCOFI (Figure 52). The CC had velocities in excess of -20.0

cm s^{-1} in May 1988, November 1988 and May 1989. The CUC had velocities in excess of 35 cm s^{-1} in August 1988, February 1989 and November 1989. These

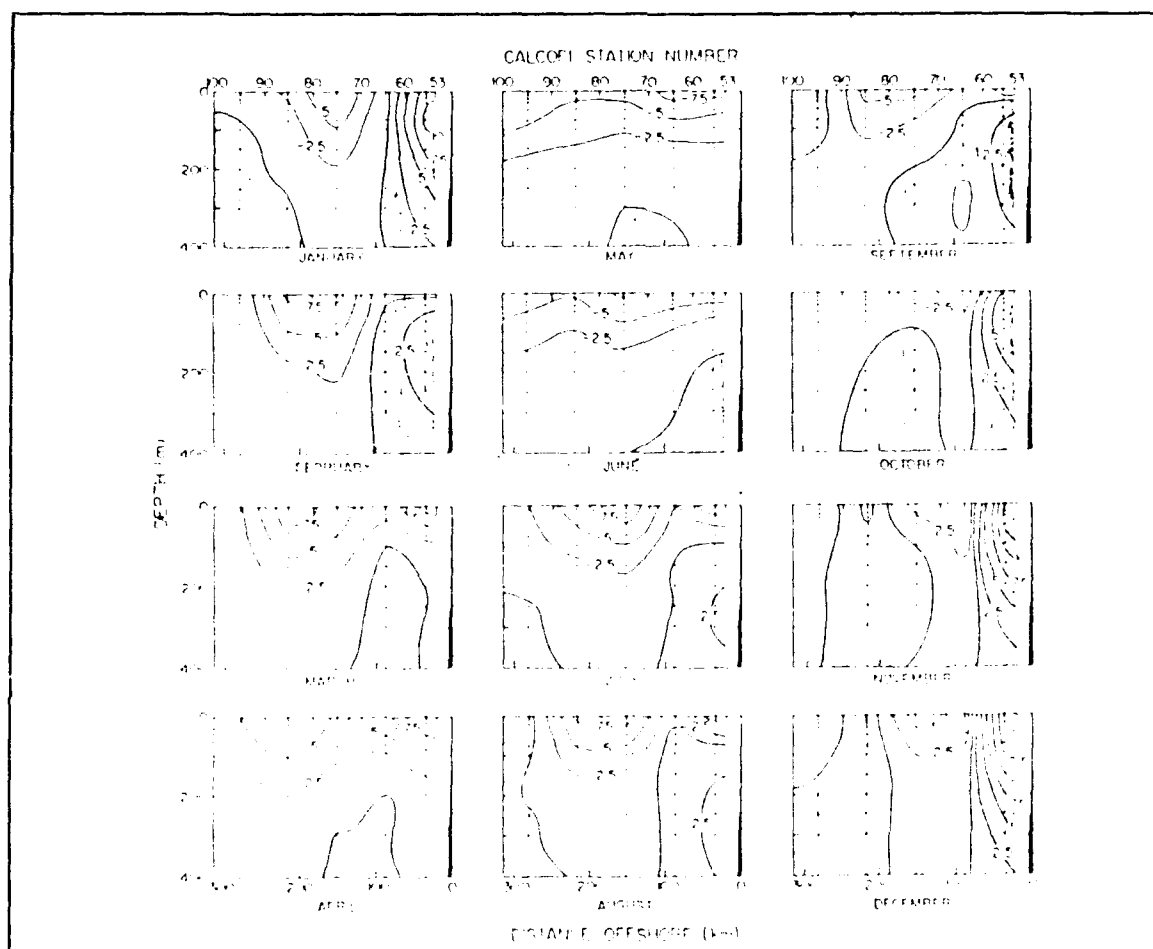


Figure 52. Vertical section (0-400 m) of seasonal alongshore geostrophic velocity relative to 500 dbar along CalCOFI line 70 off Point Sur: Shaded regions depict poleward flow. The contour interval is 2.5 cm s^{-1} . (Source: Chelton 1984)

higher geostrophic velocities were likely the result of: 1) the decreased station spacing of the POST; and 2) the deeper LNM used in this study. Chelton (1984) points out that the coarse station spacing associated with the CalCOFI sampling grid tends to provide a smoothed version of the flow field and potentially misses

narrow, higher velocity jets near the coast. The decreased station spacing inshore provides better definition of these narrow jets and increases the magnitude of the mean flow. Significant vertical shear still existed at and below 500 dbar, which suggests that the deeper LNM contributed to the larger surface velocities observed in this study.

Based upon the analysis of water mass characteristics and geostrophic velocities, the spatial extent and peak core velocities of the CUC for each of the cruises have been defined (Table 8). The core of the undercurrent was observed within 42 km of the coast and between 70 m to 460 m depths on all cruises, which generally agrees with the observations of Wickham et al. (1987). These values are much greater than those shown in Figure 50 and may be the result of decreased station spacing near the coast. The CUC was present at the surface in February 1989 and November 1989 and subsurface throughout the remainder of the year, similar to the results of Chelton (1984). Poleward flow was only present at the surface inshore of station 3 (Figure 37) due to the presence of a strong mesoscale feature in November 1988, and was below this feature offshore. Wickham et al. (1987) observed increased temperatures and salinities nearshore in winter within the upper layers. The warmest and saltiest waters were found at the depth of the CUC in agreement with the observations of Wooster and Jones (1970) off northern Baja California, who also observed the CUC at depth below shallow weak equatorward and sometimes poleward flow in summer. From their observations off northern Baja near 31°N, Wooster and Jones (1970) found the CUC to lie close to continental slope. It had a width of approximately 20 km, a thickness of 300 m, and velocities approaching 30 cm s⁻¹. These earlier studies agree favorably with the observations of this

study although their measurements were taken off Cape San Martin, roughly 70 km south of Point Sur, and northern Baja, roughly 800 km to the south,

Table 8. SPATIAL EXTENT AND CORE VELOCITIES OF THE CALIFORNIA UNDERCURRENT: Based upon the observations from seven cruises along the Point Sur Transect between May 1988 and November 1989.

Cruise	Distance from shore (km)	Core depth (m)	Maximum Velocity (cm s^{-1})
STMAY 1988	22	460	< 5
CUC-August 1988	12 / 42	190	> 35 / > 20
CUC-November 1988	20	460	> 25
CUC-February 1989	15	100	> 35
STMAY 1989	17	160	> 20
CUC-July 1989	23	400	> 10
CUC-November 1989	28	70	> 35

indicating properties of the CUC are not observed to vary widely along the California coast.

The strong poleward surface flow observed in May 1989 inshore of station 5 (Figure 43) appeared to be the result of warmer, fresher water at the surface, not associated with the CUC, which was observed at depth. This poleward flow resulted from the geostrophic adjustment of the water column in response to the warm, fresh water found near the surface farther offshore. Strong poleward surface flow was also observed in August 1988 and July 1989 although the dynamics involved differ from the flow observed in May 1989. In July 1989, a significant relaxation of equatorward winds (Figure 45) occurred two days prior

to this cruise and lasted three days. The magnitude of this relaxation was greater at the southern buoy, 46028.

The reversal of near surface currents in response to relaxation of equatorward winds has been observed using moored current meters during CODE (Davis 1985). In May 1981, equatorward winds of 10 m s^{-1} at central CODE stations relaxed to 5 m s^{-1} . Within one day after this relaxation current meters located 125 km to the south (in the southern section of the CODE region) exhibited a reversal in flow from equatorward to poleward. Three days later this flow reversal was present in current meters 70 km to the north of the southern current meters, indicating poleward propagation of this event. Davis and Bogden (1989) discuss the effect of local and remote wind forcing on shelf circulation in the CODE region. In their study, coastally trapped waves depicted in sea level records were found to be coherent with coastal winds 500 km to the south. It is hypothesized that the strong poleward flow exhibited in the July 1989 alongshore geostrophic velocities (Figure 46) was in response to remote forcing from the south, and the weak equatorward flow and deeper poleward flow offshore represent the oceanic response to the onset of equatorward winds. Further evidence to support this hypothesis comes from Chelton et al. (1988) as discussed earlier. Salinities at the 10 m level for July 1981 and July 1984 were higher than those from the seasonal average for July from the CalCOFI data set and are characteristic of those found farther south, indicative of poleward flow.

In August 1988 a region of intense poleward flow was observed at the surface within 20 km of the coast (Figure 34). A brief period of intense equatorward winds preceded the cruise by four days (Figure 33), followed by a calm period lasting two to three days into the cruise. Present understanding

suggests that inshore countercurrents may in part be driven by: 1) the wind stress curl and 2) alongshore pressure gradients which are set up to balance strong equatorward winds. When the winds relax, a residual pressure gradient produces a northward acceleration and hence poleward flow (Huyer et al. 1989). Drogue trajectories from August 1972 depict strong poleward ($v > 50 \text{ cm s}^{-1}$) flow inshore between Point Sur and Cypress Point which was much stronger than the corresponding geostrophic currents. Due to the design of these early drogues, they were not truly Lagrangian (move along with currents), but were subject to wind forcing as well, which would produce the higher speeds observed. Additionally, deformations of the reference level due to internal waves may also contribute to the observed difference between the flow observed by drogues and geostrophy (Wickham 1975). A possible explanation for the unusually intense poleward flow observed in our study is that it may be a response to the relaxation of equatorward winds, however the relaxation occurred four days prior to the cruise, a time scale longer than expected from earlier studies. The exact cause is not known.

The intense equatorward flow found inshore of station 5 during the February 1989 cruise (Figure 40) requires further discussion. Velocities in excess of -40 cm s^{-1} were observed in a time of weak or no winds (Figure 39). The vertical section of salinity depicts a salinity minimum ($S < 33.3 \text{ PSU}$) which corresponds to the minimum observed in the density field (Figure 41) between stations 4 and 7. Salinity minima in coastal regions during winter usually result from excess river run-off, however drought conditions have existed throughout central and southern California since 1988. Therefore, this lower salinity water is not expected to be the result of river run-off. An equatorward wind event which

occurred just prior to the cruise and subsequent offshore transport may be responsible for the weak frontal structure seen in the density field. It is hypothesized that the lower salinity water was just ambient surface water trapped between previously upwelled water and higher salinity water found near the coast. The observed equatorward flow would then have resulted from the geostrophic adjustment of the water column inshore. However, the lack of wind data from the Monterey Bay buoy and the exact cause of the lower salinity water leave this hypothesis unsubstantiated.

The deep equatorward flow found offshore during November 1989 suggests an error in the use of 1000 dbar as the LNM. Due to the intrusion of North Pacific Central water, the equatorward flow of the CC penetrated deep within the water column. The deep (ageostrophic) flow exhibited near the steep topography of the Monterey Canyon was a feature present in all the cruises. Shepard (1975) indicates that alternating up- and downcanyon currents with velocities reaching 50 cm s^{-1} can be found in submarine canyons. Internal waves, mostly near tidal frequencies, advance up submarine canyons and rarely downward (Shepard 1975). Strong downcanyon flows may result from unusual canyon bathymetry. It is believed that these deep ageostrophic flows are the result of high frequency motions interacting with the steep bathymetry of the Monterey canyon where it crosses the POST, and deserves closer study in the future.

VI. CONCLUSIONS AND RECOMMENDATIONS

A. CONCLUSIONS

The purpose of this study was to determine the seasonal variability of geostrophic velocities and water mass characteristics along the Point Sur Transect (POST). Observations presented throughout this study, however, appear to have revealed interannual rather than seasonal variability. This is not surprising since only seven cruises were selected for study whereas earlier studies utilized many years of data collected along the CalCOFI sampling grid to determine the seasonal means. This study excelled over the continental shelf and slope where the station spacing of the POST is considerably closer than the CalCOFI scheme. This decreased spacing enabled the study of narrow coastal jets which could not be studied effectively using the CalCOFI scheme (Chelton 1984).

On all cruises the flow pattern inshore depicted narrow bands of both poleward and equatorward flow demonstrating the complexity of the shelf/slope region off Point Sur. In general, observations of large scale features such as the CC and in some cases the CUC were in agreement with the studies of Chelton (1984) and Lynn and Simpson (1987). The nature of the alongshore geostrophic velocities and the location and spatial extent of the undercurrent appear to be strongly related to specific wind events, both local and remote. Observed differences represent deviations from the seasonal averages of these earlier studies and may fall within the standard deviations of the seasonal averages, which were not discussed by the earlier authors.

Significant deviations from these seasonal averages included;

- a weak undercurrent in the presence of strong equatorward wind stress in May 1988;
- the lack of surface equatorward flow during a period of strong equatorward wind stress in July 1989;
- the presence of unusually high surface salinities of southern origin in July 1989 suggestive of remote forcing from the south resulting in unusually strong poleward flow throughout the water column;
- the unusually strong and deep penetration of warm, saline waters offshore in November 1989 resulting in an extremely deep signature of the CC;
- generally larger magnitudes observed in equatorward flow associated with the CC resulting from a deeper LNM;
- larger magnitudes observed in poleward flow associated with the CUC resulting from the closer spacing of stations along the POST;
- definition of complex banded flow near the coast over the continental shelf and slope resulting from the closer spacing of stations along the POST;
- deep, bottom trapped ageostrophic flow along the continental slope near 2500 m depth, near the head of a branch of the Monterey Canyon.

This last feature was present on all cruises with variable intensity due to differences in station spacing and the variability normally associated with higher frequency motions. The strength and persistence of the phenomenon suggest that it is real and not the result of errors in sampling and/or computational processes.

B. RECOMMENDATIONS

This study focussed on only seven cruises selected to represent specific seasons. A better understanding of seasonal and temporal variability would be obtained by using all of the cruises to date along the POST. This not only

includes using the hydrographic data, but ADCP and PEGASUS data collected concurrently with CTD data, and current meters which have been placed at several locations along the POST since 1988. The time scales of phenomena off Point Sur can be resolved by these current meters and will aid in the interpretation of the hydrographic data. As this data base continues to grow so will our understanding of the processes which occur along the POST.

The wind relaxation and subsequent poleward flow in July 1989 were suggestive of remote forcing from farther south. Wind records from NOAA buoys to the south were not available at the time of this study however they should be obtained and incorporated into future studies along the POST. Such information would provide insight into the cause of such intense bursts of poleward flow as observed in July 1989.

The intrusion of warm, salty water in the offshore section of the POST was a feature common to several cruises. It appears to be either North Pacific Central water or an unusually strong recirculation of CUC water. A more rigorous T-S analysis is required to determine the exact cause of the warm, salty water.

Oceanographic data frequently requires interpolation to provide initial conditions for models, estimation of transports, and wave number spectra (McIntosh 1990). In recent years the use of objective analysis has gained increasing popularity in the representation of hydrographic data (Bretherton et al. 1976; Roemmich 1983), modeling of mesoscale features (Reinecker et al. 1987), and in the interpretation and analysis of satellite imagery (Kelley and Caruso 1990; Wahl and Simpson 1990). Objective analysis commonly refers to a statistical interpolation method based on the Gauss-Markov theorem (Bretherton et al. 1976) and has been used to map hydrographic station data and derived

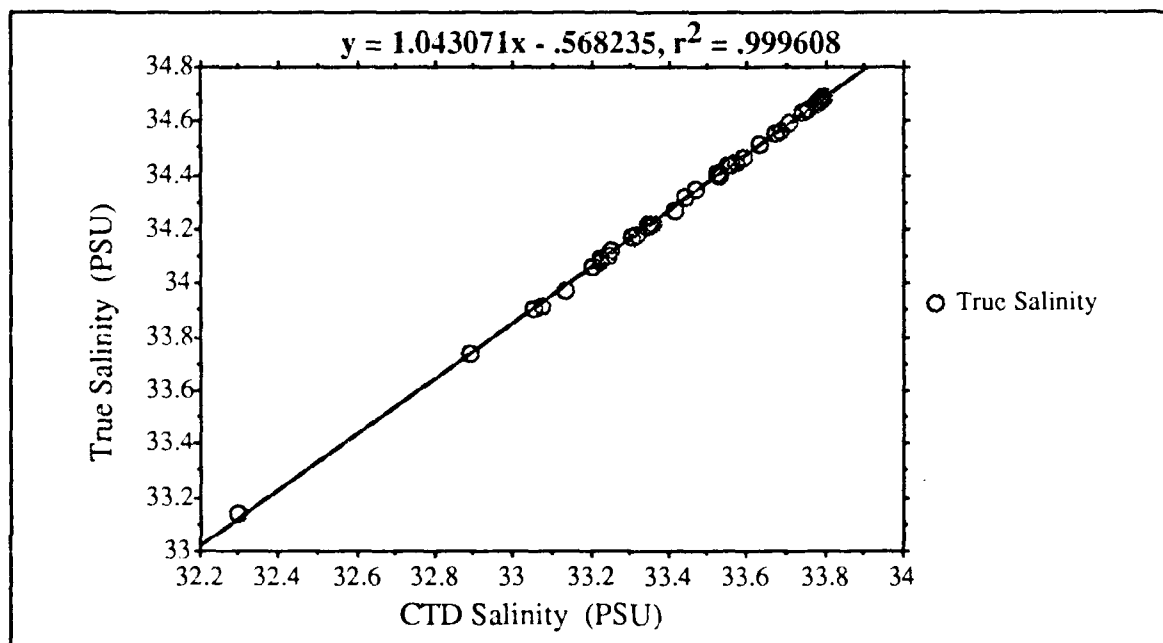
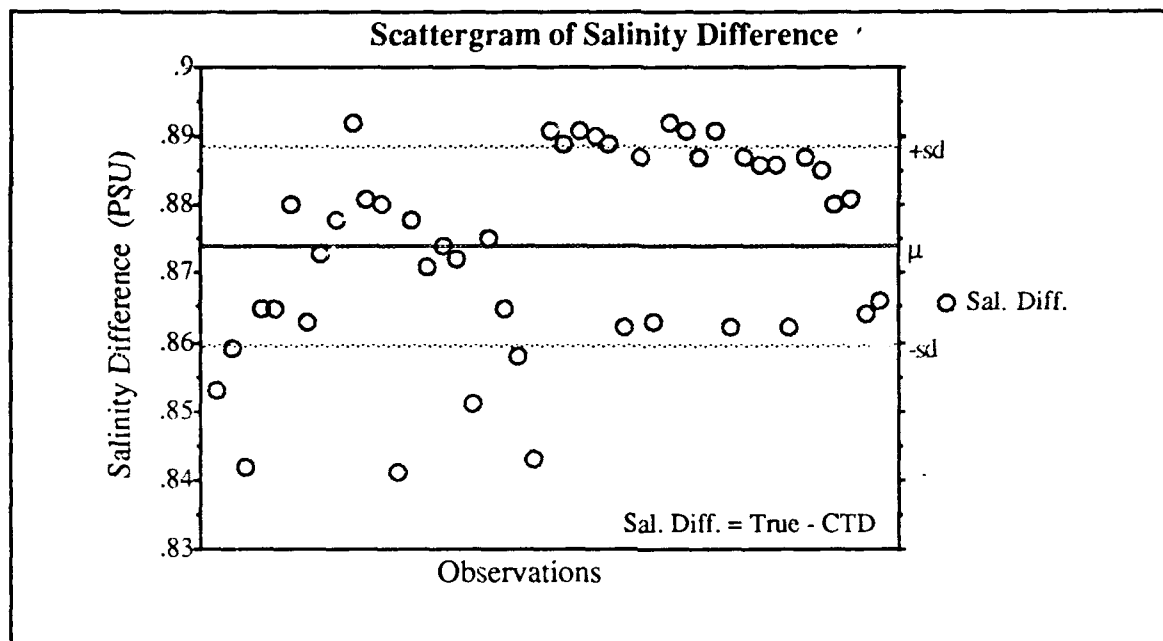
fields such as density, salinity anomaly, and geostrophic velocity to standard positions and depths. This technique provides an alternative to the shear extrapolation techniques presently used. It has the advantage of utilizing all the available data whereas present extrapolation techniques utilize data between adjacent stations pairs to fill in the region below the deepest common depth to a station pair. Such techniques are artificial and may result in larger errors than objective techniques, especially when computing transports (Roemmich 1983).

Interpolation of temperature and salinity data to a uniform grid using an objective analysis technique similar to that of Bretherton et al. (1976) or McIntosh (1990), which utilizes splines (a curve, properly weighted, so that it passes smoothly through each point) would provide a uniform basis upon which more rigorous seasonal and interannual comparisons could be made. This would eliminate problems associated with stations not being occupied on consecutive cruises due to operational considerations, and those inherent in artificial extrapolation techniques where the bottom depth becomes shallower than the reference level.

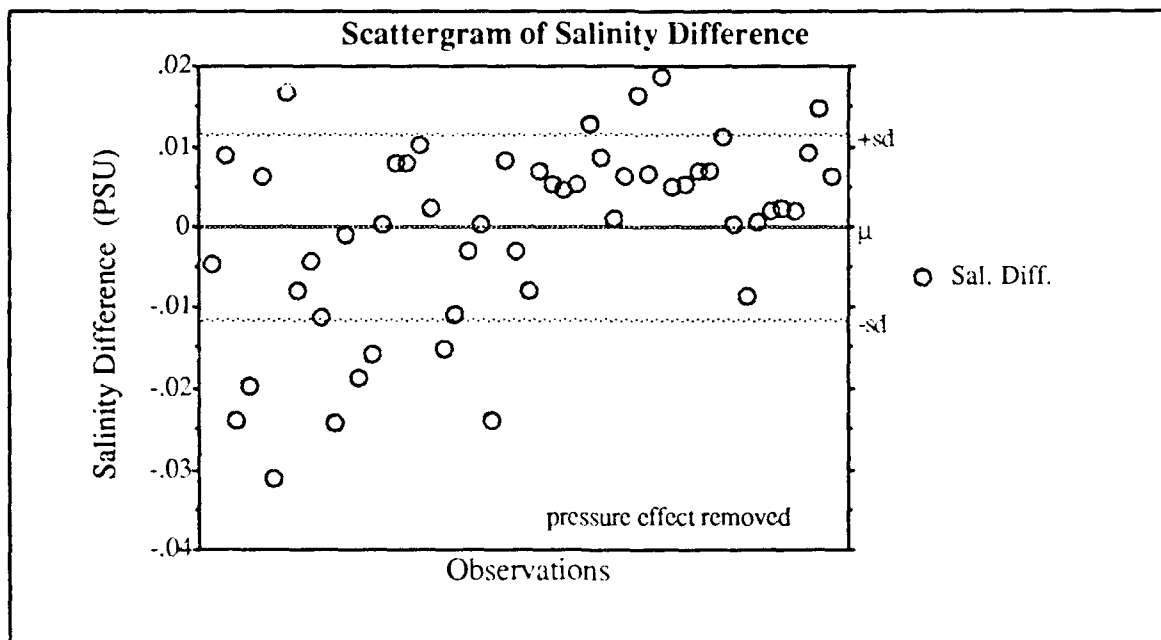
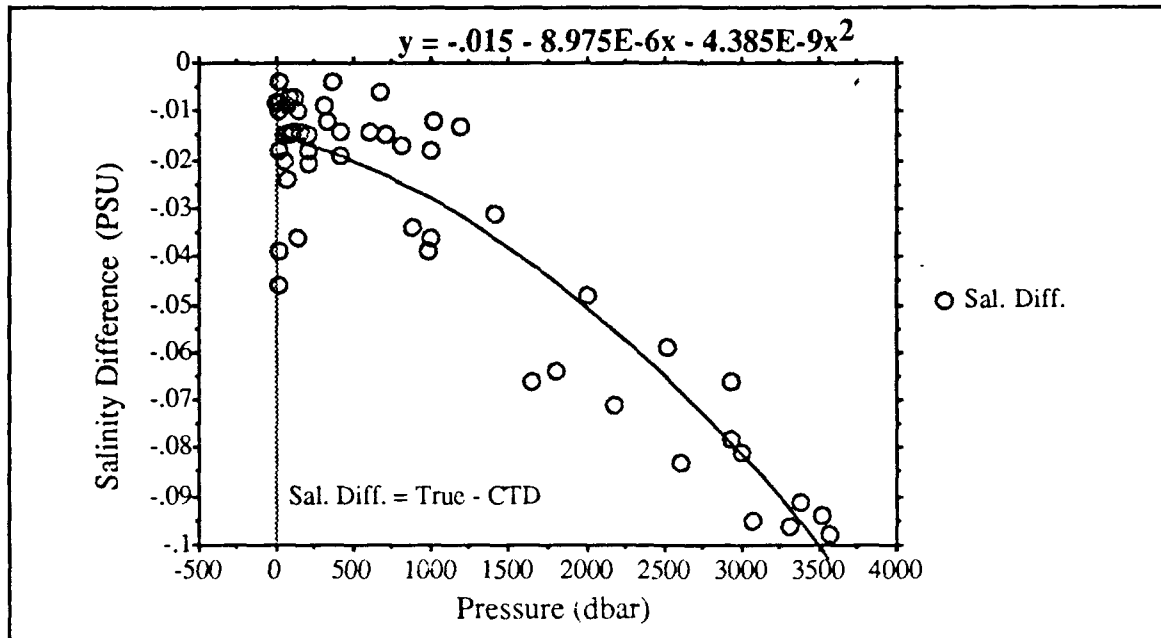
APPENDIX A. CALIBRATION INFORMATION AND DEEP T-S CURVES

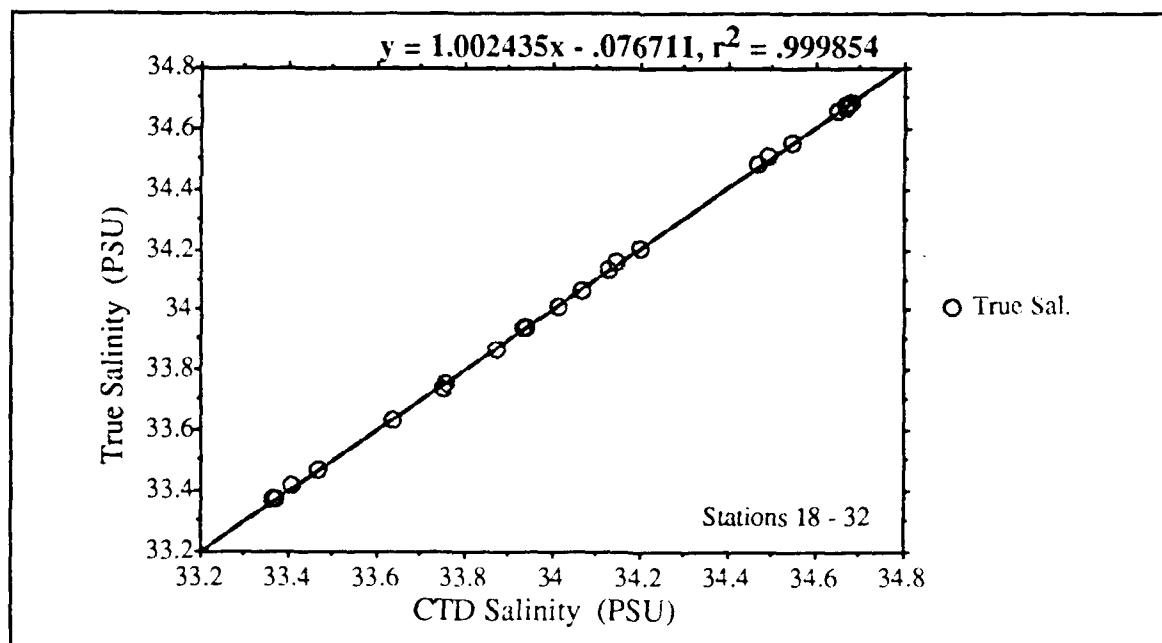
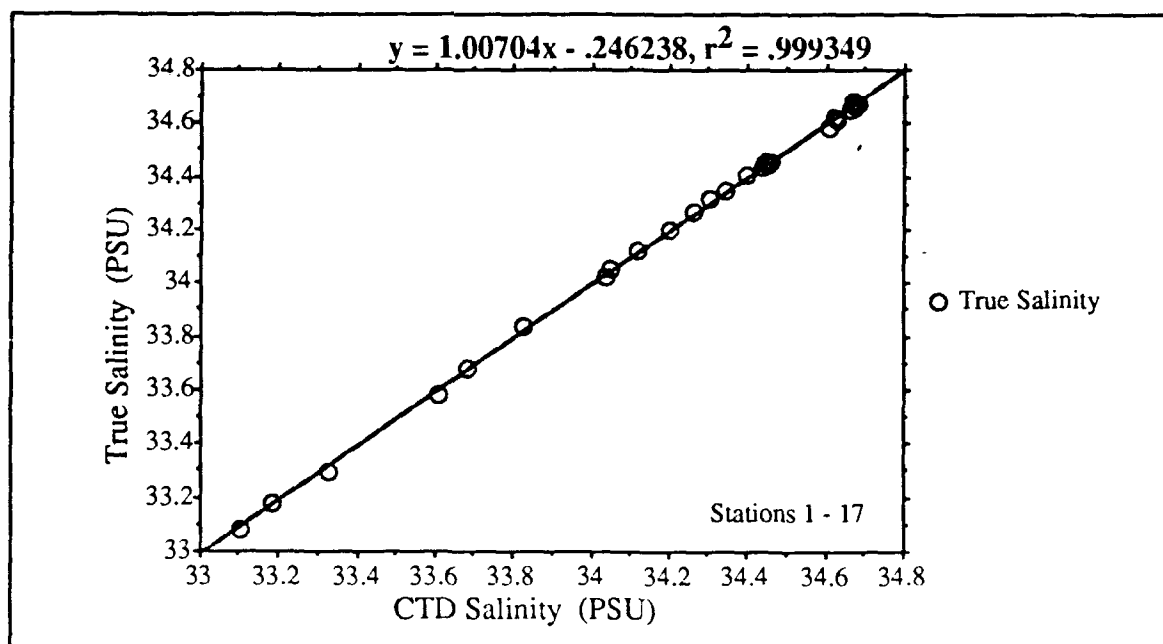
The following scattergrams and regressions were the result of the calibration procedures discussed at length in Chapter III. All cruises, with the exception of those discussed earlier, have been shown here. T-S curves for the 2800 to 3300 decibar range have also been included. These plots consist of all stations along the POST that had depths falling into this range. As mentioned in Chapter III, these T-S curves were used throughout the calibration process to determine the effectiveness of the calibrations.

August 1988 California Undercurrent Cruise : Large Neil Brown CTD

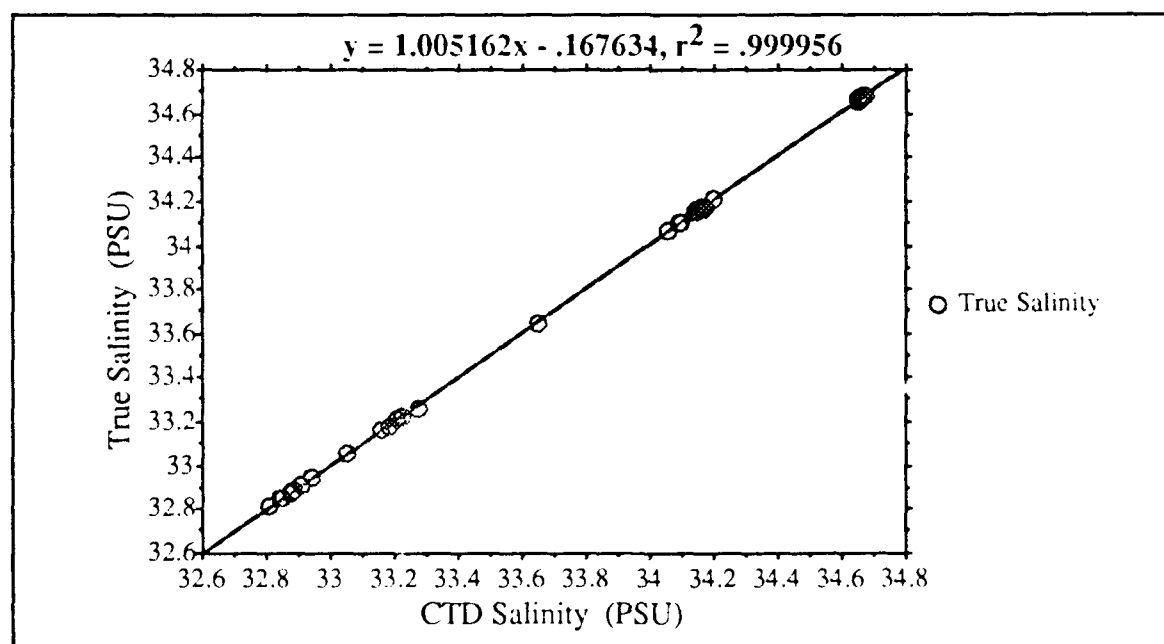
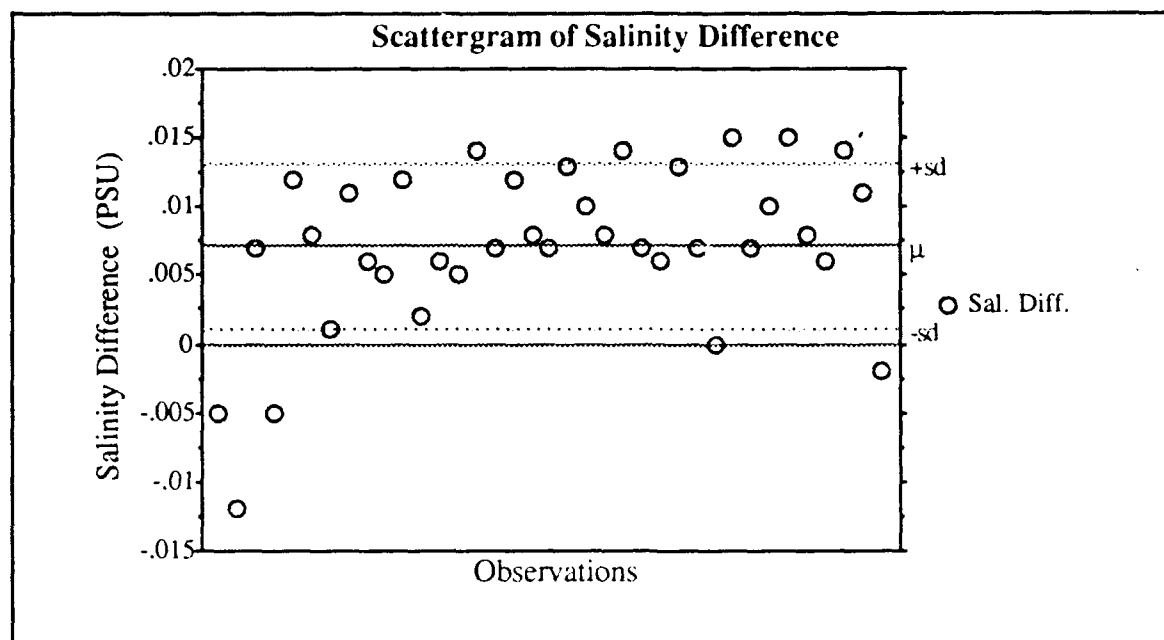


November 1988 California Undercurrent Cruise : Small Neil Brown
CTD

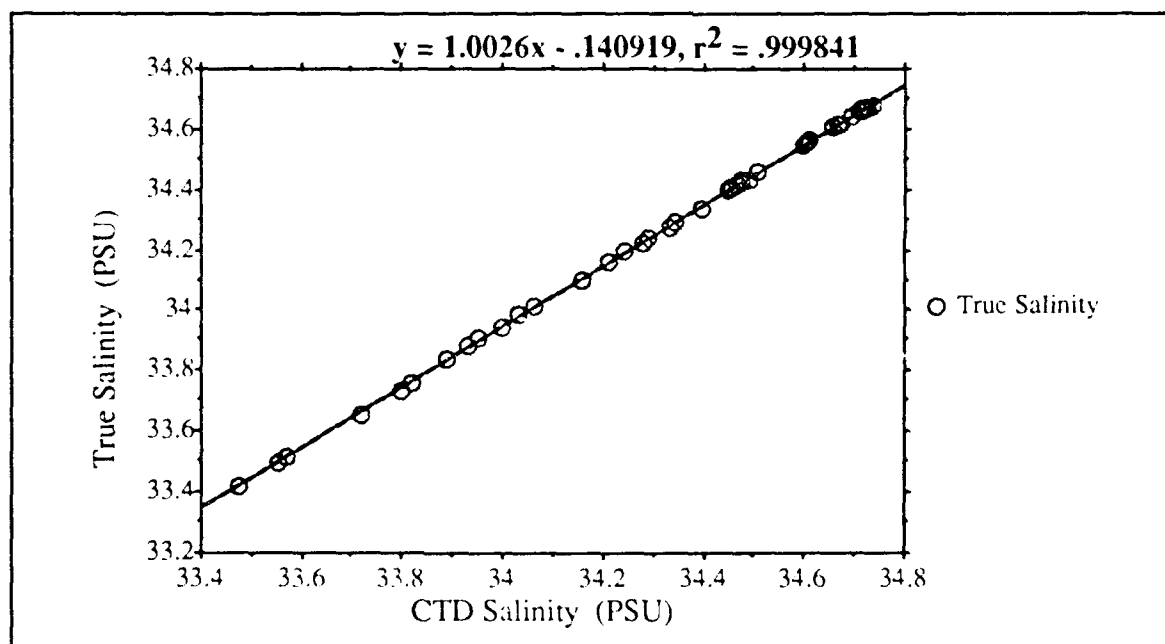
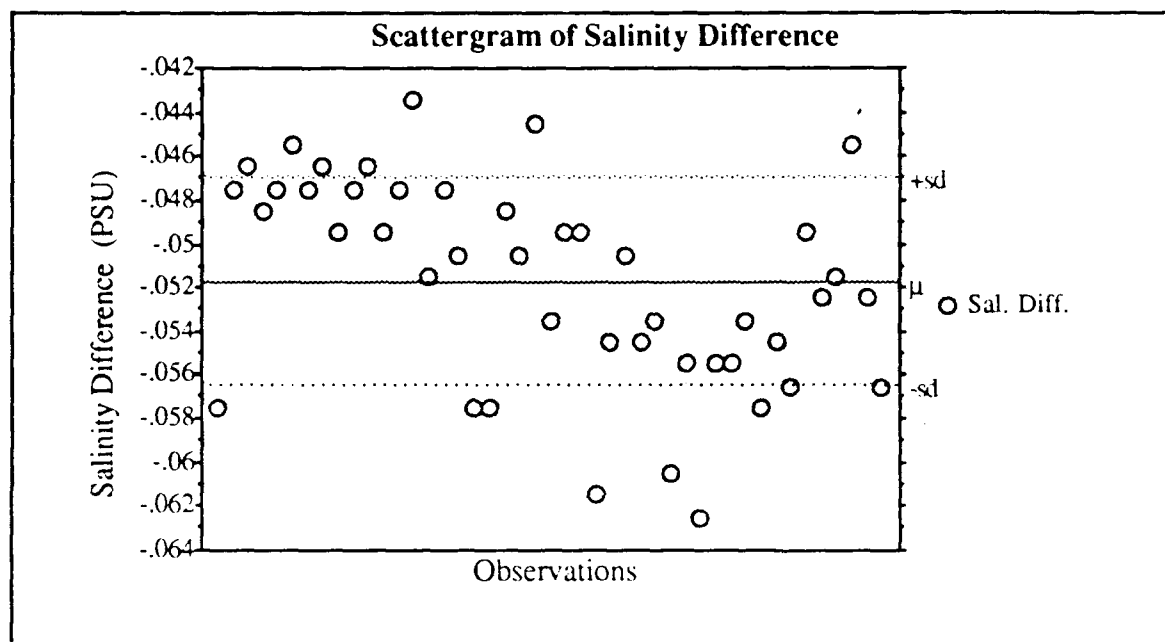




STMAY 1989 POST Cruise : Large Neil Brown CTD

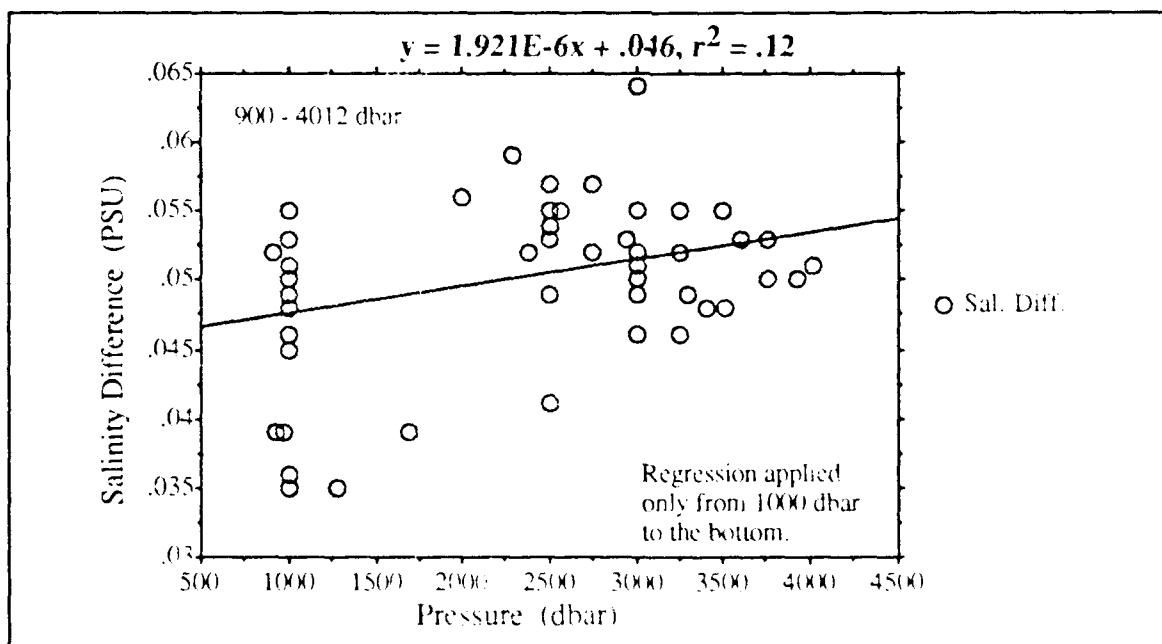
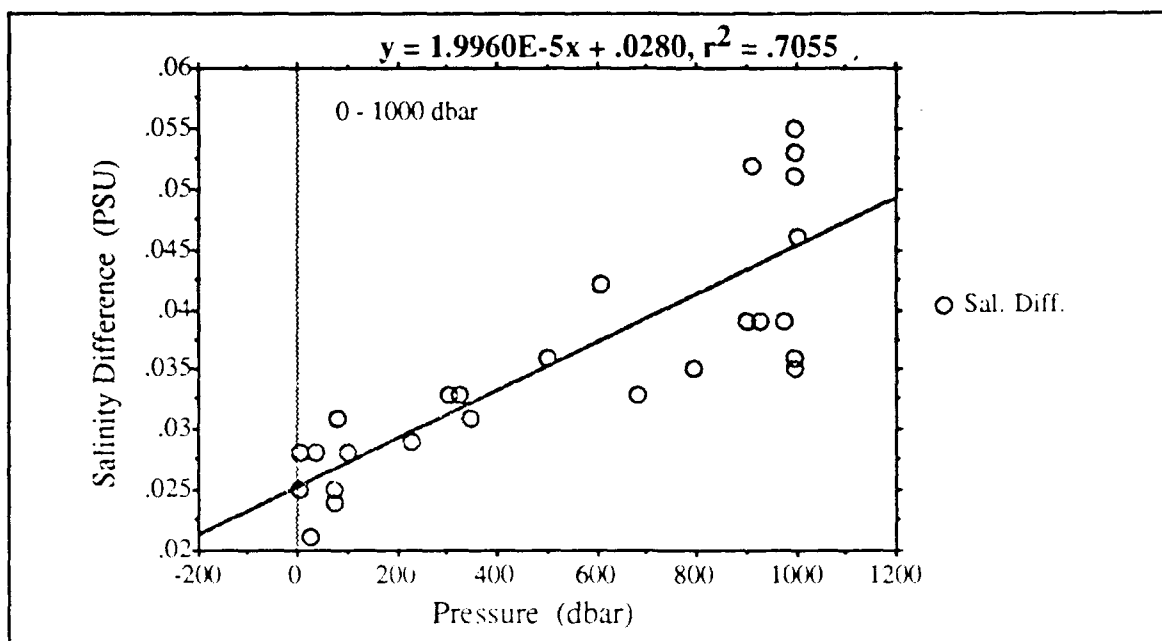


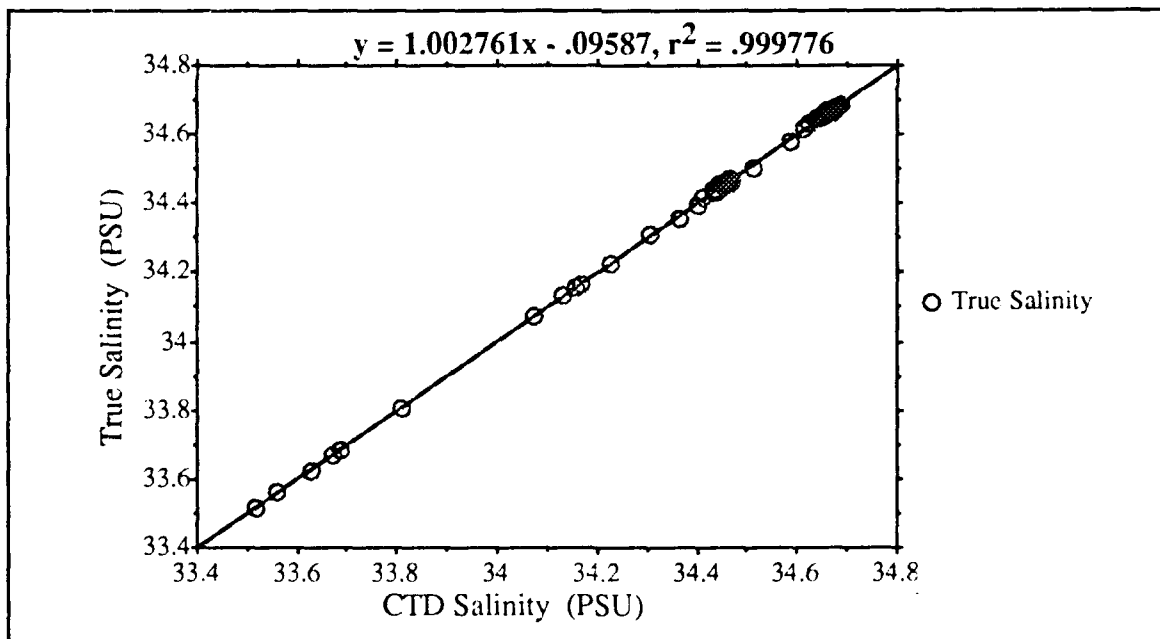
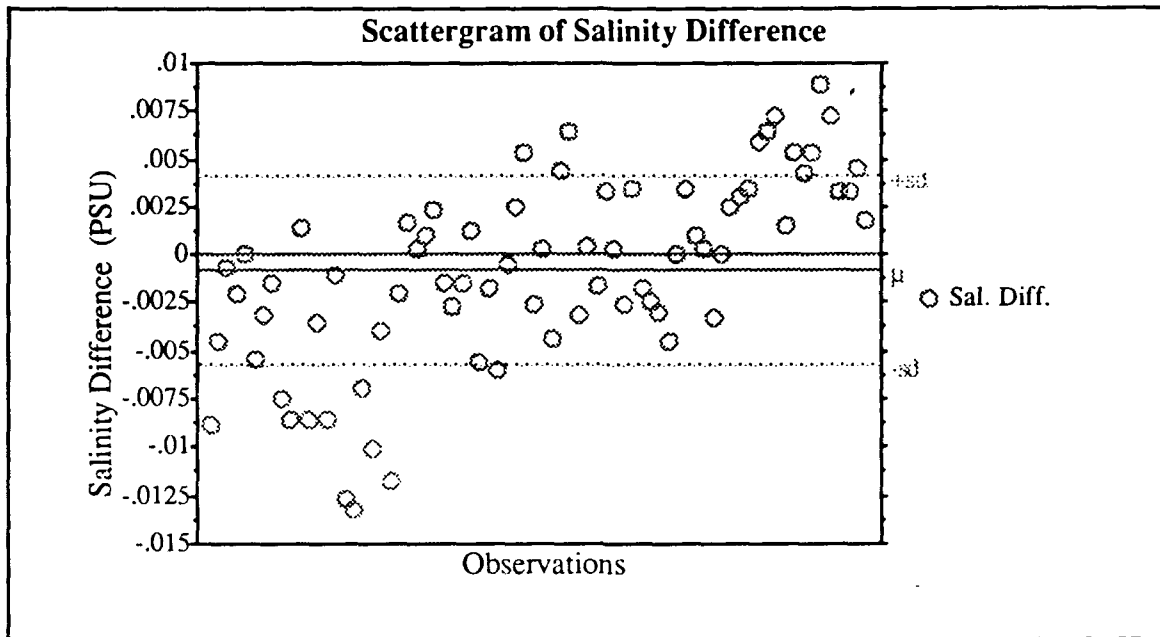
July 1989 California Undercurrent Cruise : Large Neil Brown CTD



November 1989 California Undercurrent Cruise : Small Neil Brown

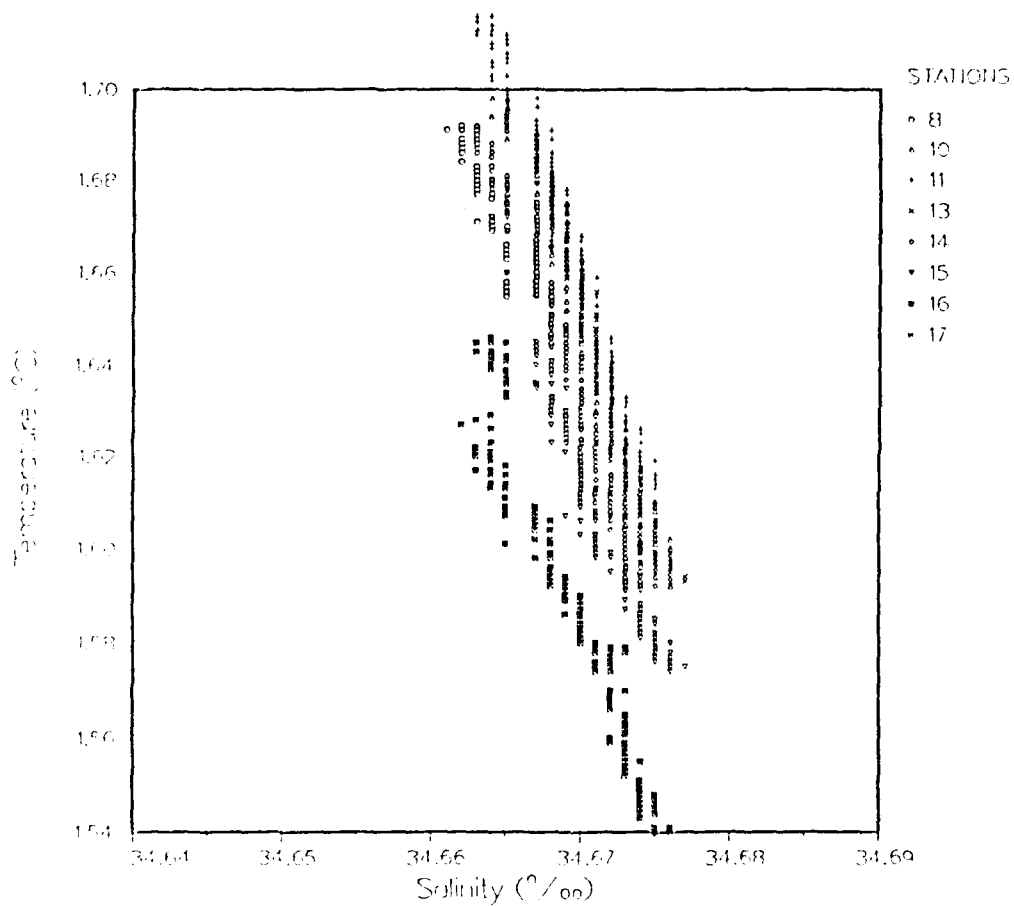
CTD





T/S Characteristics

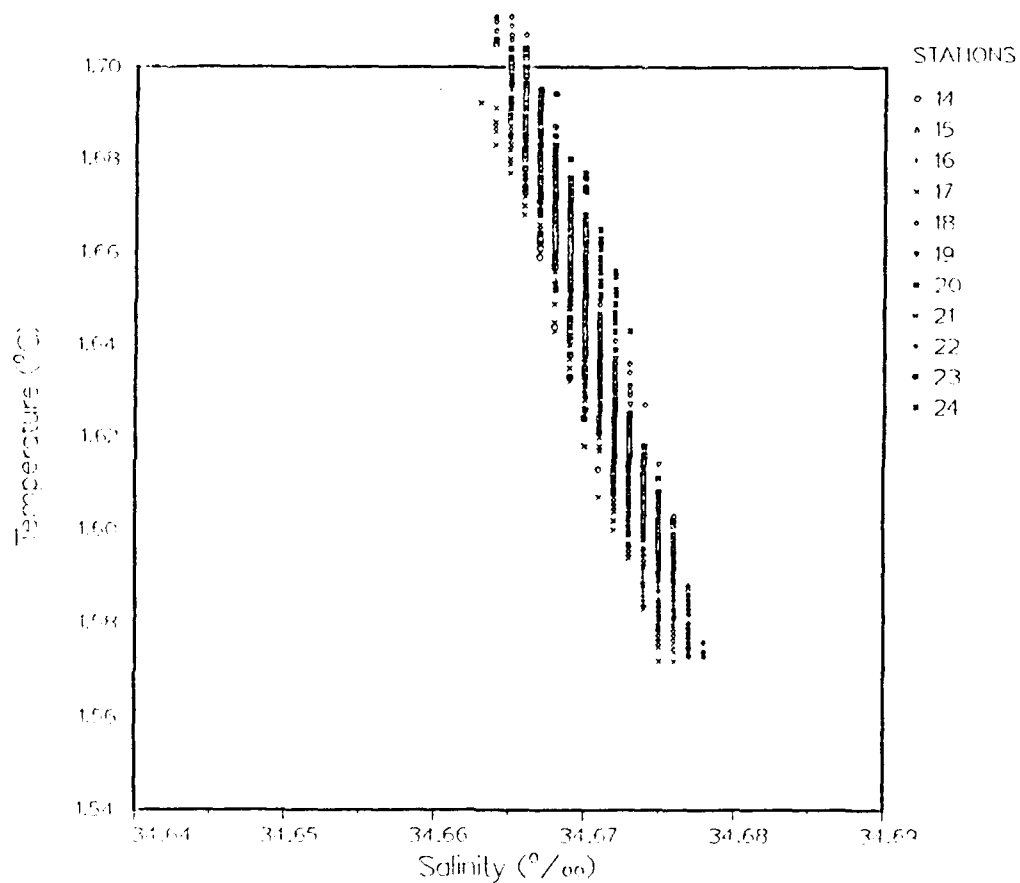
ST MAY 88-I



Pressure range: 2800. - 3200. db

T/S Characteristics

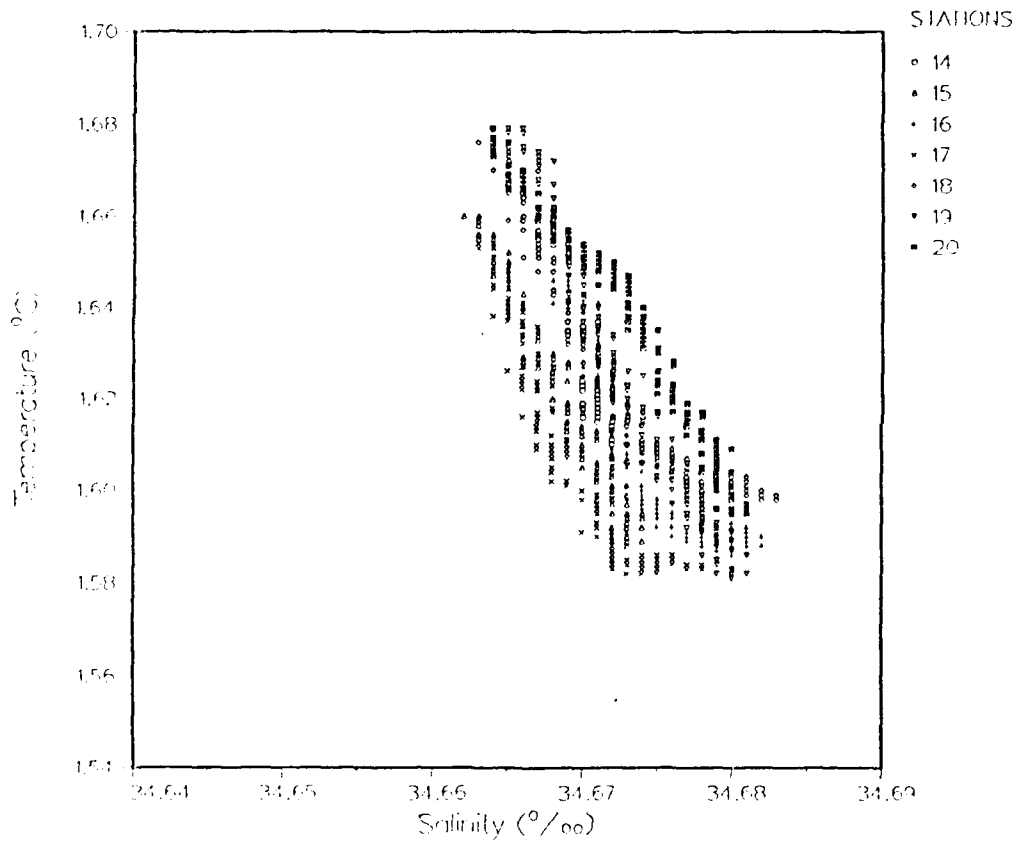
AUG88-CUC



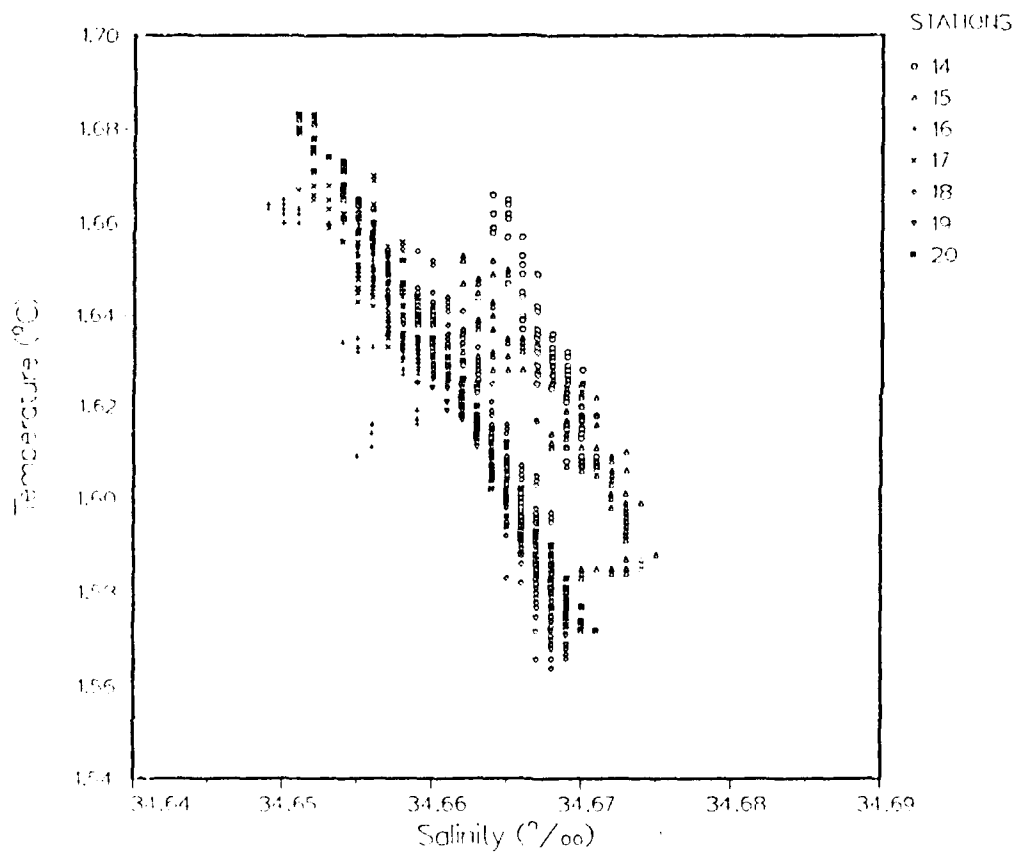
Pressure range: 2800. - 3300. db

T/S Characteristics

CUC-NOV88

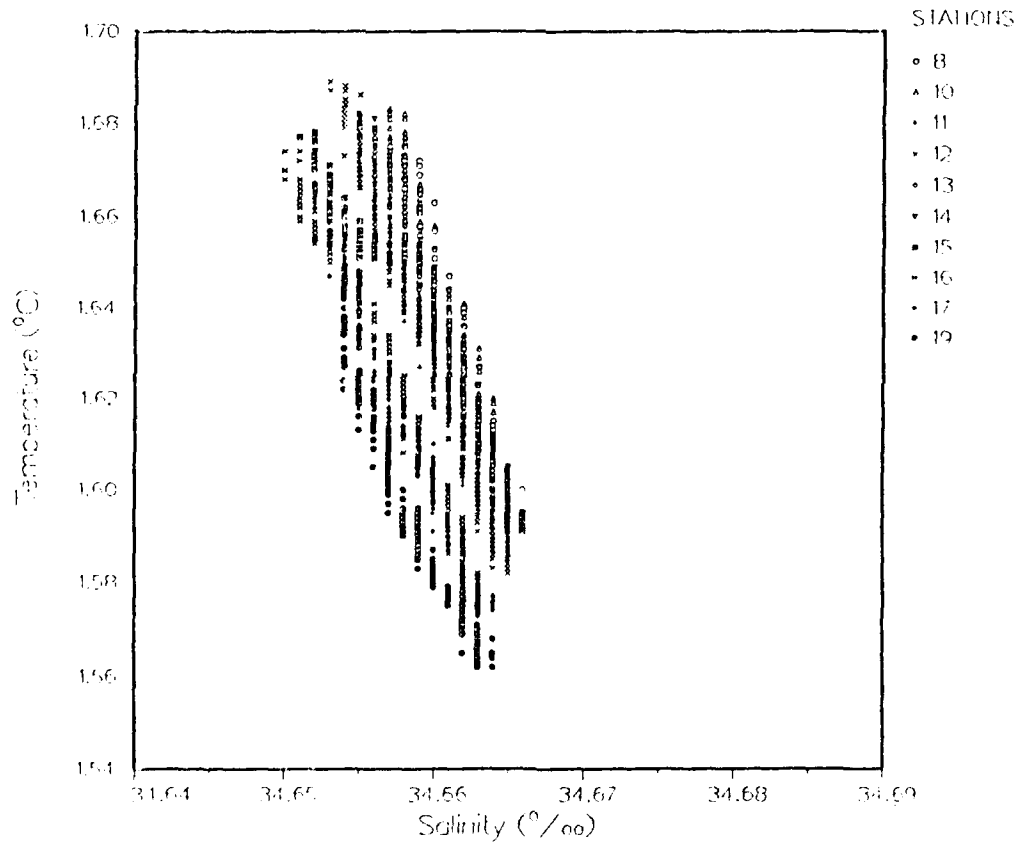


T/S Characteristics FEB89-CUC



T/S Characteristics

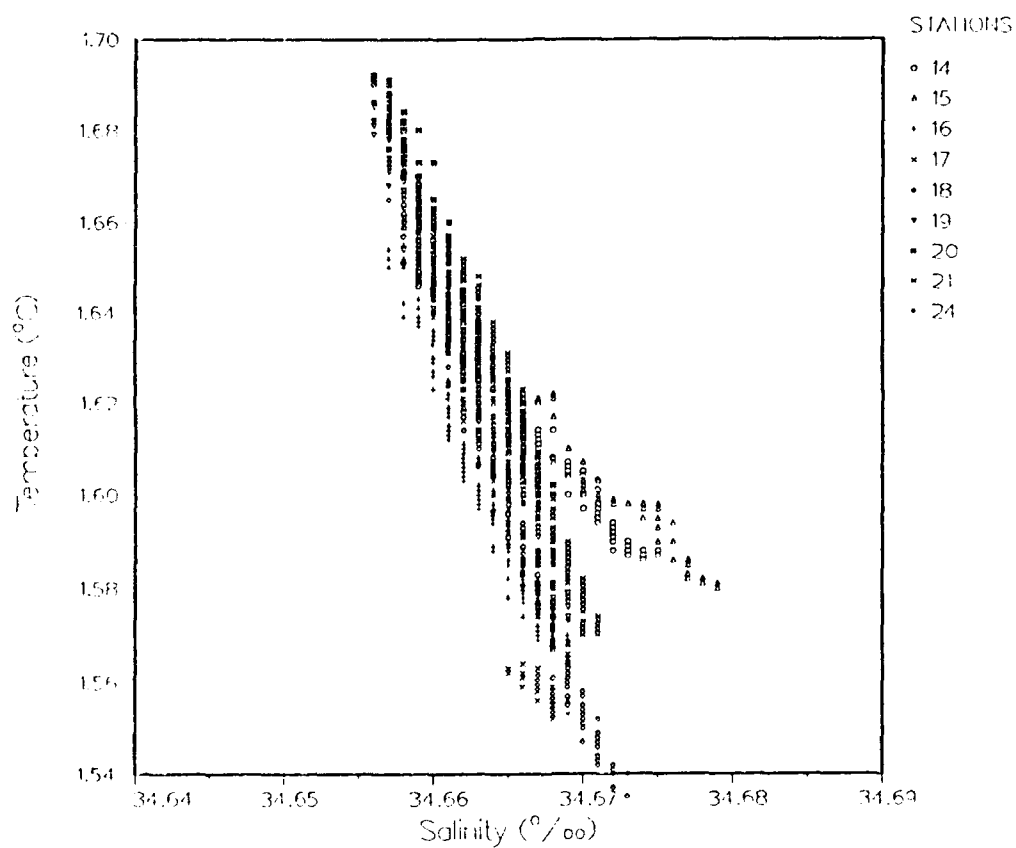
ST MAY 89



Pressure range: 2800 - 3300 db

T/S Characteristics

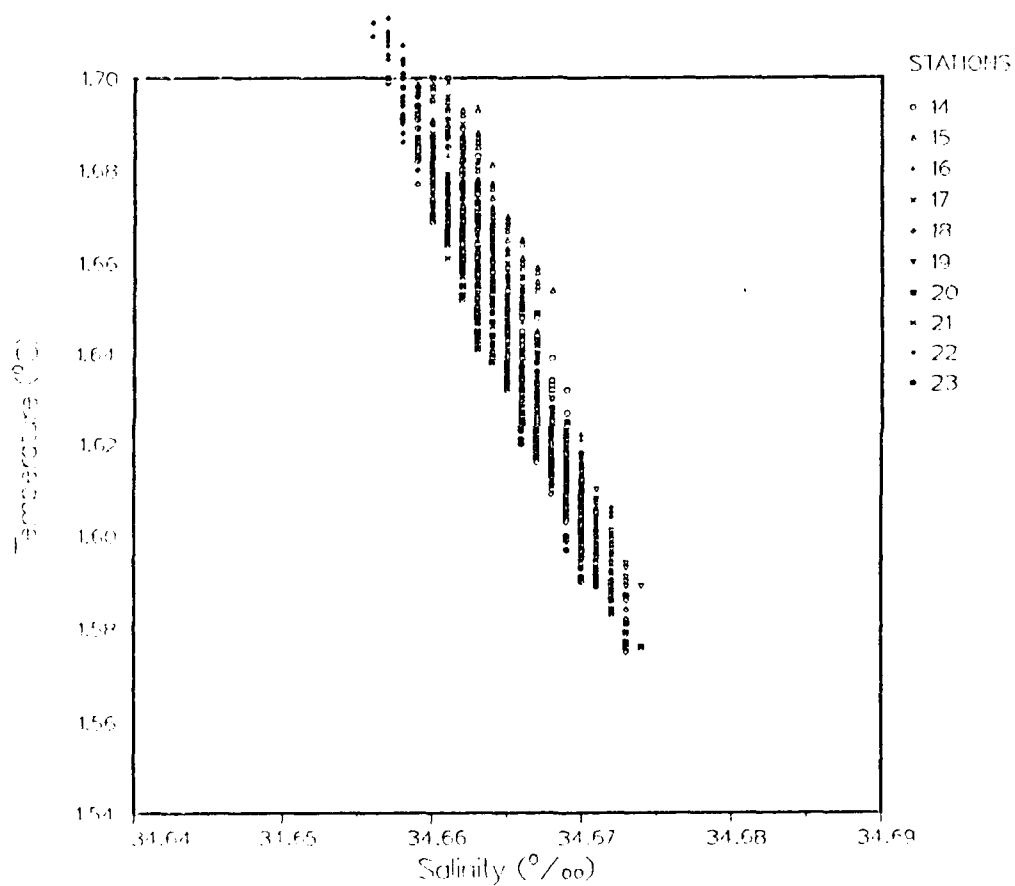
JULY 89 - CUC



Pressure range: 2800, - 3300, db

T/S Characteristics

NOV89--CUC



APPENDIX B: PROPAGATION OF VARIANCES AND COVARIANCES AND FUNDAMENTAL PROPERTIES OF A UNIFORM DISTRIBUTION

The material presented within this appendix provides a detailed description of the method of propagation of variance or propagation of errors as it is more commonly referred to, following Mikhail (1976). A general description of this process will be provided first, followed by the derivation of the equations found in Chapter IV.

In general, observations can be considered samples from probability distributions of random variables. The error properties of these observations are then considered to be statistical properties of the sampling. It is common to assume that the observations are statistically independent. By this it is meant that the results of a previous observation does not or should not influence subsequent observations. This statistical independence results in the elimination of covariance terms between random variables. If the observations are somehow correlated with each other they are no longer considered statistically independent. For the purposes of this work the observations are assumed to be statistically independent both horizontally and vertically.

Propagation of error involves determining the random characteristics of dependent variables from the random characteristics of the independent variables and the functional relationships which relate the two sets of variables. Letting x_1 and x_2 represent random variables, μ_1 and μ_2 the means and $f(x_1, x_2)$ the probability density function, the variances and covariances may be defined in the following manner:

$$\sigma_{x_1}^2 = E[(x_1 - \mu_1)^2] = \int_{-\infty}^{\infty} (x_1 - \mu_1)^2 f(x_1) dx_1 \quad B1$$

$$\sigma_{x_2}^2 = E[(x_2 - \mu_2)^2] = \int_{-\infty}^{\infty} (x_2 - \mu_2)^2 f(x_2) dx_2 \quad B2$$

$$\begin{aligned} \sigma_{x_1 x_2} &= E[(x_1 - \mu_1)(x_2 - \mu_2)] \\ &= \int_{-\infty}^{\infty} \int_{-\infty}^{\infty} (x_1 - \mu_1)(x_2 - \mu_2) f(x_1) f(x_2) dx_1 dx_2 \end{aligned} \quad B3$$

If $y_1 = g_1(x_1, x_2)$ and $y_2 = g_2(x_1, x_2)$, then the following expressions for the variances and covariances for y_1 and y_2 are obtained.

$$\sigma_{y_1}^2 = \int_{-\infty}^{\infty} \int_{-\infty}^{\infty} (g_1(x_1, x_2) - \mu_{y_1})^2 f(x_1, x_2) dx_1 dx_2 \quad B4$$

$$\sigma_{y_2}^2 = \int_{-\infty}^{\infty} \int_{-\infty}^{\infty} (g_2(x_1, x_2) - \mu_{y_2})^2 f(x_1, x_2) dx_1 dx_2 \quad B5$$

$$\sigma_{y_1 y_2} = \int_{-\infty}^{\infty} \int_{-\infty}^{\infty} (g_1(x_1, x_2) - \mu_{y_1})(g_2(x_1, x_2) - \mu_{y_2}) f(x_1, x_2) dx_1 dx_2 \quad B6$$

General formulae such as these are seldom used in practice. The propagation of variances and covariances are simplified to linear or linearized functions.

A. PROPAGATION OF VARIANCE AND COVARIANCE FOR LINEAR FUNCTIONS

Consider the following linear functions, where x_1 and x_2 are random variables with means μ_1 and μ_2 and a joint probability density function $f(x_1, x_2)$,

$$y_1 = a_0 + a_1x_1 + a_2x_2$$

B7

$$y_2 = b_0 + b_1x_1 + b_2x_2$$

From the definition of variance and covariance (B1-B3) and the fact that both the summation and integral operators are linear, expressions for the variance and covariance of y_1 and y_2 are obtained in the following manner.

$$\begin{aligned}\sigma_{y_1}^2 &= E[(y_1 - \mu_{y_1})^2] \\ &= E[(a_0 + a_1x_1 + a_2x_2 - a_0 - a_1\mu_1 - a_2\mu_2)^2] \\ &= E[(a_1(x_1 - \mu_1) + a_2(x_2 - \mu_2))^2] \\ &= E[a_1^2(x_1 - \mu_1)^2 + a_2^2(x_2 - \mu_2)^2 + 2a_1a_2(x_1 - \mu_1)(x_2 - \mu_2)] \\ &= a_1^2 E[(x_1 - \mu_1)^2] + a_2^2 E[(x_2 - \mu_2)^2] + 2a_1a_2 E[(x_1 - \mu_1)(x_2 - \mu_2)] \\ &= a_1^2\sigma_{x_1}^2 + a_2^2\sigma_{x_2}^2 + 2a_1a_2\sigma_{x_1x_2}\end{aligned}$$

B8

Similarly for y_2 ,

$$\sigma_{y_2}^2 = b_1^2\sigma_{x_1}^2 + b_2^2\sigma_{x_2}^2 + 2b_1b_2\sigma_{x_1x_2}$$

B9

The covariance is obtained as follows,

$$\begin{aligned}
\sigma_{y_1 y_2} &= E[(y_1 - \mu_{y_1})(y_2 - \mu_{y_2})] \\
&= E[(a_0 + a_1 x_1 + a_2 x_2 - a_0 - a_1 \mu_1 - a_2 \mu_2)(b_0 + b_1 x_1 + b_2 x_2 - b_0 - b_1 \mu_1 - b_2 \mu_2)] \\
&= E[(a_1(x_1 - \mu_1) + a_2(x_2 - \mu_2))(b_1(x_1 - \mu_1) + b_2(x_2 - \mu_2))] \\
&= E[a_1 b_1 (x_1 - \mu_1)^2 + a_2 b_2 (x_2 - \mu_2)^2 + (a_1 b_2 + a_2 b_1)(x_1 - \mu_1)(x_2 - \mu_2)] \\
&= a_1 b_1 E[(x_1 - \mu_1)^2] + a_2 b_2 E[(x_2 - \mu_2)^2] + (a_1 b_2 + a_2 b_1) E[(x_1 - \mu_1)(x_2 - \mu_2)] \\
&= a_1 b_1 \sigma_{x_1}^2 + a_2 b_2 \sigma_{x_2}^2 + (a_1 b_2 + a_2 b_1) \sigma_{x_1 x_2}
\end{aligned} \tag{B10}$$

Upon inspection of these equations, notice that they are independent of the density functions. Therefore propagation of variances and covariances of linear functions are valid for any distribution.

If matrix notation is introduced it is possible to consolidate equations B8-B10 into a much simpler form. Let $\mathbf{y} = [y_1 \ y_2]^t$ and $\mathbf{x} = [x_1 \ x_2]^t$, where \mathbf{x} and \mathbf{y} are vectors and t denotes the transpose of the matrix. Using \mathbf{x} and \mathbf{y} equation B7 may be rewritten as,

$$\mathbf{y} = \mathbf{c} + \mathbf{C}\mathbf{x} \tag{B11}$$

where

$$\begin{aligned}
\mathbf{c} &= [a_0 \ b_0]^t \\
\mathbf{C} &= \begin{bmatrix} a_1 & a_2 \\ b_1 & b_2 \end{bmatrix}
\end{aligned} \tag{B12}$$

Utilizing equations B8-B10 the covariance matrices for two random vectors \mathbf{x} and \mathbf{y} can be written as follows,

$$\Sigma_{\mathbf{xx}} = \begin{bmatrix} \sigma_{x_1}^2 & \sigma_{x_1 x_2} \\ \sigma_{x_1 x_2} & \sigma_{x_2}^2 \end{bmatrix} \quad \Sigma_{\mathbf{yy}} = \begin{bmatrix} \sigma_{y_1}^2 & \sigma_{y_1 y_2} \\ \sigma_{y_1 y_2} & \sigma_{y_2}^2 \end{bmatrix} \quad \text{B13}$$

which when combined with B12 yields,

$$\Sigma_{\mathbf{yy}} = \mathbf{C} \Sigma_{\mathbf{xx}} \mathbf{C}^t \quad \text{B14}$$

Here the matrix \mathbf{C} represents the Jacobian (\mathbf{J}) of \mathbf{y} with respect to \mathbf{x} , where \mathbf{J} is written as,

$$\mathbf{J}_{\mathbf{yx}} = \frac{\partial \mathbf{y}}{\partial \mathbf{x}} \quad \text{B15}$$

Finally, substitution of B15 into B14 the general form of the propagation of variance and covariance becomes,

$$\Sigma_{\mathbf{yy}} = \mathbf{J}_{\mathbf{yx}} \Sigma_{\mathbf{xx}} \mathbf{J}_{\mathbf{yx}}^t \quad \text{B16}$$

B. PROPAGATION OF VARIANCE AND COVARIANCE FOR NONLINEAR FUNCTIONS

The previous discussion dealt with linear functions, however, in practice one is usually confronted with nonlinear functions. In this case equations such as B7 are the result of a linearization of the general equations. If we now consider

$y_1 = g_1(x_1, x_2)$ and $y_2 = g_2(x_1, x_2)$ to be nonlinear, the linearized form at the initial values x_1^0 and x_2^0 will be identical to B7.

The linearized form is generally truncated after the first order terms, thus neglecting any higher order terms. The zero order terms are not required since $g_1(x_1^0, x_2^0)$ and $g_2(x_1^0, x_2^0)$ correspond to a_0 and b_0 and will not appear in the forms for propagated variance and covariance (B8-B10). All that remains are the partial derivatives and equation B6 will include all four partial derivatives,

$$J = \begin{bmatrix} \frac{\partial y_1}{\partial x_1} & \frac{\partial y_1}{\partial x_2} \\ \frac{\partial y_2}{\partial x_1} & \frac{\partial y_2}{\partial x_2} \end{bmatrix}$$

evaluated at x_1^0 and x_2^0 .

The use of linearized forms is common practice in the propagation of variances and covariances but it must be kept in mind that they are only suited to regions where the function is well approximated by its tangent. In this case, the properties of the nonlinear random variables now become properties of the increments,

$$x_i = x_{i0} + \Delta x_i \quad y_i = y_{i0} + \Delta y_i$$

In other words, the error properties are now associated with Δx_i and Δy_i instead of x_i and y_i , respectively.

C. PROPAGATION OF VARIANCE THROUGH THE EQUATION OF STATE AND EQUATION FOR GEOSTROPHIC VELOCITY

This section provides the details involved in the derivation of equation 5 in Chapter IV. Following the methods discussed earlier in the Appendix, our function becomes $\delta = \delta(S,T,P)$, and equations B13 through B16 become,

$$\Sigma_{STP} = \begin{bmatrix} \sigma_S^2 & \sigma_{ST} & \sigma_{SP} \\ \sigma_{ST} & \sigma_T^2 & \sigma_{TP} \\ \sigma_{SP} & \sigma_{TP} & \sigma_P^2 \end{bmatrix} \quad \text{B17}$$

$$J = \begin{bmatrix} \frac{\partial \delta}{\partial S} & \frac{\partial \delta}{\partial T} & \frac{\partial \delta}{\partial P} \end{bmatrix} \quad \text{B18}$$

$$J^t = \begin{bmatrix} \frac{\partial \delta}{\partial S} \\ \frac{\partial \delta}{\partial T} \\ \frac{\partial \delta}{\partial P} \end{bmatrix} \quad \text{B19}$$

$$\Sigma_{\delta} = \begin{bmatrix} \frac{\partial \delta}{\partial S} & \frac{\partial \delta}{\partial T} & \frac{\partial \delta}{\partial P} \end{bmatrix} \begin{bmatrix} \sigma_S^2 & 0 & 0 \\ 0 & \sigma_T^2 & 0 \\ 0 & 0 & \sigma_P^2 \end{bmatrix} \begin{bmatrix} \frac{\partial \delta}{\partial S} \\ \frac{\partial \delta}{\partial T} \\ \frac{\partial \delta}{\partial P} \end{bmatrix} \quad \text{B20}$$

From statistical independence the off diagonal terms have been set to zero. The final result becomes,

$$\sigma_{\delta}^2 = \left(\frac{\partial \delta}{\partial S} \right)^2 \sigma_S^2 + \left(\frac{\partial \delta}{\partial T} \right)^2 \sigma_T^2 + \left(\frac{\partial \delta}{\partial P} \right)^2 \sigma_P^2 \quad \text{B21}$$

which is equation 5 in Chapter IV.

To determine propagated errors in geostrophic velocity the same procedure shown above is followed. Starting with the equation for geostrophic velocity,

$$v_g = \frac{1}{fL} (\Delta D_B - \Delta D_A) + v_{ref} \quad \text{B22}$$

where $v_g = f(L, \Delta D_B, \Delta D_A, v_{ref})$, the covariance and Jacobian matrices become,

$$\Sigma_{\Delta D_B, \Delta D_A, L, v_{ref}} = \begin{bmatrix} \sigma_{\Delta D_B}^2 & 0 & 0 & 0 \\ 0 & \sigma_{\Delta D_A}^2 & 0 & 0 \\ 0 & 0 & \sigma_L^2 & 0 \\ 0 & 0 & 0 & \sigma_{v_{ref}}^2 \end{bmatrix} \quad \text{B23}$$

$$J = \begin{bmatrix} \frac{\partial v_g}{\partial \Delta D_B} & \frac{\partial v_g}{\partial \Delta D_A} & \frac{\partial v_g}{\partial L} & \frac{\partial v_g}{\partial v_{ref}} \end{bmatrix} \quad \text{B24}$$

$$J^t = \begin{bmatrix} \frac{\partial v_g}{\partial \Delta D_B} \\ \frac{\partial v_g}{\partial \Delta D_A} \\ \frac{\partial v_g}{\partial L} \\ \frac{\partial v_g}{\partial v_{ref}} \end{bmatrix}$$

B25

$$\Sigma_{v_g} = \begin{bmatrix} \frac{\partial v_g}{\partial \Delta D_B} & \frac{\partial v_g}{\partial \Delta D_A} & \frac{\partial v_g}{\partial L} & \frac{\partial v_g}{\partial v_{ref}} \end{bmatrix} \begin{bmatrix} \sigma_{\Delta D_B}^2 & 0 & 0 & 0 \\ 0 & \sigma_{\Delta D_A}^2 & 0 & 0 \\ 0 & 0 & \sigma_L^2 & 0 \\ 0 & 0 & 0 & \sigma_{v_{ref}}^2 \end{bmatrix} \begin{bmatrix} \frac{\partial v_g}{\partial \Delta D_B} \\ \frac{\partial v_g}{\partial \Delta D_A} \\ \frac{\partial v_g}{\partial L} \\ \frac{\partial v_g}{\partial v_{ref}} \end{bmatrix}$$

B26

or,

$$\sigma_{v_g}^2 = \left(\frac{\partial v_g}{\partial \Delta D_B} \right)^2 \sigma_{\Delta D_B}^2 + \left(\frac{\partial v_g}{\partial \Delta D_A} \right)^2 \sigma_{\Delta D_A}^2 + \left(\frac{\partial v_g}{\partial L} \right)^2 \sigma_L^2 + \left(\frac{\partial v_g}{\partial v_{ref}} \right)^2 \sigma_{v_{ref}}^2$$

B27

Substitution of the derivatives into the Jacobian matrix yields the following,

$$\sigma_{v_g}^2 = \left(\frac{1}{fL} \right)^2 \sigma_{\Delta D_B}^2 + \left(\frac{-1}{fL} \right)^2 \sigma_{\Delta D_A}^2 + \left(\frac{-v_g}{L} \right)^2 \sigma_L^2 + \left(\frac{\partial v_g}{\partial v_{ref}} \right)^2 \sigma_{v_{ref}}^2$$

B28

Because the error in dynamic height, $\sigma_{\Delta D}^2$, is the same for each station, the first two terms in equation B28 are equivalent and the derivative of v_g with respect to v_{ref} is equal to one. As a result B28 reduces to,

$$\sigma_{v_g}^2 = 2\left(\frac{1}{fL}\right)^2 \sigma_{\Delta D}^2 + \left(\frac{v_g}{L}\right)^2 \sigma_L^2 + \sigma_{v_{ref}}^2 \quad B28$$

This form is identical to equation (9) in Chapter IV where the value in (9) already incorporates the factor of two.

D. UNIFORM DISTRIBUTIONS

This section contains the development for the error in station spacing as described in Chapter IV. The source material comes from Bendat and Piersol (1986).

Consider an experiment which consists of choosing a point at random in some interval $[a, b]$ which includes the endpoints. The probability distribution for a continuous random variable $x(k)$, becomes,

$$p(x) = \begin{cases} 0 & x < a \\ \frac{x-a}{b-a} & a \leq x \leq b \\ 1 & x > b \end{cases} \quad B29$$

and the corresponding probability density function is defined as,

$$p(x) = \begin{cases} \frac{1}{b-a} & a \leq x \leq b \\ 0 & \text{otherwise} \end{cases} \quad B30$$

The mean or expected value is defined as,

$$E[g(x(k))] = \int_{-\infty}^{\infty} g(x)p(x) dx \quad \text{B31}$$

and for this example becomes,

$$\mu_x = \frac{a+b}{2} \quad \text{B32}$$

The variance or second moment is defined as,

$$E[x^2(k)] = \int_{-\infty}^{\infty} x^2 p(x) dx \quad \text{B33}$$

and for this example becomes,

$$\sigma_x^2 = \frac{(b-a)^2}{12} \quad \text{B34}$$

For the case of the error in station spacing due to vessel drift, the value of the error is assumed to lie between 0 and $L/2$, or $1/2$ the differential drift between stations. Substituting these values in for a and b in equations B19 through B22, the following result is obtained,

$$\sigma_L^2 = \frac{\left(\frac{L}{2} + 0\right)^2}{12} = \frac{L^2}{48} \quad \text{B35}$$

Taking the square-root of this result provides the root mean square error which for the error in station spacing is simply the differential distance, $L/2$, divided by two times the square-root of three.

REFERENCES

- Bendat, J.S., and A.G. Piersol, 1986: *Random Data, Analysis and Measurement Procedures*, 2nd Ed., John Wiley and Sons, Inc., NY, 586 pp.
- Berryman, P., 1989: Study of currents along the Pt. Sur transect in February 1989, Master's Thesis, Naval Postgraduate School, Monterey, California, 51 pp.
- Bowditch, N., 1984: *American Practical Navigator, Vol. I*, Pub. No. 9, Defense Mapping Agency Hydrographic/Topographic Center, 1428 pp.
- Breaker, L.C., and W.W. Broenkow, 1989: The circulation of Monterey Bay and related processes, Moss Landing Marine Laboratories, Moss Landing, Calif., *Technical Publication*, 89-1, 99 pp.
- Bretherton, F.P., R.E. Davis, and C.B. Fandry, 1976: A technique for objective analysis of oceanographic experiments applied to MODE-73, *Deep Sea Res.*, 23, pp. 559-582.
- Brink, K.H. and E.O. Hartwig, 1985: Office of Naval Research Coastal Transition Zone workshop report, 65 pp.
- Chelton, D.B., 1984: Seasonal variability of alongshore geostrophic velocity off central California, *J. Geophys. Res.*, 89, 3473-3486.
- Chelton, D.B., A.W. Bratkovich, R.L. Bernstein, and P.M. Kosro, 1988: Poleward flow off central California during the spring and summer of 1981 and 1984, *J. Geophys. Res.*, 93, 10,604-10,620.
- Davis, R.E., 1985: Drifter observations of coastal surface currents during CODE: The method and descriptive view, *J. Geophys. Res.*, 90, 4741-4755.
- Davis, R.E., and P.S. Bogden, 1989: Variability on the California shelf forced by local and remote winds during the Coastal Ocean Dynamics Experiment, *J. Geophys. Res.*, 94, 4763-4784.
- Defant, A., 1950: Reality and illusion in oceanographic surveys, *J. Mar. Res.*, 9(2), 120-138.

- Flament, P., submitted 1986: A note on seawater spiciness and diffusive stability, *Deep Sea Res.*
- Fofonoff, N.P., 1985: Physical properties of seawater: A new salinity scale and equation of state for seawater, *J. Geophys. Res.*, **90**, 3332-3342.
- Halpern, D., R.L. Smith, and R.K. Reed, 1978: On the California Undercurrent over the continental slope off Oregon, *J. Geophys. Res.*, **83**, 1366-1372.
- Hickey, B.M., 1979: The California Current System - hypotheses and facts, *Prog. Oceanogr.*, **8**, pp. 191-279.
- Huyer, A., 1980: The offshore structure and subsurface expression of sea level variations off Peru, 1976-1977, *J. Phys. Oceanogr.*, **10**, 1755-1768.
- Huyer, A., 1983: Coastal upwelling in the California Current System, *Prog. Oceanogr.*, **12**, pp. 259-284.
- Huyer, A., P.M. Kosro, S.J. Lentz, and R.C. Beardsley, 1989: Poleward flow in the California Current System, in *Poleward Flows along Eastern Oceanic Boundaries*, Coastal and Estuarine Studies No. 34, pp.142-156, Springer-Verlag New York Inc.
- Huyer, A., P.M. Kosro, J. Fleischbein, S.R. Ramp, T. Stanton, L. Washburn, F. Chavez, and T. Cowles, submitted 1990: Currents and water masses of the Coastal Transition Zone off northern California, June to August 1988, *J. Geophys. Res.*
- Jessen, P.F., S.R. Ramp, and C.A. Clark, 1989: Hydrographic data from the pilot study of the Coastal Transition Zone (CTZ) program, 15 - 28 June 1987, *NPS-69-89-004*, Naval Postgraduate Sch., Monterey, Calif., 250 pp.
- Johns, E., 1984: Geostrophy and potential vorticity in the Gulf Stream northeast of Cape Hatteras, N.C., Ph.D. Dissertation, Univ. of Rhode Island, Kingston, 223 pp.
- Kelley, K.A., and M.J. Caruso, 1990: A modified objective mapping technique for scatterometer wind data, *J. Geophys. Res.*, **95**, 13,483-13,496.
- Large, W.G., and S. Pond, 1981: Open ocean momentum flux measurements in moderate to strong winds, *J. Phys. Oceanogr.*, **11**, 324-336.
- Lewis, E.L. and R.G. Perkin, 1981: The Practical Salinity Scale 1978: conversion of existing data, *Deep Sea Res.*, **28A**, 307-328.

- Lynn, R.J., and J.J. Simpson, 1987: The California Current System: The seasonal variability of its physical characteristics, *J. Geophys. Res.*, **92**, 12,947-12,966.
- Lynn, R.J., and J.J. Simpson, 1990: The flow of the undercurrent over the continental borderland off Southern California, *J. Geophys. Res.*, **90**, 12,955-13,008.
- McIntosh, P.C., 1990: Oceanographic data interpolation: Objective analysis and splines, *J. Geophys. Res.*, **90**, 13,529-13,541.
- Mikhail, E.M., 1976: *Observations and Least Squares*, Thomas Y. Crowell Company Inc., 511 pp.
- Millero, F.S., and A. Poisson, 1981: International one-atmosphere equation of state of seawater, *Deep Sea Res.*, **28A**(6), 625-629.
- Nelson, C.S., 1977: Wind stress and wind stress curl over the California Current, *Tech. Rep. NMFS-SSRF-714*, Nat. Oceanic and Atmos. Admin., Wash. D.C.
- Pickard, G.L., and W.J. Emery, 1982: *Descriptive Physical Oceanography an Introduction*, 4th Ed., Pergamon Press Inc., Elmsford, NY, 263 pp.
- Pond, S., and G.L. Pickard, 1983: *Introductory Dynamical Oceanography*, 2nd Ed., Pergamon Press Inc., Elmsford, NY, 349 pp.
- Rago, T.A., and C.A. Collins, 1989: Measurements of ocean currents across the continental margin off Pt. Sur, California, from April 1988 to March 1989, abstract in *Trans. Amer. Geophys. Un.*, **70**(43), 278-286.
- Reid, J.L., 1956: Observations of internal tides in October 1950, *Trans. Amer. Geophys. Un.*, **37**, 278-286.
- Reid, J.L., G.I. Roden, and J.G. Wyllie, 1958: Studies of the California Current System, CalCOFI Progress Reports 1 July 1956 to 1 January 1958, Calif. Coop. Oceanic Fish. Invest., La Jolla, pp. 27-56.
- Reid, J.L., and R.A. Schwartzlose, 1962: Direct measurements of the Davidson Current off central California, *J. Geophys. Res.*, **67**, 2491-2497.
- Reid, J.L., and A. W. Mantyla, 1976: The effect of the geostrophic flow upon coastal sea elevations in the North Pacific Ocean, *J. Geophys. Res.*, **81**, 3100-3110.

- Reid, R.O., 1958: Influence of some errors in the equation of state or in observations on geostrophic currents, *Physical and Chemical properties of seawater*, *Publ. 600*, Nat. Acad. Sci., Nat. Res. Council., Wash., D.C., pp. 10 - 29.
- Reinecker, M.M., C.N.K. Mooers, and A.R. Robinson, 1987: Dynamical interpolation and forecast of the evolution of mesoscale features off northern California, *J. Phys. Oceanogr.*, **17**, 1189-1213.
- Roemmich, D., 1983: Optimal estimation of hydrographic station data and derived fields, *J. Phys. Oceanogr.*, **13**, 1544-1549.
- Simpson, J.J., 1984: El Niño-induced onshore transport in the California current during 1982-83, *Geophys. Res. Lett.*, **11**, 233-236.
- Shepard, F.P., 1975: Progress of internal waves along submarine canyons, *Marine Geology*, **19**, pp. 131-138.
- Sverdrup, H., 1938: On the process of upwelling, *J. Mar. Res.*, **1**, 155-164.
- Sverdrup, H.U., R.H. Johnson, M.W. Fleming, 1942: *The Oceans*, Prentice-Hall, Inc. Englewood Cliffs, NJ, 1066 pp.
- Tibby, R.B., 1941: The water masses off the west coast of North America, *J. Mar. Res.*, **4**, 112-121.
- Tracy, D.E., 1990: Surface circulation of Monterey Bay using AVHRR Satellite Imagery, Master's Thesis, Naval Postgraduate School, Monterey, California.
- UNESCO, 1983: Algorithms for computation of fundamental properties of seawater, *UNESCO Tech. Pap. in Mar. Sci.*, No. 44, 53 pp.
- UNESCO, 1987: International Oceanographic Tables, *UNESCO Tech. Pap. in Mar. Sci.*, Vol 4.
- Wahl, D.D., and J.J. Simpson, 1990: Physical processes affecting the objective determination of near-surface velocity from satellite data, *J. Geophys. Res.*, **95**, 13,511-13,528.
- Warren, B.A., and W.B. Owens, 1988: Deep Currents in the Central Subarctic Pacific Ocean, *J. Phys. Oceanogr.*, **18**, 529-551.

- Wickham, J.B., 1975: Observations of the California countercurrent, *J. Mar. Res.*, **33**, 325-340.
- Wickham, J.B., A.A. Bird, and C.N.K. Mooers, 1987: Mean and variable flow over the central California continental margin, 1978-1980, *Continental Shelf Res.*, **7**(8), pp. 827-849.
- Wiseman, W.J., C.N.K. Mooers, and G.D. Forristall, 1983: Ocean current processes, *Ocean Science and Engineering*, **8**(4), 367-459.
- Wooster, W.S., and B.A. Taft, 1958: On the reliability of field measurements of temperature and salinity in the ocean, *J. Mar. Res.*, **17**, 552-566.
- Wooster, W.S., and J.H. Jones, 1970: California undercurrent off northern Baja California, *J. Mar. Res.*, **28**, 253-260.
- Worthington, V., 1981: The water masses of the World Ocean: some results of a fine-scale census, in *Evolution of physical oceanography*, pp.42-69, The MIT press, Cambridge, Massachusetts.

INITIAL DISTRIBUTION LIST

	No. Copies
1. Defense Technical Information Center Cameron Station Alexandria, Virginia 22314	2
2. Library, Code 52 Naval Postgraduate School Monterey, CA 93943-5000	2
3. Chairman (Code OC/Co) Department of Oceanography Naval Postgraduate School Monterey, CA 93943-5000	1
4. Professor C.A. Collins (OC/Co) Department of Oceanography Naval Postgraduate School Monterey, CA 93943-5000	1
5. Professor Steven. R. Ramp (OC/Ra) Department of Oceanography Naval Postgraduate School Monterey, CA 93943-5000	1
6. LT Timothy D. Tisch Department of Oceanography Naval Postgraduate School Monterey, CA 93943-5000	1
7. Director Naval Oceanography Division Naval Observatory 34th and Massachusetts Avenue NW Washington, DC 20390	1
8. Commander Naval Oceanography Command Stennis Space Center MS 39529-5000	1

- | | |
|--|---|
| 9. Library
Scripps Institution of Oceanography
P.O. Box 2367
La Jolla, CA 92037 | 1 |
| 10. Chief, Ocean Services Division
National Atmospheric and Oceanic
Administration
8060 Thirteenth Street
Silver Springs, MD 20910 | 1 |
| 11. Chief, Career Development Division (CPC2)
Commisioned Personnel Center
National Atmospheric and Oceanic
Administration
Rockville, MD 20852 | 1 |
| 12. NOAA Library
7600 Sand Point Way NE
Building 3
Seattle, WA 98115 | 1 |
| 13. Professor J.L. Reid, Jr
Scripps Institution of Oceanography
La Jolla, CA 92038 | 1 |